2009

Effects of diluent addition and metal support interactions in heterogeneous catalysis: SiC/VPO catalysts for maleic anhydride production and co/silica supported catalysts for FTS/

Ala'a Hamed Kababji
University of South Florida

Effects of Diluent Addition and Metal Support Interactions in Heterogeneous Catalysis:

SiC/VPO Catalysts for Maleic Anhydride Production and

Co/Silica Supported Catalysts for FTS

by

Ala'a Hamed Kababji

A dissertation submitted in partial fulfillment
of the requirements for the degree of
Doctor of Philosophy
Department of Chemical and Biomedical Engineering
College of Engineering
University of South Florida

Major Professor: John T. Wolan, Ph.D.
Babu Joseph, Ph.D.
Elias Stefanakos, Ph.D.
Vinay K. Gupta, Ph.D.
Stephen E. Saddow, Ph.D.
Casey W. Miller, Ph.D.

Date of Approval:
March 23, 2009

Keywords: exothermic reaction, adsorption, fixed-bed reactor, synthetic liquid fuel,
incipient wetness impregnation

Dedication

I would like to dedicate this dissertation to my beloved mother who passed away during the time I was completing this work. To my father, whose love and support have always helped me throughout those years I spent far from home. I would also like to dedicate this work to my beloved sisters and brother. You all have been there for me in the rough time and in good times. To S. C.: thank you for your support, encouragement and for believing in me from the beginning and to my cousin A. Z. for standing beside me, without your help and support, I would not have made it. I miss you all.

Acknowledgements

I would like to express my gratitude to my graduate advisor and major professor Dr. John Wolan for his support and help through my entire education and research experience here at USF. Special thanks to the Chair of the Chemical Engineering Department, Dr. Babu Joseph for the support, advice and the "weekly meeting" valuable discussions. I would also like to collectively thank all my committee members for their motivation and valuable remarks and recommendations.

Many thanks go to Dr. Take Constantinescu from Chemont S.A. in Belgium for his continued interest and recommendations regarding the VPO catalytic experiments. Special thanks go for my other co-workers (current and graduated) in the Applied Surface Science Laboratory: Dr. Timothy Fawcett, Dr. Benjamin Grayson, Ali, Chris, Brad, and Dr. Jonathan Mbah for their help and technical assistance. I also extend my thanks to Haito Li for help in conducting the BET measurements of the synthesized catalyst samples.

The VPO work was supported by the Defense University Research Initiative on Nanotechnology (DURINT) program administered by the Office of Naval Research under grant N00014-0110715 monitored by Dr. Colin Wood. For the Fischer-Tropsch synthesis experiments, financial support from the National Aeronautics and Space Administration (NASA) under grant 16266038-27 through a subcontract from the University of Central Florida is gratefully acknowledged. Graduate support in the form of a teaching assistantship from NSF grant on curriculum reform EEC-0530444 is also acknowledged.

Table of Contents

List of Tables

List of Figures

Effects of Diluent Addition and Metal Support Interactions in Heterogeneous Catalysis: SiC/VPO Catalysts for Maleic Anhydride Production and Co/Silica Supported Catalysts for FTS

Ala'a Hamed Kababji

ABSTRACT

This work begins with an introduction to catalysis focusing on heterogeneous systems and surface science phenomena. A study on the partial oxidation reaction of *n*-butane to maleic anhydride (MA) is presented in the first part. MA supplies are barely adequate for market requirements due to continued strong demand. Only slight improvement in catalytic performance would be welcome in the industrial community. The vanadium phosphorus oxide (VPO) catalyst was used in this work. The reaction is highly exothermic and the need to properly support the catalyst, not only for good dispersion but adequate heat dissipation is of crucial importance. For this, α-SiC commercial powders were used in synthesizing the catalyst due to its high thermal conductivity. Up to 25% MA yields were obtained and the reaction temperature was lowered by up to28% using SiC/VPO mixed catalysts.

The second part of this work is focused on the Fischer-Tropsch synthesis (FTS) process using cobalt silica supported catalysts. The main objective is the production of

synthetic ultra high purity jet fuel (JP5). This is a very timely topic given the energy issues our world is facing. Almost all aspects of the FTS process have been extensively studied, however the effects of calcination temperature and silica support structure on the catalyst performance are lacking in literature. The catalysts were prepared using various silica supports. The catalysts had different drying and calcination temperatures. It was found that lower support surface area and calcination temperature catalysts exhibited higher activity due to lower support cobalt phase interaction. Co/silica catalysts calcined at 573K showed the highest CO conversion and the lowest CH_4 selectivity. Catalysts prepared with 300m^2/g support surface area exhibited 79.5% C_{5+} selectivity due to higher reducibility and less metal support interaction.

The properties and performance of various prepared catalysts in both VPO and Co/silica systems are characterized by FTIR, XRD, BET, GC and XPS techniques. Theoretical FTS deactivation by sintering calculations and SiC/VPO particle temperature gradient calculations are presented as well. Finally, conclusions and future work on improving the yield and selectivity and scaling up the bench top setups are also presented.

Chapter 1: Introduction

1.1 Introduction to Catalysis

Catalytic processes have been applied by humans for centuries, however, it was not until 1836 that Berzelius introduced the term 'catalysis' [1]. Later, in 1895, William Ostwald was the first to write down a definition of a catalyst: 'A catalyst is a substance that changes the rate of a chemical reaction without itself appearing in the products.' It is important to note that a catalyst does not influence the thermodynamic equilibrium of reactants and products. Therefore, the current definition is slightly better, though close to Ostwald's description: 'A catalyst is a substance that increases the rate of approach to thermodynamic equilibrium of a chemical reaction without being substantially consumed' [1,2]. The principal theme in catalysis is the desire to control the rate of chemical reactions and the secondary theme is to understand the mechanism of the control. Catalysts do undergo chemical changes during the course of a reaction. However, these changes are reversible so that the catalyst is not consumed as the reaction proceeds. While early attempts at improving reaction rates and conversions were successful by relying on high temperature and high pressure processes, these conditions are energy intensive, corrosive, and result in undesirable side products [2]. The extensive use of catalysts along with improvements in fluid flow characteristics have led to lower operating temperatures, lower operating pressures, higher efficiencies and cost reduction.

The catalyst usually reacts with the reactants to form a stable complex, and then the complex rearranges to yield products and regenerate the catalyst. Notice that the catalyst is regenerated at the end of the reaction which means that there is no net consumption of catalyst.

Global value demand for catalysts will grow 5% yearly through 2008 based on increased production of end use products and a shift toward higher value catalyst materials [2]. Catalysis is used in over 90% of the manufacturing process in the U.S. chemical industry, transforming raw chemical ingredients into petroleum products, synthetic rubber and plastics, food products, chemicals, and pharmaceuticals as well as controlling vehicle and industry emissions [3]. In economic terms, the U.S. chemical industry produces over 7,000 different products worth an estimated $375 billion per year [3, 4], and generates 10% of the national total exports. Worldwide, the manufacture of catalysts themselves, which come in forms as disparate as biological enzymes (specialized proteins) to fine metal powders to complex inorganic compounds called zeolites, is a $10 billion industry [4]. Improving catalysts and catalytic processes promise several important payoffs downstream in manufacturing. New catalysts that are more precisely designed than ones currently used can maximize desired products while minimizing byproducts. New catalysts will enable engineers to produce the same products using less expensive feed stocks or even to replace feed stocks based on nonrenewable and depletable resources, such as petroleum, with renewable ones, such as biomass. Another payoff, one that analysts predict will grow in relative importance in the coming years, will come from catalysis technologies that reduce pollution by obviating the need for organic solvents, eliminating troublesome byproducts that subsequently need

to be disposed of [2]. The key technical challenges of catalysis include: improved understanding of the relationships between catalyst structure and function; innovative techniques for increasing the reliability of manufacturing processes for catalysts; and innovative approaches to modeling, designing, and scaling catalytic reactors. This will lead to strategic business goals, which include: significantly reducing the manufacturing cost and environmental impacts of the commercial production of chemicals and plastics; significantly reducing the time and costs involved in the development both of new catalysts and of catalytic processes and products; and significantly accelerating the availability of computational tools for catalysis [4].

Today, almost 90% of all chemicals that are produced in industry worldwide have been in contact with a catalyst somewhere in their synthesis process. This number stresses the importance of the role of catalysis in the chemical industry. Without a catalyst, processes are less clean and many times impossible to perform. For example, the purpose of the vanadium phosphorous oxide (VPO) catalyst in the partial oxidation of *n*-butane to maleic anhydride (MA) is to achieve a higher product yield and less undesired byproduct [1]. The effects of using a modified VPO catalyst on this partial oxidation reaction are presented in detail in Chapters 3 and 4. Chapter 2 discusses the partial oxidation reaction to MA using *n*-butane and provides an insight on the tools used in this research.

In general, commercial catalysts are biphasic or heterogeneous being composed of a support material and one or more active phase components (metal or oxide). Support materials provide a porous framework of high surface area and active phase dispersion. This, in turn allows access to the active phase for the reactants and free exit for the

products from the catalyst particles. For example: in cobalt silica supported Fischer-Tropsch synthesis (FTS) catalysts, porous high surface area silica supports are used to disperse the active cobalt phase, thus, providing a high reaction surface area. The support must also have high mechanical and thermal stability in order to avoid surface area collapse during reaction or oxidative regeneration, which can induce the formation of hot spots. All of this must be achieved with the support being chemically resistant or interactive with the active site, cheap, abundant and not strategically limited. Usually, industrial supports are based on high surface area γ -Al_2O_3 or SiO_2, pure or doped with different elements in order to improve the mechanical and thermal stability of the support [5]. Under normal reaction conditions, γ-Al_2O_3 and silica are stable, but at temperatures between 700 and 1000^{o}C and in the presence of steam, a phase transformation occurs for γ-Al_2O_3, first to metastable δ and θ-Al_2O_3 leading to the formation of α-Al_2O_3 with a low surface area.

In addition, the chemical interactions between alumina and silica supports with the active phase can lead to the formation of additional compounds such as silicates, resulting in loss of the active phase and as a consequence, the catalytic activity [6]. The effects of such metal support interactions (MSI) between the active cobalt species and the silica support in FTS catalytic systems are investigated in Chapter 5.

Finally, during an oxidative regeneration, in order to burn off the carbonaceous residues deposited on the catalyst during the catalytic operation, hot spots or temperature runaway can occur resulting in the support sintering mainly due to the low thermal conductivity of alumina and silica. For these reasons, it is of interest to find new supports resistant to the sintering phenomenon. In Chapter 5 of this dissertation, an investigation

into what causes the cobalt or silica support sintering is presented. In addition, the cobalt metals used as active phases are generally precious metals or environmentally dangerous metals and should be recovered or reused to prepare new catalyst systems.

Thermodynamics limits the concentration of the desired product, and since the catalyst does not affect the thermodynamics of the reaction, it is important to develop the proper catalyst for a specific reaction. In addition, the reaction conditions (temperature, pressure and the reactant concentration) must be optimized to maximize the equilibrium concentration of the product(s). Once the reaction conditions of temperature, pressure and concentration have been found, but the rate is too slow for reasonable production, the search for a suitable catalyst begins [7]. It is not necessary that optimal catalysts have the highest reaction rates, usually catalysts with high activity exhibit very large mass and energy transfer rates which make them unstable to survive under feasible reaction conditions [7]. At present, there are no modeling or theoretical methods for determining an optimum catalytic system for a reaction scheme. However, a great deal of theoretical research is underway to do so. Therefore, catalysis remains both a science and an art, requiring much experimentation, insight, and determination.

1.2 Homogeneous and Heterogeneous Catalysts

There are two kinds of catalysts: homogeneous and heterogeneous catalysts. Homogeneous catalysts are those that are in the same phase (solid, liquid or gas) as the reactants. Examples include acids, bases, enzymes and in some cases solvents. A heterogeneous catalyst (usually a solid) is not in the same physical state as the reacting system. It ideally does not dissolve in the mixture, but is still able to promote a desired

reaction or a series of desired reactions. This work is focused on heterogeneous catalytic systems only. Heterogeneous and homogeneous catalysts are fundamentally different. A homogeneous catalyst dissolves into the gas phase or solution and acts uniformly throughout the liquid or gas mixture. On the other hand, heterogeneous catalysts do not dissolve. Instead, the reaction usually occurs on the surface of the solid catalyst structure [2]. Surface area is directly proportional to activity therefore researchers have always tried to compress as much surface area as possible in as little volume as possible. Heterogeneous catalysts are more important industrially, and are used extensively in chemical processing because they are easier to separate from the products of a reaction mixture than a homogeneous catalyst [2].

Figure 1.1 attempts to graphically explain the details of a heterogeneous reaction. One of the processes by which a catalyst increases the reaction rate is through lowering of the activation energy or energy barrier to the formation of products.

The typical mechanism for heterogeneous catalysis starts with incoming reacting compounds adsorbing onto the surface of a solid catalyst. This process must be energetically profitable or it will not occur. Figure 1.1 demonstrates that the chemisorbed species do lower their energy states when adsorbing onto the active surface. These adsorbed species are then rapidly and selectively transformed into adsorbed products. The products then desorb from the surface returning the solid catalyst back to its original state to recycle the process.

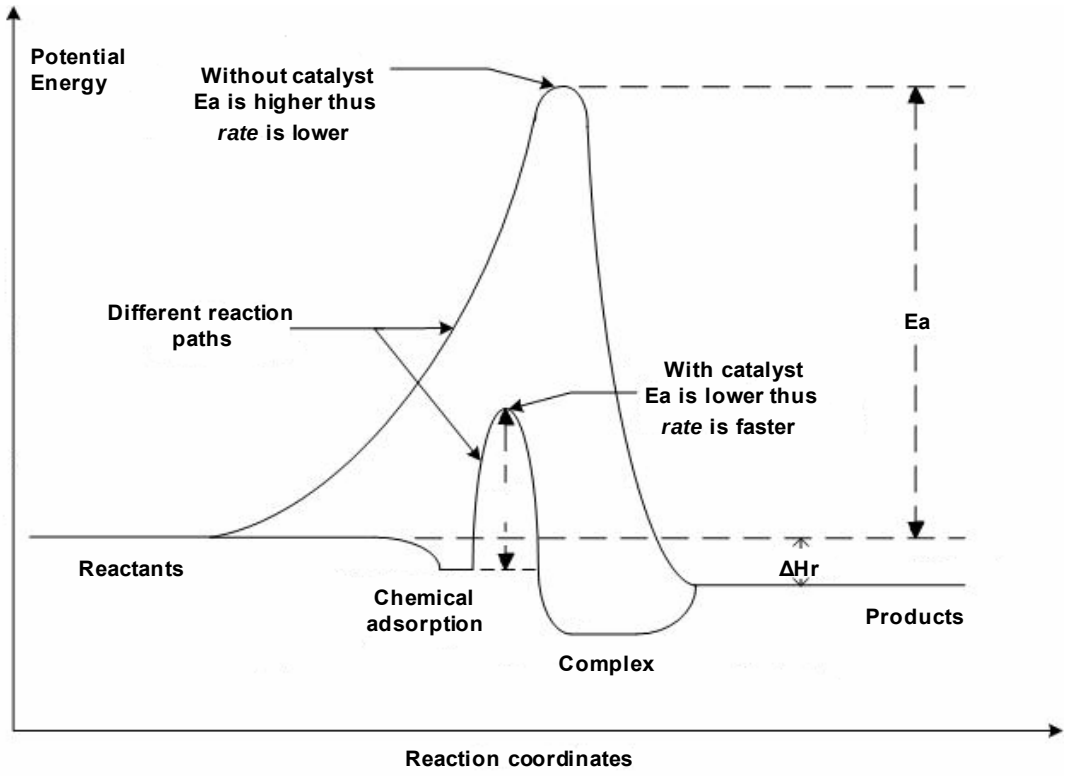

Figure 1.1: Catalytic potential energies versus reaction coordinate. Figure adapted from reference [8] for a heterogeneous reaction.

The idea that reactions are activated dates back to Faraday's work in 1834 [2]. He proposed that chemical reactions are not instantaneous because there was an electrical barrier to reaction. Over the years, many models were proposed to understand how elementary chemical reactions are activated. Most recent studies indicate that activation barriers are subtle. There are many different explanations why activation barriers arise during elementary chemical reactions, bonds need to stretch or distort during reaction and this requires energy. Another major cause of barriers to reactions is that in order to get molecules close enough to react, the molecules need to overcome Pauli repulsions (i.e.,

electron-electron repulsions). There are also a few special cases where the reactants need to be promoted into an excited state before a reaction can occur [2].

1.3 Surface Reaction Theory and Chemical Kinetics

Chemical kinetics is the study of reaction rates. More than 200 years ago, it was found that chemical reactions do have finite rates that could be measured and understood in principle. The rate of chemical reactions can be described at two levels: dynamics and kinetics. The detailed microscopic description of a chemical reaction in terms of the motion of the individual atoms taking part in the event is known as reaction dynamics. The molecule has a well defined energy; it may even start in a well defined quantum state. At this level, temperature has little meaning since it is a property of an ensemble, not individual molecules [7]. Kinetics is the description of the rate of reaction for a large number of molecules. However, the temperature may change in the course of the reaction [2, 7].

One of the most important concepts about surface reactions is that the reactions occur on distinct active surface sites. Active sites consist of a specific arrangement of metal atoms or electrically conducting entities. Specific arrangements of atoms or sites can greatly enhance the rate of the surface reaction. In a heterogeneous catalyst, the reaction takes place at the surface. In order to maximize the reaction rate, the active material is present as small particles. In turn, the different faces of the crystal have different energies [2,7].

Rates typically increase by factors of 10^3-10^9 with gas phase heterogeneous catalysts due to a higher molecule-molecule interaction. Solid gas or solid liquid phase

catalysts can often increase rates by factors of 10^{10}-10^{20} and there are cases where rate enhancements are as large as 10^{40} [2]. Clearly these effects are of great interest to be fully understood.

1.4 Adsorption Principles

The mechanism of a reaction occurring on a surface involves the adsorption of one or more of the reactants onto that surface. The properties of the now adsorbed species exhibit a change in electronic structure. The surface reaction occurs within this thin layer of adsorbed molecules, which can be disordered like a liquid or ordered like a solid [2].

Two types of adsorption exist: molecular adsorption, in which the molecule adsorbs intact and dissociative adsorption in which a bond breaks during the adsorption process. It is not unusual for a molecule to dissociate on adsorption since it is easy to break a bond during a surface reaction. The fact that bonds can easily break during adsorption is important since reactive species in the adsorbed layer can be formed, and that is why surface reactions are quite rapid and often referred to as the rate limiting step.

The surface and interface of a catalytic material is of particular importance since that is where the active region is and where unique material properties exist, the result of a better understood surface science theory leads to improved and better understood heterogeneous reaction processes.

1.5 Summary

Catalysts play a key role in nature and society since almost every reaction requires a catalytic material. Catalysts facilitate a chemical reaction by lowering the

energy barrier of the reaction pathway and thus increasing the reaction rate. Monitoring the events taking place in such materials is of crucial importance for the understanding of the reaction mechanisms occurring.

One of the most important concepts about surface reactions is that the reactions occur on active sites which are a specific arrangement of metal atoms or electrically conducting entities, in other cases, only a single bare metal atom or conducting site is sufficient. Specific arrangements of atoms or sites can greatly enhance the rate of a surface reaction. Surface reactions occur so rapidly that they are often the rate limiting step in chemical reactions. Heterogeneous catalytic reactions occur in three main steps: adsorption of reactants, surface reaction and desorption of products.

There are two types of adsorption: molecular adsorption, in which the molecule adsorbs intact on the active surface and dissociative adsorption in which a bond breaks during the adsorption process on the surface. It is not unusual for a molecule to dissociate on adsorption since it is easy to break a bond during a surface reaction. The fact that bonds can easily break during adsorption is very important since very reactive species in the adsorbed layer can be formed, and that is why surface reactions are often quite rapid.

There are two types of catalysts: homogeneous and heterogeneous, in which their main objective is to lower the activation barrier of a reaction, thus greatly increasing the rate of reaction without interfering with the thermodynamic equilibrium of that reaction. In this dissertation, the focus is only on heterogeneous catalytic systems. From a practical standpoint, one of the key roles of a catalyst is to lower the temperature where a reaction takes place.

High thermal budgets can greatly increase capital costs of production; safety due to explosion hazards at higher temperatures is also of great concern. In industry, over 90% of all chemical processes utilize catalytic systems with over 700 billion dollars of products were made with catalysts in the United States alone.

Chapter 2: Partial Oxidation of *n*-Butane to Maleic Anhydride

2.1 Introduction

MA as a raw chemical has many different applications and uses. The development in the chemical processes to produce MA ($C_4H_2O_3$) has been highly modified since the 1940s in terms of the reactant (benzene or *n*-butane) or the reactor (fluidized or fixed-bed), which will all be discussed later in Chapter 2.

MA biggest single use is in the manufacture of unsaturated poly ester (UPE) and alkyd resins. These resins are added to fiberglass reinforced plastics to make a strong, lightweight, and corrosion resistant material found in boats, autos, trucks, pipelines and electrical goods [9,10]. In a secondary capacity, MA is employed in the manufacture of lacquers, lubricating oil additives, and agricultural products [10]. The addition of MA to drying oils decreases the required drying time and improves the coating quality of lacquers. Agricultural products made from MA include herbicides, pesticides, and plant growth regulators. Furthermore, fumaric and malic acid are important MA derivatives used in paper sizing resins and as food and beverage acidulants [9].

MA supplies are barely adequate for market requirements due to planned and unplanned downtime arising from the complexity of the process and continued strong demand [10]. The motivation behind this work was to improve the selectivity and yield to MA by addressing some of the issues regarding the activity of the catalyst used in the *n*-

butane partial oxidation reaction. Some physical and chemical properties of MA are shown in Table 2.1.

Table 2.1: Selected physical and chemical properties of MA. Data taken from reference [10].

Physical state	White crystals
Melting point	52°C
Boiling point	202°C (decomposes)
Solubility in water	Slowly hydrolyzes
NFPA ratings	Health:3, Flammability:1, Reactivity:1

In MA production, a major advantage of using *n*-butane (a four carbon molecule) over benzene (formerly used as the main reactant) is that no carbon is lost in the reaction to form MA. Benzene, although easily oxidized to MA with high selectivity, is an inherently inefficient feedstock [1], since only four out of six carbon atoms are recovered in the product. For a theoretically achievable conversion of 100%, the yield from *n*-butane is a third greater than that from benzene. From a raw material viewpoint, the relatively low purchase price of *n*-butane is much more attractive than the expense of benzene [9,10].

Other influential factors that favor *n*-butane are safety, health, and the environment. Benzene is a known carcinogen and one of the chemicals most stringently regulated by the EPA. The flammability limit for *n*-butane is also lower than that for benzene, which is an additional safety advantage of the process. For all of these reasons, the fixed-bed process with *n*-butane has been the only MA route used commercially since 1985 in the United States [9-11].

n-Butane is a colorless, flammable gas. It is normally shipped as a liquefied gas under its own vapor pressure. Classified as an alkane, or paraffin, hydrogen saturates the carbon atoms via covalent single bonds. Alkanes such as *n*-butane are non polar, thus insoluble in polar solvents such as water. *n*-Butane is typically used in the manufacture of aviation fuels, organic chemicals, and as a heating fuel. Some physical properties of *n*-butane are shown in Table 2.2.

Table 2.2: Selected physical properties of *n*-butane. Data taken from reference [11].

Molecular weight	58.1 g/mol
Vapor pressure	16.3 psig @ 22°C
Boiling point	-0.5°C @1 atm
Specific gravity (gas)	2.1 @ 15°C and 1 atm
Density (liquid)	0.58 g/ml @ 20°C
Flammable limits in air	1.9-8.5 vol %
Specific heat (gas)	0.39 cal/g °C @ 15°C and 1 atm

2.2 Motivation

The production of MA has been in steady growth since the 1940s. It is estimated that MA and its two derivatives, maleic acid and fumaric acid, are produced with an annual worldwide capacity of over 10^6 tons [1]. MA and its two acid derivatives were first prepared in the 1830s, but it took about 100 years before commercial manufacturing took place. In 1933 the national aniline and chemical company (NACC) started a process for the production of MA based on benzene oxidation using a vanadium oxide catalyst,

but the first commercial production of MA from *n*-butane was not until 1974 by Monsanto [1,12].

The average annual demand growth is estimated to be about 4%. By the year 2004, total worldwide consumption was increased by about 30% as compared to 1998 [10]. The capacity to produce MA from *n*-butane in 2004 doubled since 1994 and half of the total MA produced worldwide is used in the production of the UPE resins. These numbers, together with the fact that the current yield to MA of the catalyst only amounts to about 58%, indicate that improvement of the process is of great economic and environmental interest [9-12].

2.3 Processes for the Production of MA From *n*-Butane

In general, there are three different types of processes for the production of MA from *n*-butane; the fixed-bed process, fluidized-bed, and the recirculating-solids process.

2.3.1 Fixed-Bed Reactor

The commercially predominant *n*-butane partial oxidation process employs a fixed-bed, but the other processes are also being developed. In the fixed-bed process, a low concentration of *n*-butane is passed over a catalyst in tubular reactors similar to the benzene process [9,10]. A fixed-bed reactor was used in this doctoral research for safety reasons and because they are easy to control and provide a simple way of collecting the product MA.

The reactor is operated at temperatures from 400-480°C, and the pressure is held at 0.3-0.4 MPa in order to force the exit gases downstream for scrubbing and purification.

As a result of the obstruction of the gas flow by the catalyst bodies, a pressure drop across the bed is exhibited. Therefore, pressure has to be applied to the inlet stream to ensure an adequate flow rate. The magnitude of the pressure drop depends on the flow rate, the length of the catalyst bed and the size of the catalyst particles [1]. Since the selective oxidation to MA is a highly exothermic process, hot spots of 350-500°C occur in the catalyst. Molten salts are used to dissipate the heat generated, in other cases of fixed-bed reactors; a facility to remove the reaction heat can be built. This can be done by splitting the bed into different sections and cooling the gas in between the sections, or by having a cooling gas or recirculating liquid flowing along the process tubes. Other ways of preventing hot spots from occurring inside the reactor would be to use larger catalyst bodies, a less active catalyst, or by dilution of the catalyst with an inert solid [1,10,12]. All of the above methodologies have some disadvantages ranging from excessive cost to greatly reduced reagent conversions. In a pilot plant, it has been shown that a fluidized sand bath reactor with a titanium tube can achieve good temperature control and help minimize hot spots [1].

Upon exiting the reactor, the vapor mixture is cooled to 150-160°C by heat exchangers. Partial condensers further cool the gas to around 55°C, the melting point of MA. The condensed MA must be removed as soon as possible to avoid prolonged contact with the water in the reaction gas. Exposure of liquid MA to water results in the undesired formation of maleic acid that further limits recovery if allowed to continue for an extended period of time. Thus, only a small amount of MA can be condensed from the reactor effluent due to the increased formation of water.

The MA that cannot be recovered is eventually washed out with water as maleic acid. Water scrubbing and subsequent dehydration of the maleic acid stream is required to purify and recover the remaining MA [9,11,12]. An alternative recovery method absorbs the MA from the reaction gas by organic solvents. The MA is then distilled from the high boiling solvent in a fractional distillation column [9].

Only low concentrations of *n*-butane can be used (<4%) in view of the explosion and flammability limits. Furthermore, the gases should be mixed and preheated. Sate of the art fixed-bed processes are currently offered from Huntsman, Pantochim and Scientific Design [1].

2.3.2 Fluidized-Bed Reactor

In a fluidized-bed process, reaction gases flow upward through a bed of catalyst particles. When the force of the gas flow on the catalyst bed is equal to the weight of the bed, the catalyst bed expands significantly and the catalyst particles are brought in continuous motion. This motion permits better heat transfer; consequently, hot spots are greatly reduced in the fluidized-bed. No heating or premixing is necessary in fluidized-bed reactors. Another advantage of using fluidized-bed reactors is that higher *n*-butane concentrations can be used due to a decreased explosion risk compared to the fixed-bed reactors.

For the fluidized-bed reactor, the size of the catalyst particles are of extreme importance, if they are very small, then they will be blown away. Large particles, on the other hand will allow high linear gas flow rates [1].The particle size for the fluidized-bed reactors usually range from 10-150 microns. Another major development is that the

catalyst used in the fluidized-bed reactor should exhibit a higher attrition resistance in order to withstand the fluidized-bed conditions (catalyst particles will continuously collide against each other and the internals of the reactor) [1,10].To solve this problem, various methods have been developed. Treating the bulk particles with an acid can lead to agglomerating the catalyst particles, the results proved that this method improved the resistance to attrition, but with a significant decrease in catalytic performance, probably because of diffusion limitation problems associated with those big agglomerated particles. Another method introduced to improve the attrition resistance, is to add silica to the catalyst particles as a colloidal silica sol which resulted in a decrease in the selectivity to MA [1,6,10].

DuPont has developed a new method of imparting attrition resistance of the bulk catalyst without loss of selectivity to MA. Instead of large quantities of colloidal silica, 5-10wt% of polysilicic acid which is spray dried in the presence of the catalyst precursor is used [1]. The result is a thin layer of porous silica at the periphery of the spray dried catalyst particles. This layer is very durable and porous to both reactants and products and does not lead to a detectable degradation of catalytic properties in microreactor experiments. However serious problems such as the expensive preparation and the long equilibrium time are issues not yet solved by this method [1,10].

2.3.3 Recirculating-Solids Process

The third type of process to produce MA from *n*-butane involves the partial oxidation of *n*-butane and then regenerating the catalyst in two separate reaction zones.

DuPont operates this process commercially. In the first stage; *n*-butane reacts with lattice oxygen in the catalyst, thus the selectivity to MA is increased, and since the reaction is carried out in the absence of O_2, MA is formed selectively since the catalyst is reduced [1,10]. Following this, MA is removed in a stripper. In the next stage, regeneration of the reduced catalyst is done with O_2. Another advantage of this process is the ability to control the catalyst oxidation state very well. However the reoxidation (regeneration) of the catalyst is far more difficult to control in a large scale plant.

2.4 Heat of the Reaction

When a reaction is so fast that the heat released or absorbed by the support/diluent cannot transport rapidly enough to keep the support/diluent close to the temperature of the bulk fluid, nonisothermal effects may be encountered. These include temperature variation within the support pellet or a temperature gradient between the pellet and the surrounding fluid. The latter is generally due to a stagnant layer or film between the surrounding flowing fluid and the support pellet. For exothermic reactions, heat is released and the support pellets are hotter than the surrounding fluid. However, for endothermic reactions the pellet is cooler than the surrounding fluid. Thus, harmful effects of thermal shock, sintering of the catalyst surface, or drop in selectivity can result.

The *n*-butane partial oxidation reaction to produce MA is highly exothermic. The main reaction products are carbon monoxide (CO) and carbon dioxide (CO_2). Stoichiometry and heat of reaction for the three principal reactions are shown in Table 2.3 [1]. It is obvious that carbon monoxide and carbon dioxide are the thermodynamically more favored products since they are in the lowest energy state. Only kinetic control by a

catalyst will enhance the formation of MA [1]. The reactor should be designed such that a sufficient heat transfer capability is met to ensure the dissipation of the heat generated by the oxidation reactions to carbon oxides. These unselective and very exothermic reactions are responsible for the hot spots frequently met in the MA production plants [1]. To solve the hot spots issue, the concept of adding a highly thermal conductive material was proposed. In this work, silicon carbide (SiC) was chosen as a diluent to be added to the catalyst used. The preparation of this mixture and its effects on the reaction are discussed in Chapters 3 and 4.

Table 2.3: *n*-Butane oxidation reactions and their respective heat of reaction. Notice that CO and CO_2 are thermodynamically more favored as products than the desired product MA [1].

Reaction	Heat of reaction
$C_4H_{10} + 3.5\ O_2 \rightarrow C_4H_2O_3 + 4\ H_2O$	ΔH=-1236 kJ/mole *n*-butane
$C_4H_{10} + 4.5\ O_2 \rightarrow 4\ CO + 5\ H_2O$	ΔH=-1521 kJ/mole *n*-butane
$C_4H_{10} + 6.5\ O_2 \rightarrow 4\ CO_2 + 5\ H_2O$	ΔH=-2656 kJ/mole *n*-butane

2.5 Verifying MA Using FTIR in the ATR Mode

The attenuated total reflectance (ATR) mode is designed to analyze liquid and semi liquid samples, pastes, gels and soft powders [13]. The accessory comes with a trough and a flat crystal plate to accommodate all types of samples. Usually called HATR, or horizontal ATR, the accessory is carefully designed to provide excellent results with minimum effort. It can be easily placed in the sample compartment and locked into position. The single reflection ATR has become quite a popular method for

analyzing samples. One of the reasons for this is that the ATR method has reduced the sampling area (smaller sample volume/size requirement), ease of cleaning and the introduction of more rigid crystals capable of withstanding higher pressures. For these reasons, ATR has gained the reputation of a "universal" sampling device [13]. Figure 2.1 shows the ATR accessory and crystal, adapted from Pike Technologies.

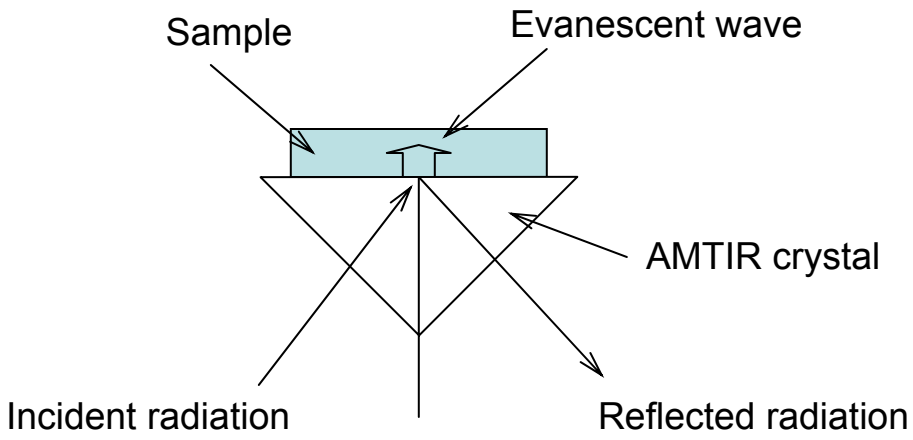

Figure 2.1: A schematic of the AMTIR crystal. The sample should be in intimate contact with the crystal. ATR crystal schematic adapted from Pike Technologies [13].

The AMTIR crystal is produced as a glass from selenium, arsenic and germanium, and is very toxic during manufacturing, however the brittle nature of this material and its total insolubility in water makes it safe for use as an internal reflectance element [13]. The ATR range for the AMTIR crystal is between 11000-650 cm^{-1} wavenumbers, its operating pH range is from 1-9, hence alkalies are considered harmful to its surface. The surface hardness is quite low at 170 kg/mm^2 compared, for example, to diamond 5700 kg/mm^2. This type of crystal can be used to detect solids powders to gel/paste to liquids [13]. The ATR crystal was used to analyze the MA product and compare it to commercial

samples to ensure product purity. Also, this technique was used to characterize all catalyst samples studied at three different stages: after preparation, after calcination and after reaction. ATR correction was done using Digilab Win IR Pro version 3.4 software.

Figure 2.2 shows the spectrum of MA obtained using the AMTIR crystal with FTIR resolution equal to 4 cm^{-1} and number of scans equal to 128.

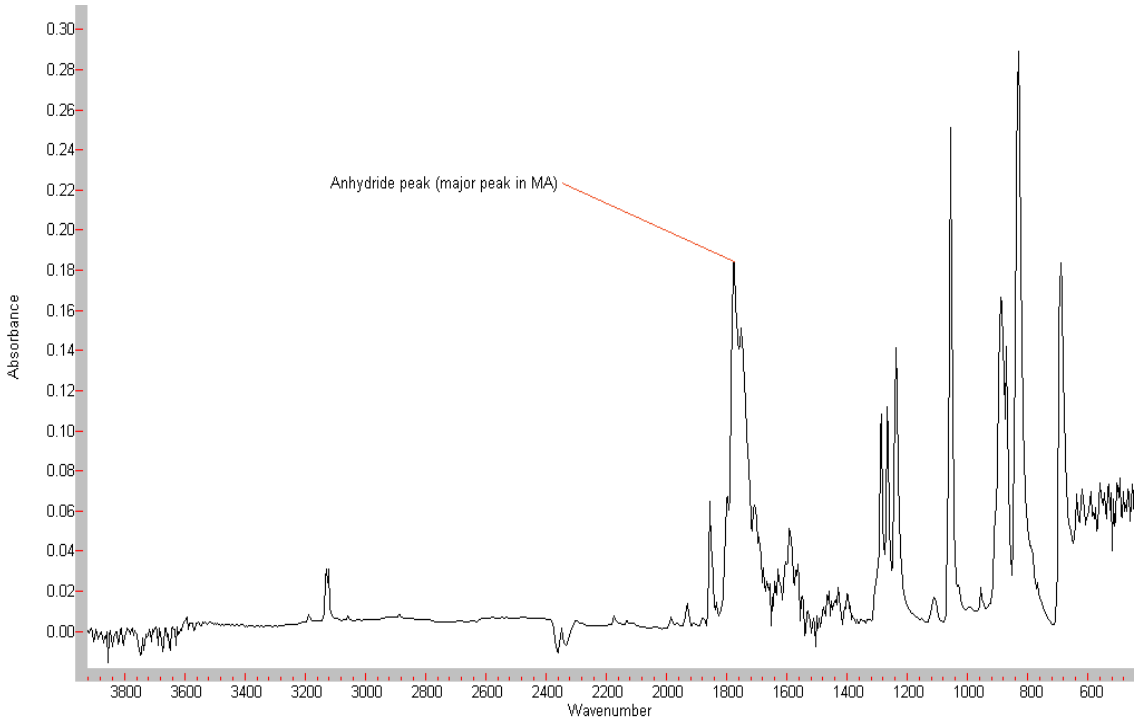

Figure 2.2: Solid maleic anhydride FTIR-ATR spectrum.

2.6 Verifying MA Using FTIR in the Gas-Cell Mode

Gas-cell verification (compound qualitative analysis) was performed and verified in every single experiment. The method was to compare the experimental FTIR spectra to the literature reference spectra of the same compound. A problem with using computer software for qualitative purposes (compound identification) is that the hit quality index (HQI) gives more than one compound result (the number of compound hits returned is

large). In other words, one may find that the highest rated hit or the first hit in the hit list is not always the best result; also, sometimes the percentage matching index would not be too high as to what is expected.

For example, Figure 2.3 represents experimental FTIR *n*-butane spectrum in the vapor phase. This spectrum matches *n*-butane FTIR spectra obtained from the literature (spectra online or NIST) [14] in the vapor phase. The spectrum is in units of absorbance versus wavenumber with a 4 cm^{-1} resolution. Figure 2.4 shows FTIR MA spectrum in the vapor phase which also shows *n*-butane peaks and CO_x peaks at 420°C (reaction temperature). This spectrum also matches for example, environmental protection agency (EPA) [14] vapor phase maleic anhydride IR spectrum obtained from spectra online. The peaks in the spectra represent the IR stretching and bending vibrations of the organic groups that *n*-butane and MA are composed of.

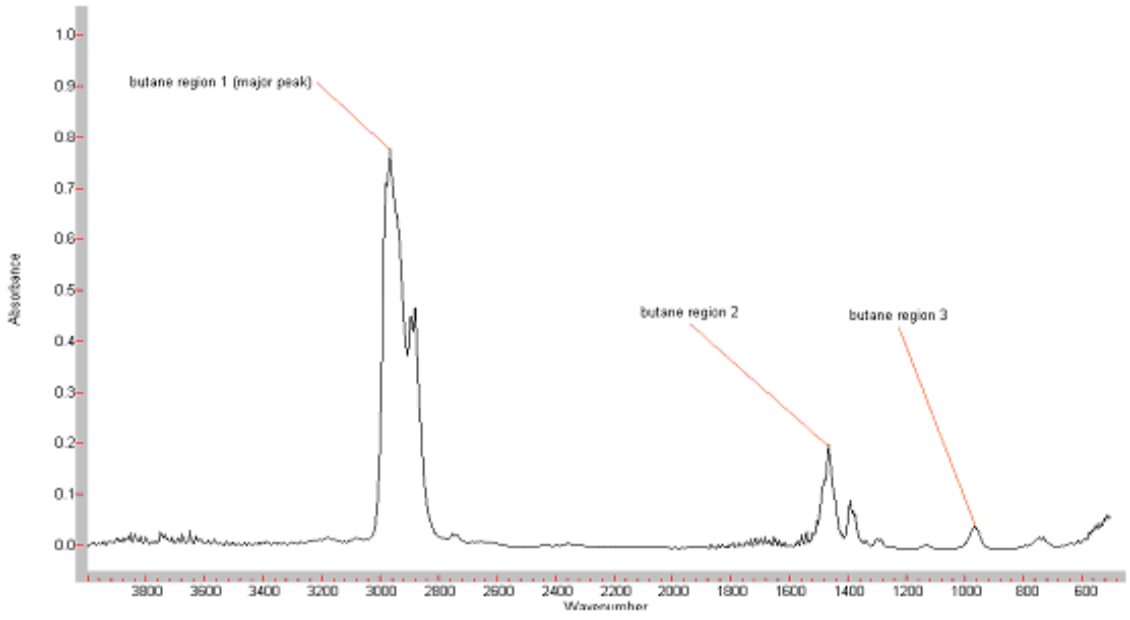

Figure 2.3: Experimental *n*-butane vapor FTIR spectrum.

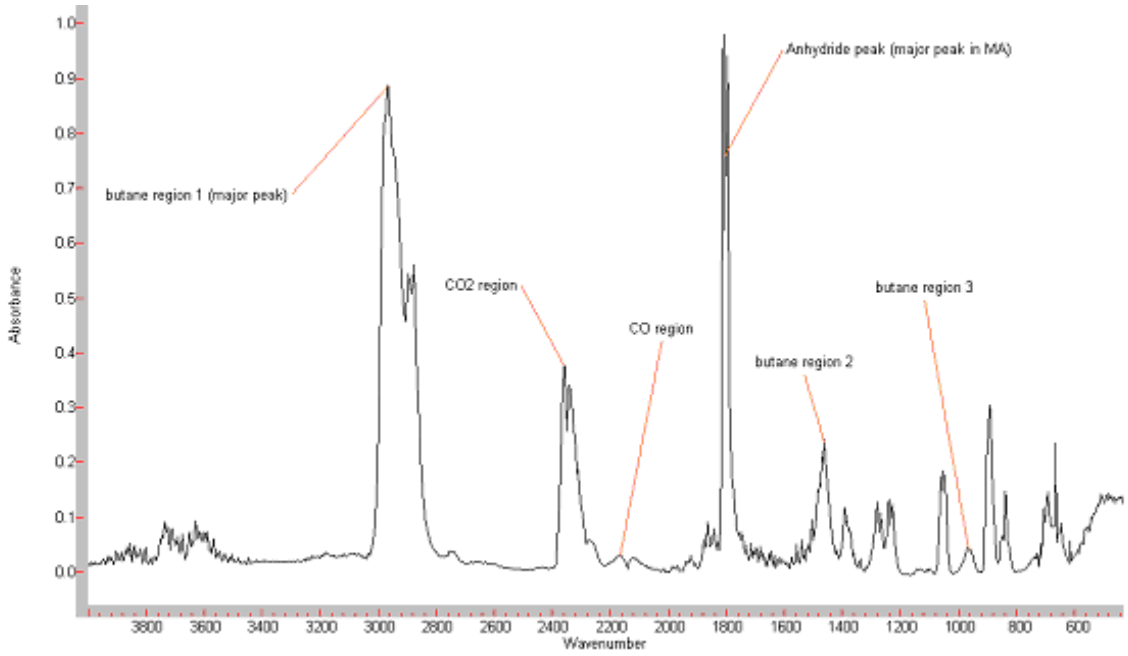

Figure 2.4: Experimental vapor MA FTIR spectrum. Notice the other reaction products (CO and CO_2) and the reactant *n*-butane IR characteristic peaks.

2.7 Data Analysis Technique

The procedure to interpret a spectrum was performed as follows: After collecting the spectrum, unique peaks (specifically those above 1500 wavenumbers) were examined. Weak peaks may be overtones or combination bands of lower frequencies or impurities. Weak peaks are used to support possible functional group identification. The peaks are correlated either using the system software or in a reference text or website to see if they match the selected peaks or not. The results are reviewed to include or exclude functional groups. Steps 1 and 2 are repeated for other peaks observed in the spectrum.

2.8 Data Analysis Software

Two software packages were used in these experiments: Digilab Win IR Pro software used for FTIR conversion calculations and the Know-It-All informatics systems software for quantitative analysis and qualitative peak identification. For *n*-butane conversion calculations, these steps were followed: data is collected using the FTIR and the resultant spectra are converted into absorbance versus wavenumber, then they are ratioed against a reference spectrum taken at initial conditions (at the beginning of the experiment). *n*-Butane peaks are identified and the areas under these peaks are calculated. These areas can be used to represent species concentration. Conversion rates are calculated by subtracting the outlet area (concentration) at specific reaction temperature from the inlet area (concentration) at initial conditions (room temperature) and the resultant area is divided by the inlet area (concentration), again at initial room temperature conditions. Conversion is plotted versus temperature. The gas-cell FTIR resolution through out the experiments was 0.25 cm^{-1} and 128 scans while the resolution used for the FTIR in the ATR mode experiments was 4.0 cm^{-1}, and 128 scans.

2.9 Summary

MA as a raw chemical has many different applications and uses. The development in the chemical processes to produce MA ($C_4H_2O_3$) went through a lot of modification since the 1940s in terms of the reactant (benzene or *n*-butane) or the reactor (fluidized or fixed-bed). The *n*-butane partial oxidation reaction to produce MA is highly exothermic. The main reaction products, other than MA, are carbon monoxide (CO) and carbon dioxide (CO_2). Careful control of the reaction ensures partial oxidation rather than

complete oxidation of the *n*-butane reactant. The three different types of processes for the production of MA from *n*-butane are: The fixed-bed process, the fluidized-bed and the recirculating-solids processes.

FTIR is a powerful instrument for both qualitative (compound identification) and quantitative (amount of concentration present) analysis. In this work, the FTIR was used to analyze the gas effluent from the catalytic reactor. Conversion of *n*-butane was calculated after obtaining the absorbance spectra from the experiments, where eventually conversions versus temperature plots were generated. FTIR was also used in the ATR mode, equipped with an AMTIR crystal accessory for compound identification purposes. Some disadvantages might occur while using FTIR for qualitative analysis, such as overlapping peaks and low signal/noise ratios. Despite these possible disadvantages, it was decided that IR analysis was the best means available for this work. Therefore, most of the data collected was gathered using this instrument.

Chapter 3: Vanadium Phosphorous Oxide (VPO) Catalyst

3.1 The VPO Catalyst

Vanadium phosphorus oxide (VPO), also known as the vanadyl pyrophosphate catalyst has been applied commercially in the selective oxidation of *n*-butane to MA since 1974. Specifically, VPO is a compound containing the elements vanadium, phosphorous and oxygen, which is catalytically active in exothermic reactions such as hydrocarbon oxidation [15]. The currently applied bulk VPO catalyst has several problems, such as poor reproduction of the synthesis, high production costs, long and difficult activation procedures and deactivation under reaction conditions. Furthermore, the real nature of the active sites in the VPO catalyst is still unknown and therefore a valuable subject of further study.

In this dissertation, the goal is to develop an in-house synthesized VPO catalyst in order to overcome the sited drawbacks of bulk VPO. This prepared catalyst was designed to show superior characteristics over bulk VPO, with a cheap and reproducible preparation procedure, a short activation process and a high mechanical strength. Ruitenbeek [1] has shown that silica (SiO_2) and titania (TiO_2) supported VPO catalysts show interesting, and in some cases enhanced properties for the *n*-butane partial oxidation to MA. However, a newly developed titania supported VPO catalyst did not show reasonable catalytic performance (yield<20%), but in general, the titania supported

VPO catalysts are much more active than their silica counterparts. However silica supported VPO catalysts are more selective, resulting in better overall yields (>20%) [1]. Ruitenbeek from Utrecht University has prepared several silica supported VPO catalysts and showed a catalytic yield to MA of 26% (7.5wt% V, P/V atomic ratio=1.1).

The ratio of phosphorus to vanadium determines the activity of the catalyst, and, in turn, the life. Catalyst activity is greater at high phosphorus to vanadium ratios, but the catalyst life is sacrificed as the activity increases. A phosphorus to vanadium atomic ratio of 1.1-1.2 in the catalyst appears to provide the optimal balance between activity and catalyst life [1,16].

Selectivity to produce MA is the extent to which the catalyst accelerates the reaction to form this desired product. Using VPO catalyst favors the partial oxidation over the complete oxidation of *n*-butane according to the following reactions:

$$C_4H_{10} + 3.5O_2 \rightarrow C_4H_2O_3 + 4H_2O \quad (3.1)$$

$$C_4H_{10} + 6.5O_2 \rightarrow 4CO_2 + 5H_2O \quad (3.2)$$

The VPO catalyst provides the proper mechanism with lower activation energy for faster rate towards the desired first reaction shown above. Optimum temperature was found to be around 420°C, the optimum pressure was between 1-5 bar [10].

Much effort has been devoted to the development of a diluent promoted VPO catalyst in this work. Promoted VPO catalysts have superior characteristics over bulk VPO catalysts, such as reproducible preparation procedure, a large number of active sites per unit surface area, a short activation period and high mechanical strength. The development of diluent mixed VPO catalyst particles is of particular importance especially for the fluidized-bed reactor process. Furthermore the application of a well

dispersed VPO phase with a diluent material opens new opportunities for characterization, since no interfering bulk contributions are expected in the various analytical characterization methods.

Preparation of the catalyst begins by mixing vanadium pentoxide (V_2O_5) with nearly anhydrous phosphoric acid and an organic solvent. Next, the mixture is heated and the organic solvent is removed by volatilization. The product is dried and calcined to yield the catalyst precursor, which is then pelletized or formed into spheres. Finally, the catalyst is loaded into the reactor where it is activated under carefully controlled conditions. According to Wen *et al.* [17], acid concentration and reaction temperature exhibit strong effects on the conversion of *n*-butane, selectivity and yield to MA where other factors like reaction time and solvent/solute ratio are minor factors influencing the behavior of the catalyst.

3.1.1 Catalyst Preparation

The catalyst can be prepared by the reduction of vanadium oxide (V_2O_5) with a V^{+5} valence number to a V^{+4}- $V^{+4.6}$ oxidation state in an organic or aqueous medium. Organic medium (preferably substantially anhydrous alcohol +95% having 1-10 carbon atoms, 1-3 hydroxyl groups) like *n*-propyl, isopropyl, *n*-butyl, isobutyl and benzyl alcohols where the aqueous medium includes, for example, concentrated HCl or H_3PO_4 [18]. The possible reaction route is as follows:

$$V_2O_5 + H_3PO_4 \rightarrow VOHPO_4 0.5H_2O \rightarrow (VO)_2P_2O_7 \qquad (3.3)$$

The first product is the vanadyl hydrogen phosphate (catalyst precursor), which upon careful and controlled heating through the activation process yields the final VPO

catalyst; (vanadyl pyrophosphate) phase. One of the important features of the VPO catalyst is the surface composition which is still debated in the literature, but it is known that the vanadyl pyrophosphate is the main component of this catalyst. About 63% in the bulk VPO based on Ruitenbeek electron spin resonance spectroscopy (ESR) results.

The use of an organic medium yields an increase in surface area of the precursor. This increase in surface area is carried over to the resulting vanadyl pyrophosphate phase and is desirable because it increases the activity of the catalyst [19]. An additional effect of the use of an organic medium in the catalyst preparation is the creation of more defects in the crystalline lattice when compared to a catalyst made by the aqueous route. These defects result in the creation of strong Lewis acid sites on the surface of the catalyst and are thought to persist in the active phase of the catalyst [19].

The procedure to prepare the unpromoted VPO catalyst in this work consists of the following steps and is based on Bither work [18]: A 3-neck 1 liter flask equipped with a stirrer, reflux condenser and a heating mantle is charged with 50 g of vanadium oxide (V_2O_5), 500ml of isobutyl alcohol and 50ml of benzyl alcohol (Alfa Aesar). This mixture was heated at reflux for 2h to bring about the reduction of (V_2O_5) according to the following reactions:

$$C_4H_{10}O + V_2O_5 \rightarrow C_4H_{10}O + V_2O_4 + H_2O \quad (3.4)$$

$$C_7H_8O + V_2O_5 \rightarrow C_7H_8O + V_2O_4 + H_2O \quad (3.5)$$

Following the reduction step in which tetravalent vanadium is formed; 73 g of 85% ortho-phosphoric acid (σ-H_3PO_4) was added drop-wise while stirring. The initial dark green mixture is heated at reflux overnight (typically 15h) to give light blue slurry according to the following reaction:

$$2H_3PO_4 + V_2O_5 \rightarrow 2(VO)HPO_4 0.5H_2O + H_2O \quad (3.6)$$

Following cooling, the solid product is filtered and air dried, first at 120°C, and then at 200°C. The resultant gray-green solid is the VPO precursor. This VPO precursor is washed with boiling water to remove undesired oxide phases like the γ-vanadyl orthophosphate and $VO(H_2PO_4)_2$.

The catalyst precursor is pelleted (1-2mm) for firing and charged into a 0.25" diameter quartz tube mounted vertically in an electrically heated furnace to begin the activation process of the catalyst.

A 45cm^3/min stream of air is passed over the catalyst bed for 2h while ramping (3°C/min) to 380°C. This was maintained for 8h. In this step the residual organic solvent in the pellets was removed.

n-Butane at about 1.64 vol% is introduced into the air stream and the total flow rate increased to about 135cm^3/min. The temperature is raised to about 480°C at a rate of 3ºC/min and was held for 16h.

The temperature is then dropped to 275°C to avoid uncontrolled hot spots in the catalyst, and the flow of 1.64vol% *n*-butane in air was maintained during this process with a space velocity between 50-500h^{-1}. Solid VPO catalyst particles which have been working for longer periods of time like in industrial plants are usually referred to as an equilibrated catalyst particles [20]. The activation process which takes approximately 30h to complete is shown in Figure 3.1. The temperature was slowly raised at a rate of 3°C/min to about 400-420°C (reaction temperature) and the partial oxidation of *n*-butane to MA was carried out under these conditions for 20h.

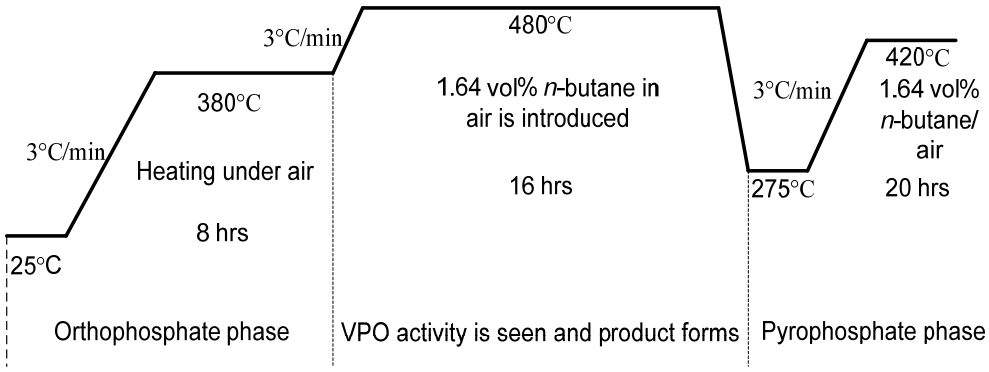

Figure 3.1: Activation by *n*-butane process for the prepared VPO. The process is divided into three sections: heating under air, introducing *n*-butane and starting the partial oxidation of *n*-butane to MA at atmospheric pressure.

At present, there are two types of patented technologies for the activation of the catalyst precursor into the active phase [19]. In the first procedure, the vanadyl hydrogen phosphate is heated to 415°C in a controlled environment with combinations of nitrogen, air and steam. The second procedure consists of slow heating of the vanadyl hydrogen phosphate in air with gradual introduction of *n*-butane to the gas stream. The possibility of inhomogeneities in the activated catalyst exists due to nonuniformities in reactor flow distribution. The procedure completed in a controlled environment can solve this problem. In this work, the activation procedure was done using *n*-butane after which the final catalyst product was sturdy, uniformly light brown pellets.

The VPO catalyst sample loses about 12% of its weight during the activation procedure as verified by thermo gravimetric analysis (TGA) done on an orthophosphate sample shown in Figure 3.2. The loss is attributed to the vaporization of isobutyl alcohol, water and benzyl alcohol.

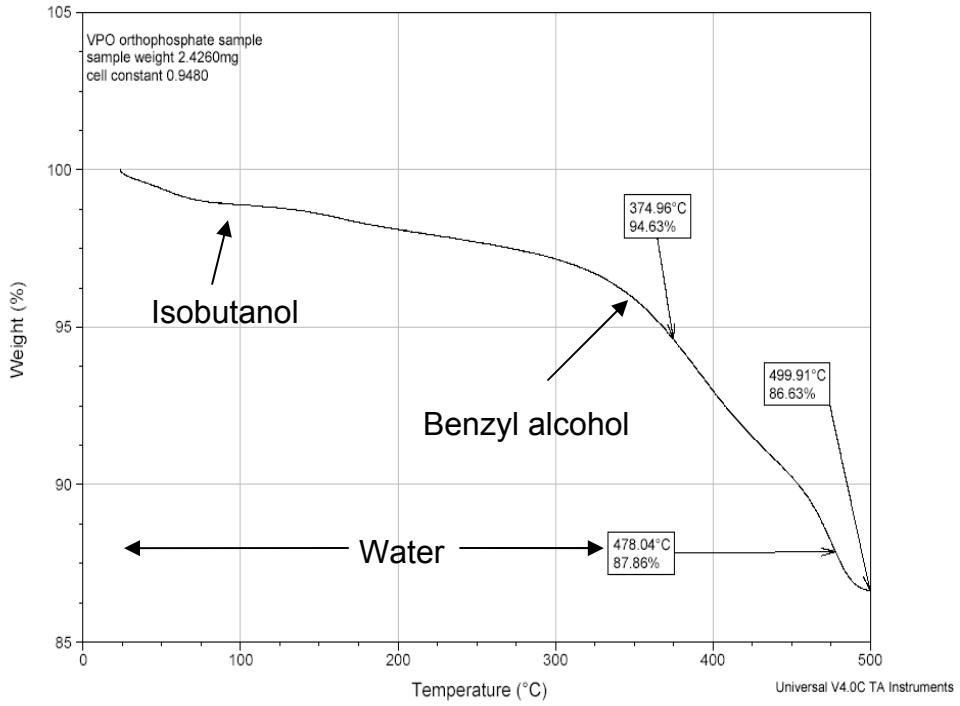

Figure 3.2: TGA analysis showing weight loss of the orthophosphate phase. The loss occurs during catalyst *n*-butane activation process.

3.1.2 Diluent Mixed VPO Catalyst

A catalyst comprising VPO combined with a thermally conductive material is particularly useful for such a highly exothermic reaction. The precursor solutions can be impregnated, mixed or spin coated on almost any kind of support.

The thermally conductive material has to have a thermal conductivity of at least 1W/m.K [15]. Typically the conductive material is selected from the group consisting of SiN, BN or P treated nitride. In this work, SiC was used as a diluent material. Both α and β-SiC were used since their thermal conductivity values range from 3.7-4.9 W/cm.°C for the α type and 3.6 for the β type SiC [3]. β-SiC mixed with VPO has been previously

reported in literature [21]. The focus of this work is to study the effects of mixing α-SiC commercial powder with the bulk synthesized VPO catalyst.

3.1.2.1 Silicon Carbide Mixed VPO

SiC exhibits high chemical and thermal stability [15]. Its melting point exceeds 3100°C. SiC also maintains its physical structure in extreme environments and has high mechanical strength making it resistant to attrition. These properties are very attractive for heterogeneous catalyst supports. Since one of the major difficulties for the production of MA by the partial oxidation of *n*-butane is the highly exothermic behavior of the reaction that leads to the formation of hot spots, the concept of introducing the highly thermal conductive SiC was proposed. In this work, size (2μm) silicon carbide (α-SiC) crystalline commercial powder was used as a diluent to modify the in-house prepared VPO catalyst as means to extract the heat generated from this reaction. In addition, the α-SiC utilized has a relatively high surface area ($10.2 m^2/g$). Ledoux *et al.* have shown a significant gain in MA yield using heat conductive supports such as β-SiC, Si_3N_4 and BN particles. The β-SiC support protected the VPO catalyst against high temperature excursions [21].

α-SiC was added to the vanadium (+4) hydrogen phosphate hemi hydrate suspension (precursor) under vigorous agitation in an isobutanol medium at moderated temperatures of 80-120°C for 1h. The resulting mixture was then placed in a furnace at 250°C for an additional 2h to dry in air. This process yields vanadium phosphorous oxide precursor mixed with α-SiC. The α-SiC/VPO mixture was then activated by the *n*-butane procedure.

3.1.3 Metal Ion Promoted VPO

The effect of a metal ion promoter in this system is to change the structural characteristics of the catalyst phases by providing extra active surface area (sites) [22]. It also plays a role in having an effect on the adsorption of oxygen and its diffusion within the lattice, by which a nonselective route of *n*-butane oxidation is suppressed [22].

Palladium (Pd) has a melting point of 1555°C and has two oxidation states +3 and +2. Pd is the least dense and has the lowest melting point of the entire platinum group of metals. At room temperature, Pd has the unusual property of absorbing up to 900 times its own volume of hydrogen gas. Finely divided Pd is a good catalyst and is used for hydrogenation and dehydrogenation reactions [23]. Pd addition to VPO catalyst and its effect on the catalyst performance is also lacking in literature. According to Volta [24], the defects in the crystalline structure of the vanadyl pyrophosphate create strain in the V-O-P bonds leading to the generation of very strong Lewis sites. This polarization of the V-O-P bonds could be induced by the presence of some promoters especially Co [24].

Pd also affects the adsorption of oxygen and its diffusion within the lattice to suppress a nonselective route of *n*-butane oxidation [25]. The mechanism is based on providing active sites on which *n*-butane will react with lattice oxygen in the appropriate configuration to produce MA, thus improving the selectivity and yield to MA. Combinations of (Pd) promoted VPO, and Pd/α-SiC/VPO modified catalysts were investigated in this dissertation.

The procedure to prepare the catalyst is quite the same as described in Section 3.1.1. Promotion with Pd was done using palladium nitrate (Pd $(NO_3)_2$) (Alfa Aesar) salt. The salt was dissolved in an appropriate volume of deionized water and added drop-wise

to dry VPO precursor particles at room temperature under vigorous agitation for 1h. The temperature was then ramped slowly (1°C/min) to 75°C and held for an additional 1h. The product was then left to dry at 100°C for 2h. The loading range was from 0.5-1.5wt% Pd in VPO.

3.1.4 Kinetic Investigation

For systematic kinetic study of the *n*-butane oxidation to MA, a commercial VPO catalyst was used. The ranges of investigated kinetic variables include total pressure and *n*-butane concentration. Experiments with the addition of the main reaction products: H_2O, CO, CO_2, MA, acrylic acid and acetic acid to the test reactor feed are also performed in order to assess their role in the reaction network [26]. Figure 3.3 shows an example adapted from reference [26] of an assumed reaction network for kinetic analysis.

These kinetic investigations have yielded good results such as the one recently reported by Xue *et al.*, who claimed drastic increments of MA selectivity upon feeding *n*-butane/air mixtures rich in CO_2 over a DuPont VPO catalyst [26].

The most significant products of the partial oxidation reaction to MA are acrylic acid and acetic acid in addition to the CO_x gases. In fact their concentration in the effluent stream from the fixed-bed reactor is relevant to the design of the downstream separation and purification sections of the plant [26].

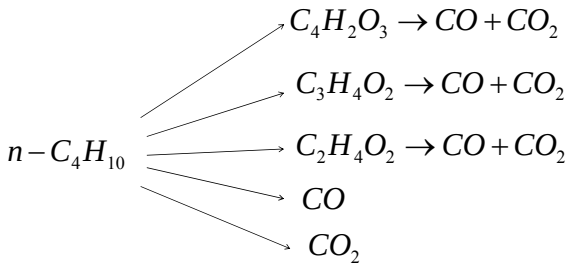

Figure 3.3: *n*-Butane reaction network assumed for kinetic analysis. The first pathway shown is the desired reaction that forms MA, other products formed includes acrylic acid, acetic acid, CO and CO_2.

3.2 Effect of Lattice Oxygen on the Reaction

The lattice oxygen in the VPO catalyst can be used instead of molecular oxygen to participate in *n*-butane oxidation. The point is that since the reaction occurs between *n*-butane and lattice oxygen in the absence of gas phase oxygen, complete oxidation can be prevented and the selectivity to MA can be improved dramatically so that the utilization of raw material is increased and environmental pollution reduced [27]. Since seven oxygen atoms are required to convert an *n*-butane molecule to MA, studies have shown that only about four surface layers of lattice oxygen are involved in the reaction, thus there is a need for a larger amount of VPO [27]. CeO_2, because of its high oxygen storage capacity, has been used as a promoter in which it was reported that it increased the conversion of *n*-butane, while Fe_2O_3 promoted VPO increased the selectivity to MA [27].

However, this lattice oxygen is very easily lost in the fresh catalyst due to defects in the pyrophosphate structure [20].

3.3 VPO Phases

Vanadium, phosphorous and oxygen catalysts can form a large number of distinct compounds, e.g., α-$VOPO_4$, γ-$VOPO_4$, $VOHPO_4$, $VO(PO_3)_2$ and $VO(H_2PO_4)_2$. However, the most active catalytic phase is believed to be $(VO)_2P_2O_7$ [15], as shown in Figure 3.4 [28], which is also the predominant oxide phase in VPO catalyst. Nevertheless, VPO catalysts are usually referred to as "mixed oxides" in recognition of the probable presence of other oxide phases [15]. The main phases are usually the V^{+4} phase $(VO)_2P_2O_7$, and secondly the V^{+5} phase δ-$VOPO_4$ [17].

The experimental conditions (temperature, composition of the flow, contact time and time of activation) will determine the nature of the active sites. The presence of the residual V^{+5} entities on the V^{+4} matrix [20] in a none equilibrated VPO catalyst (disordered $(VO)_2P_2O_7$, V^{+4} phase with some residual V^{+5} entities) has favored the *n*-butane transformation to MA. But the optimal V^{+5}/V^{+4} ratio is still not known [20].

The average valence state of vanadium giving maximum yield of MA is slightly above 4, thus the amount of the V^{+4} phase (vanadyl pyrophosphate) determines the dehydrogenation extent of *n*-butane. On the other hand, when the relative amount of the V^{+5} phase increases, the *n*-butane conversion still continues to increase, but the selectivity to MA decreases. In other words, when the relative amount of the V^{+5} phase reaches a given quantity, the oxidation proceeds further to carbon oxides [17].

Ruitenbeek has found that the structure of the VPO catalyst is affected by the adsorbed reactants and products and the reaction temperature. The presence of the V-O-P bond seems to be a prerequisite for optimal catalytic selectivity to MA. So weakening that bond (V-O bond) means an increase in activity and selectivity and that is the goal behind adding a promoter (promoters like P weakens that bond) [22].

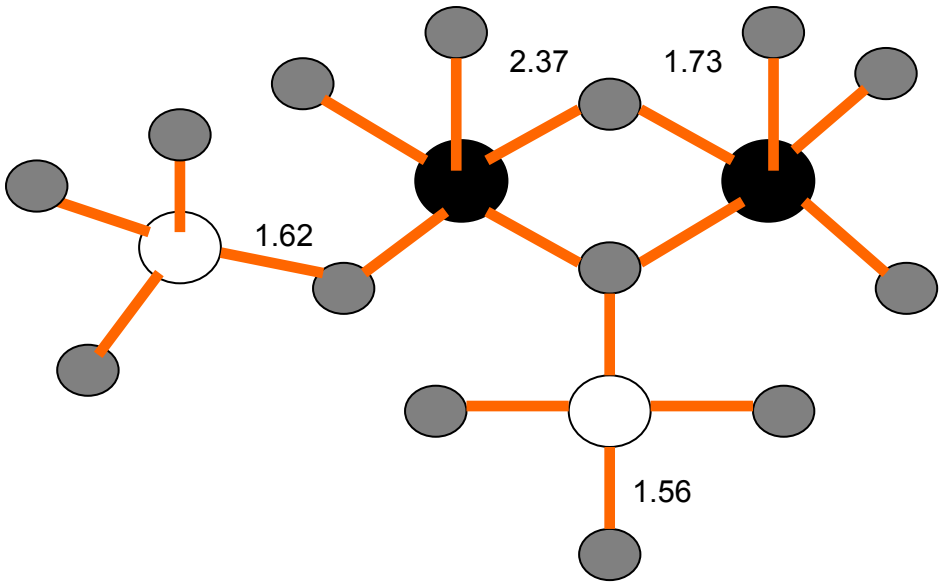

Figure 3.4: Geometrical structure of the pyrophosphate phase. Two local sections at the surface are emphasized. P centers are in white, V centers are in black O in gray. All distances are in A°. The schematic is adapted from reference [28].

3.4 Reaction Mechanism

The mechanism of the partial oxidation reaction is defined as the sequence of elementary reactions that occur at appreciable rates when the oxygen and *n*-butane

reactants come together and react to form products. The mechanism represents the principal route from reactants to products; of course other reactions can occur.

A reaction pathway from *n*-butane to MA obtained from reference [16] in which mass spectroscopy (MS) was the main instrument of analysis and verification proceeds via the intermediate products: *n*-butene, butadiene, crotonaldehyde, dihydrofuran, furan and crotonlactone as shown in Figure 3.5. This mechanism is similar to the proposed Mars-Van-Krevelen mechanism [1] which is applied when VPO is supported on silica.

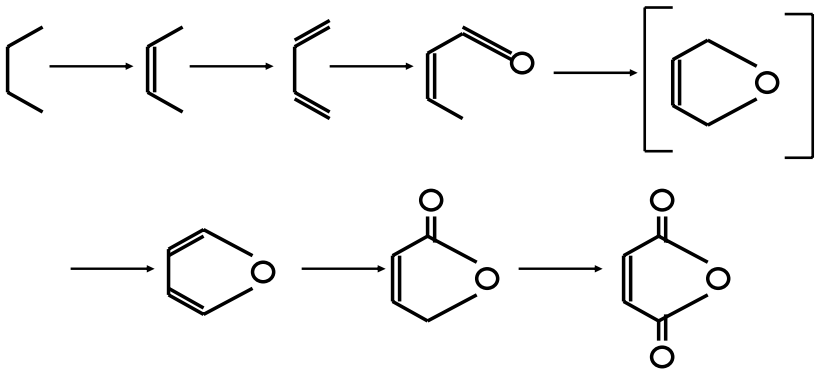

Figure 3.5: *n*-Butane to MA reaction pathway. A total of eight hydrogen atoms are removed, and three oxygen atoms are introduced into the C_4 molecule. Schematic is adapted from reference [16].

Results also show that side products like phathalic anhydride, acrylic acid and acetic acid might be formed by oxidation of some of the above intermediates like butadiene [16]. The rate of desorption of the olefinic intermediates and furan was observed to be low as compared to the rate of their transformation to MA, which implies that MA should be rapidly desorbed to avoid its combustion [20].

3.5 Summary

Vanadyl pyrophosphate exhibits a unique ability to activate and selectively oxidize *n*-butane to MA. It is generally agreed upon that the best catalyst precursor is vanadium phosphate hemihydrate obtained by the reduction of pentavalent vanadium compounds with organic reductive agents, such as a mixture of isobutanol and benzyl alcohol. The precursor is converted to $(VO)_2P_2O_7$ during activation.

The VPO catalyst has a low thermal conductivity. With the high temperatures of the reaction used in the vapor phase partial oxidation of *n*-butane to MA and the large amounts of heat released in this exothermic reaction, the catalyst deteriorates in activity over a short period of time. The nonisothermal operating conditions can also lead to decreased productivity through severe hot spotting in the catalyst bed. The need to properly dissipate the heat generated in this reaction is of crucial importance; hence the concept to mix the VPO catalyst with a high heat conductive material such as SiC was introduced.

The high thermal conductivity of SiC may turn out to facilitate new process designs for highly exothermic or endothermic reactions in which heat transfer must be carefully controlled. Furthermore, because the SiC can be formed from carbon in any shape or porosity due to the "shape memory effect", a catalyst with good activity and selectivity in a particular reaction can be formed closer to a commercially acceptable form without an extensive development project [10].

A VPO catalyst that has a high concentration of very strong Lewis acid sites, very low concentration of isolated V^{+5} centers and minimum V^{+5} phases would definitely improve the yield to MA. The presence of the right promoters enhances surface

phosphorous enrichment, which modifies the surface acidity. However, excess phosphorous limits the total oxidation of the surface.

It is important to emphasize here that the reaction mechanism for the selective oxidation of *n*-butane to MA is different for the supported or mixed catalyst than the bulk catalyst. According to Matthijs Ruitenbeek, the Mars-Van-Krevelen mechanism is operative for VPO/SiO_2.

Although there are many publications on the topic of chemistry of VPO catalysts, there is very little information regarding the optimization of the variables together to obtain the maximum yield to MA.

Chapter 4: Catalyst Characterization and Performance

4.1 X-ray Diffraction

X-ray diffraction using (Philips Pananlytical X'Pert Diffractometer) was utilized to characterize the catalyst using Cu Kα radiation in a step-scan mode. The XRD spectra of bulk VPO (hemihydrate phase) precursor, and of the activated VPO (30h) are shown (Figure. 4.1). All features corresponding to bulk and activated VPO are in good agreement with literature [21,29]. The identification of XRD diffraction peaks of $VOHPO_4.0.5H_2O$ and $(VO)_2P_2O_7$ were assigned according to Bordes *et al.* [30]. Thus, the $VOHPO_4.0.5H_2O$ line at the $2\theta=15.5$ is indexed as the (001) plane and the second prominent line at $2\theta=30.4$ as the (220) plane. The activated VPO features at $2\theta=23.2$ and at $2\theta=28.3$ are identified as the (200) and (024) planes respectively [31].

A comparison of the XRD spectra (Figure. 4.2) of bulk activated VPO after 30h, and of the activated mixture of 10wt%α-SiC/VPO is also shown. According to Ledoux *et al.*, 2θ features between the angles of 20° through 25° are larger than the remaining peaks corresponding to different planes of diffraction. This confirms that no negative interaction between the pure SiC diluent and the VPO occurred during activation and that the prepared activated VPO can be described as a "true" VPO [21]. The XRD spectra of the bulk activated (orthophosphate phase) VPO (30h.), pure (commercial) α-SiC particles and 10wt% α-SiC/activated VPO confirm these results (Figure. 4.3).

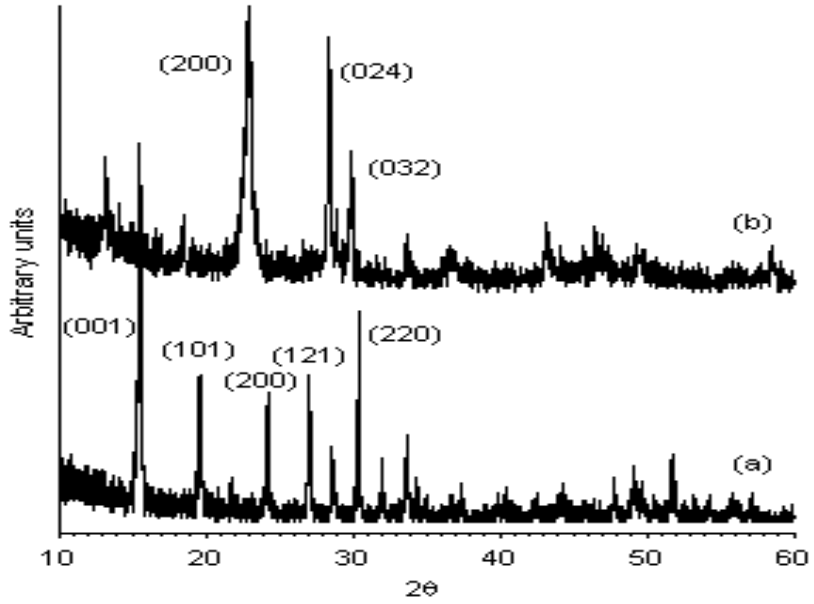

Figure 4.1: Comparison of XRD patterns of the VPO catalyst phases. (a) Bulk VPO (hemihydrate phase), and (b) activated VPO (30h).

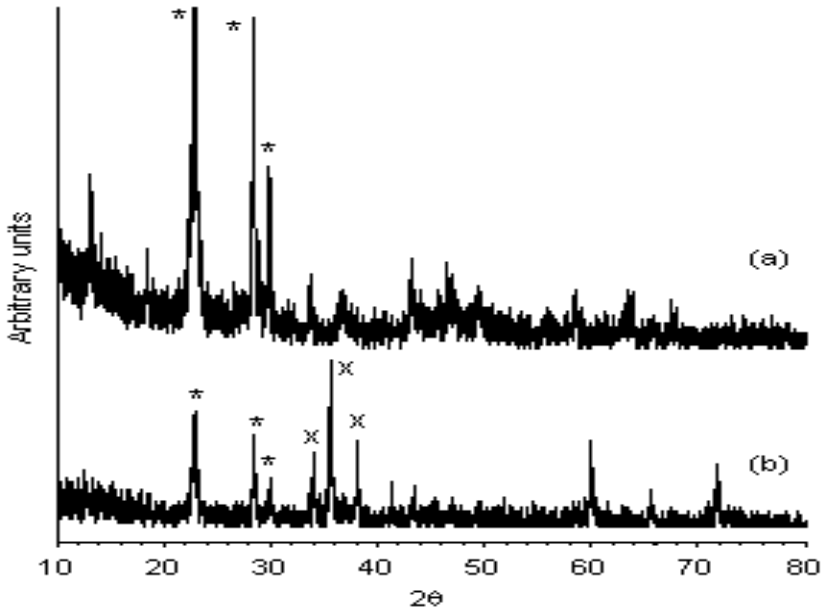

Figure 4.2: Comparison of XRD patterns of the VPO/SiC catalyst phases. (a) Activated VPO (30h), and (b) activated mixture of 10wt% α-SiC (2μm)/ VPO. x: SiC, *: VPO.

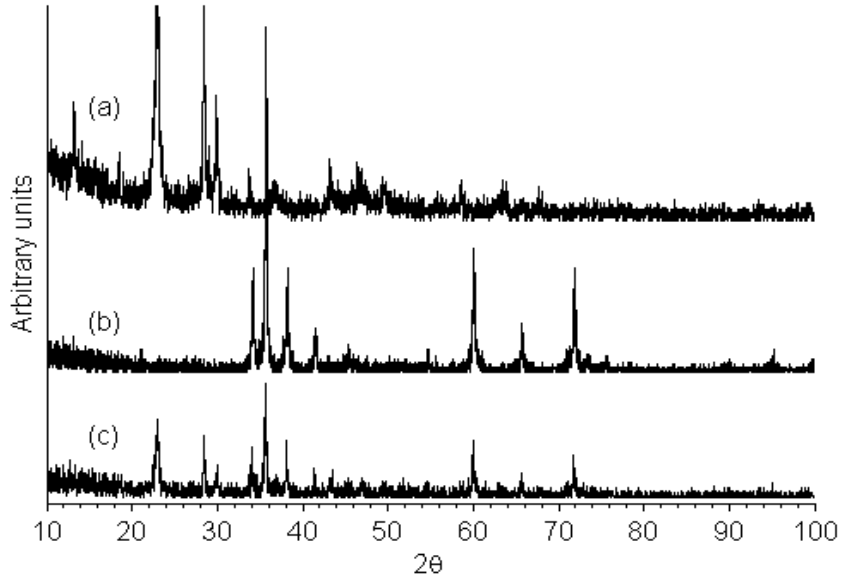

Figure 4.3: Comparison of XRD patterns of pure and activated SiC/VPO. (a) Activated after (30h), (b) pure α-SiC (2μm) diluent particles and (c) 10wt% α-SiC (2μm)/ activated VPO after (30h).

4.2 Experimental Setup

The screening of a catalyst starts with the measurement of the catalytic activity and performance in a microreactor. In this work, a 4 mm diameter quartz tube with a constriction in the center was loaded with a measured amount of catalyst and then placed vertically or horizontally in a Lindberg/blue furnace with a maximum heating temperature of 1100°C. The electric furnace is controlled by a temperature controller. Four MKS mass flow controllers (MFC) were used to regulate the flow rate of the gases. The MFCs were controlled by MKS 247-D four channel flow controller readout. The gases were mixed in a 150 mm static inline mixer and the gas feed introduced to the catalytic reactor from the top in a vertical arrangement (fixed-bed). Upon exiting the fixed-bed catalytic reactor, the gas effluent is passed through a 500 nm filter and then

analyzed using a BIO-RAD Excalibur FTS 3000 FTIR as shown in Figure 4.4. The FTIR is equipped with a permanently aligned gas-cell. The 2.5" diameter gas-cell provides an infrared beam path length of 2.4 m through multiple reflections from gold coated mirrors. It has a borosilicate glass body with a KBr window and a total volume of 0.1 liter. The detector is a mercury cadmium telluride (MCT) detector. The effective range of analysis is between 4000 and 600 cm^{-1} wavenumbers. A vacuum pump with 25.5"Hg maximum vacuum was attached to the system to assist the outflow of the gas effluent from the FTIR gas-cell chamber.

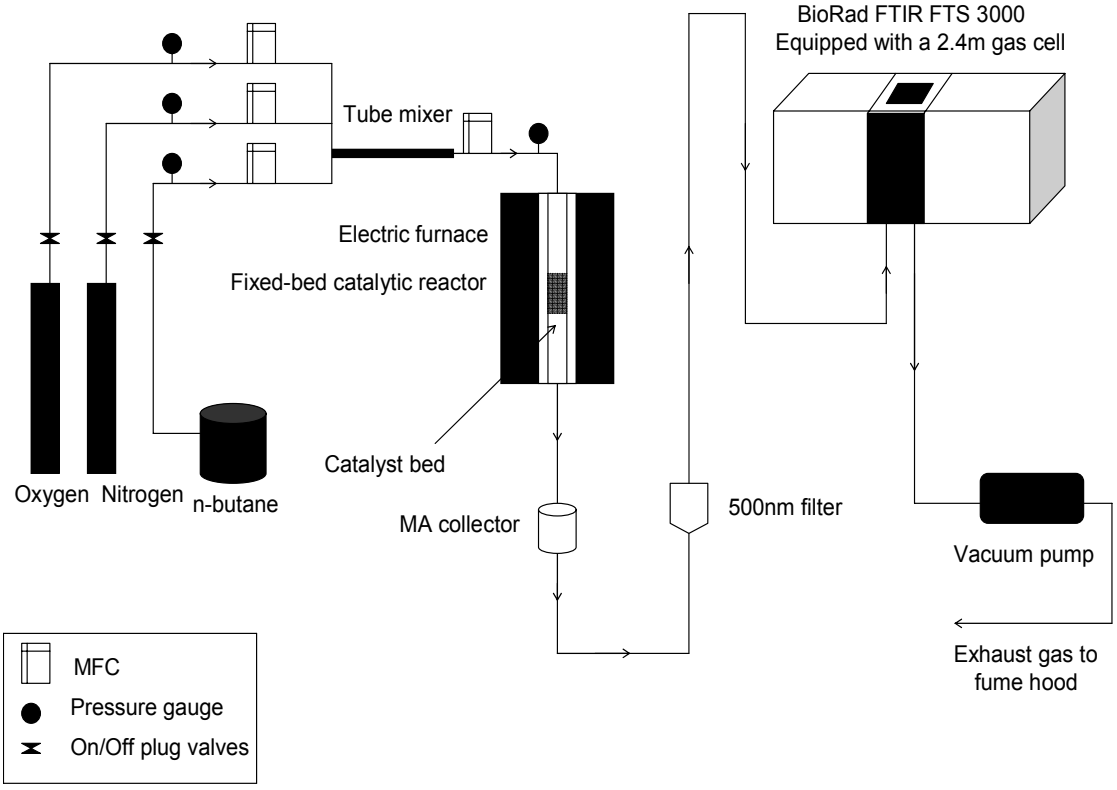

Figure 4.4: Catalytic reactor setup. The gases are mixed and introduced into a fixed-bed catalytic reactor containing a catalyst bed in the middle. The effluent stream is analyzed using FTIR equipped with a gas-cell.

Once the FTIR detector was cooled with liquid nitrogen, the gas-cell was purged with gaseous nitrogen to get rid of any CO_2 and water vapor residue. Three infrared (IR) spectra were collected every 50°C or 100°C depending on the experiment to ensure uniformity in all data collecting runs.

A pilot plant is the next step in developing a catalyst after its preliminary testing in the microreactor. The main difference between a pilot plant and a real industrial process is the number of reaction tubes. Temperature, pressure and flow rates are kept identical to allow heat and mass transfer phenomena to be studied.

4.2.1 Reaction Conditions

The explosive potential of a wide range of oxygen/ *n*-butane mixtures combined with inert diluent gases must be recognized. Thus a concentration of up to about 1.5-2.0 vol% *n*-butane in air represents the maximum safe range for the lower explosive limit [18]. In order to achieve maximum productivity of MA, it is also desirable to maximize the *n*-butane concentration [18]. The *n*-butane flow rate concentration used in this work was 1.64 vol% *n*-butane in air as shown in Table 4.1, with some experiments up to 2.3 vol% *n*-butane in air. Other experiments in this work had a mixture of O_2 and N_2 rather than air.

Table 4.1: Different gas flow rates used in the partial oxidation to MA.

Gas used	1.64 vol% *n*-butane in air	1.64 vol% *n*-butane in air
n-butane	1.04 sccm	1.04 sccm
UHP air	63.3 sccm	N/A
0.21 mol%O_2/ 0.79 mol%N_2	N/A	13.3 sccm/ 50.0 sccm

Oxidation is carried out at a temperature range of 300-550°C with operating pressure that can vary from about 0.5-20 atm but preferably should be held in the range of 1-7 atm. Contact time can vary between 0.1 to 15 seconds, preferably between 0.2 to 4.0 seconds [15,18]. In this work contact time was determined based on limitations of the MKS MFCs capacities, safety measures when using high *n*-butane volume concentrations and the reactor quartz tube 4 mm diameter. It is important to note that increasing reaction pressure increases contact time for the same mass flow rate. In this work, the pressure was kept at approximately 1 atm in most of the experiments, thus contact time values were less than optimal. On the other hand, according to Bither, based on VPO catalyst results shown in U.S. patent # 4,442,226 [18], increasing pressure can cause significant decrease in catalyst activity or conversion. Contact times are shown in Table 4.2.

Table 4.2: Contact time values used in the reaction to MA. Contact time is based on 20 mm average bed height.

Purpose of reaction	*n*-Butane concentration in Air	Contact time
MA yield determining reactions	2.3 vol % (1.46 sccm *n*-butane)	0.10 seconds
n-Butane conversion reactions	1.64 vol% (1.04 sccm *n*-butane)	0.07 seconds

The results are categorized based on the catalyst used, starting with fresh activated and calcined VPO precursor as shown in Table 4.3. Catalyst particles were crushed and sieved to have a size range between 40-60 mesh, and then pressed to form 1 mm diameter particles. In the next sections, the results are presented as *n*-butane conversion versus temperature plots. It is important to note here that when referring to reaction, it is meant partial oxidation of *n*-butane to MA and when using the VPO catalyst, this implies that it is already been calcined and activated.

Table 4.3: Analyzed samples weight loading range and space velocity.

Sample	Weight (g)	Loading range (wt%)	Space velocity ($h.^{-1}$)
VPO only	0.38	-	116
SiC wafers	0.13	-	500
Pd / α-SiC (2μm)	0.32-0.50	0.5wt% Pd / α-SiC (2μm)	110-115
Pd / VPO	0.50	0.5-1.5	110-116
α-SiC (2μm) / VPO	0.38-0.50	6.60-90.0	110-120
Pd / α-SiC (2 μm)/ VPO	0.50	1.5wt%Pd/ 10wt% α-SiC (2μm)/ VPO	113

The gas effluent stream was connected to the FTIR. Temperature was ramped at a rate of 50°C every 30 minutes. Three spectra were collected every 50°C or 100°C depending on the experiment and to ensure uniformity in all experimental runs. The spectra were ratioed against initial concentration spectrum and analyzed later using the FTIR Know-It-All Informatics system software to calculate the conversion values presented in the following result figures. The resultant FTIR spectra of the product stream were converted into absorbance. Conversion was calculated once inlet and outlet concentrations at specific temperatures were known. The FTIR resolution and number of scans used through out these experiments were 0.25 cm^{-1} and 128 scans, respectively.

4.3 Surface Area of the Catalyst (BET Results)

The total surface area of different SiC diluents as well as the VPO catalyst was measured by the Brunauer-Emmet-Teller (BET) method which included two steps: degassing and BET analysis using nitrogen as adsorpate at 77K. This was done using a NOVA 2000 series instrument. The results are shown in Table 4.4. It is clear that the α-SiC (2μm) had the closest surface area (SA) to the activated VPO catalyst, thus becoming a good candidate as a diluent.

Table 4.4: BET results and particle size of the SiC diluent and VPO catalysts.

Powder sample	Size (μm)	Specific surface area (m^2/g)
α-SiC	150	0.160
α-SiC	2	10.26
β-SiC	0.03	110.5
VPO (precursor)	200-1000	8.100
VPO (activated)	200-1000	10.90
-BET specific surface area of the catalysts was determined by nitrogen physisorption using a Quantachrome AUTOSORB-1 automated system. -Each sample was degassed for 4h prior to nitrogen physisorption. -Bath temperature: 77K -Elapsed time: 412 min -α-SiC: commercial particles obtained from Alfa Aesar. -β-SiC: commercial particles obtained from Sigma. -VPO (precursor): obtained after washing with hot water before activation. -VPO (activated): activated by *n*-butane procedure. -Error of measurement=±12%		

Surface area measurement done using the BET method showed that the average surface area was in the range of 10-15m^2/g for the VPO catalyst prepared via the aqueous medium process and in the range of 15-50m^2/g for VPO catalysts prepared using the organic medium [20]. The results in Table 4.4 agree with the literature results [15, 18, 20]. It is well known that an increase in the surface area of the prepared VPO catalyst is achieved using an organic solvent rather than the use of an aqueous medium as discussed earlier [1].

Regardless of the preparation method (aqueous or organic), a significant amount of carbon contaminant is deposited on the surface of the VPO catalyst during reaction that shields the vanadium, phosphorous and oxygen atoms on the surface, thus affecting the catalyst performance. Although the solution to this problem is to combust the carbon in air at 300°C, this will also bring about the oxidation of vanadium (seen as a color change) which indicates a structural change has occurred as well [18].

4.4 Reaction Using α-SiC Diluents and Wafers

In this section, different commercial SiC powder/wafer samples were used as modifiers, which were loaded in the catalytic reactor, and were all run under the exact reaction conditions.

As stated, SiC is expected to act as an efficient heat transfer medium to distribute heat and assist with hot-spot reduction associated with the very high exothermicity of this reaction. The use of SiC as a catalyst diluent was expected to result in an increase in catalyst lifetime and the prevention of VPO over oxidization. In addition, the small reactor inner diameter (4mm) ensures that isothermal conditions are favored.

Figure 4.5 shows two wafer samples denoted as D5-AK08 and D2-AK08 under reaction regime, the only difference between the two wafers is their location in the original manufactured wafer. The wafers are 6H-SiC, 100% porous with 1.6μm layer. The wafers were cut into similar smaller slices (<4mm in size). Previously, the two wafers were treated according to the following procedure: Wafers were already etched with HF solution to remove the oxide layer. Reactive ion etching (RIE) was used to

expose pores (50 nm average diameter). The wafers were immersed in acetone-filled beaker. The beaker was placed in an ultra sonic bath for 15 minutes.

No desired product (MA) was formed in the two wafer runs and the FTIR results indicated low *n*-butane conversion to CO_x gases. The two other plots; one for a wafer mixed VPO catalyst with a 1:1 weight ratio mixture, and the other for a 6.6wt% α-SiC (2μm)/VPO system. Both samples gave a 5% *n*-butane conversion at 450°C, but the VPO mixed with α-SiC powder gave better overall results than the VPO/wafer mixture. The amount of product was almost doubled when using α-SiC powder.

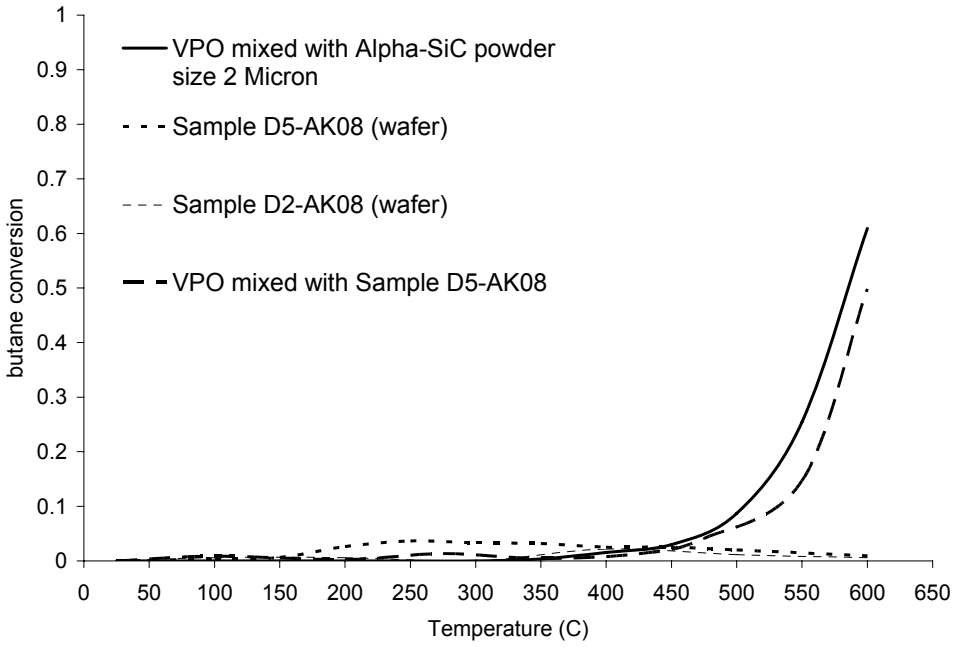

Figure 4.5: *n*-Butane conversion results using VPO mixed 6H-SiC. The sample weight was 0.13g. Wafers alone did not produce any MA.

It should be noted that in all sample runs containing VPO catalysts, MA was formed along with other products such as acetic acid. Using SiC lowered the light off temperature which is the temperature at which conversion of *n*-butane, CO_2, water or

maleic anhydride begins. Repeated experiments were done on different types of SiC powder with different loading percentages for comparison. This will be discussed in the next section.

Figure 4.6 shows results using different commercial SiC diluent particles. The partial oxidation reaction of *n*-butane to MA was performed using these samples, but no desired product (MA) was formed; only CO_x gases and water vapor. This means that bare SiC has no intrinsic catalytic selectivity to produce the desired product MA. From Figure 4.6, the α-SiC (2μm) powder had the lowest light off temperature (less than 600°C) in comparison to the other powder samples used in the experiments. For this reason, the α-SiC (2μm) powder was used in all future SiC/VPO mixtures with loadings ranging from 6wt% α-SiC (2μm) in VPO up to 90wt% α-SiC (2μm) in VPO. *n*-Butane combustion is shown as a reference.

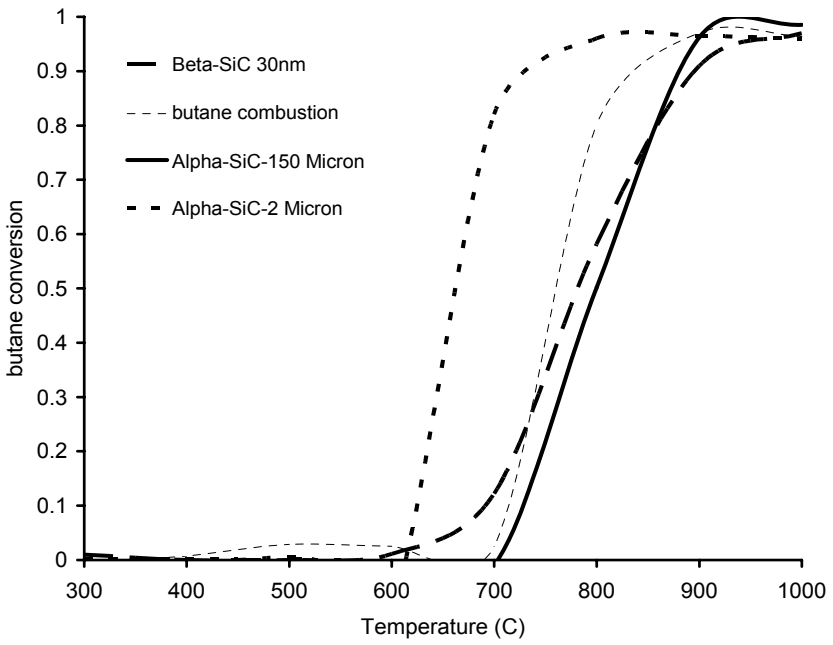

Figure 4.6: *n*-Butane conversion using different commercial SiC diluents. The sample weight was 0.13g. No MA was formed, only oxidation products: CO_x gases and water vapor. α-SiC (2μm) had the lowest light off temperature. *n*-Butane combustion is shown as a reference.

4.5 Reaction Using Unpromoted SiC Modified VPO Catalysts

The conversion of *n*-butane as a function of reaction temperature for a range of α-SiC/VPO mixtures, with bulk VPO as a reference is shown in Figure 4.7. The 10wt% α-SiC modified VPO resulted in at least a 70°C reduction in the light off temperature (The temperature at which *n*-butane starts to convert into products) converting *n*-butane to MA, water, CO_x gases and other products. At a reaction temperature of approximately 400°C, samples with 10wt% and 26wt% SiC/VPO gave 54% and 28% *n*-butane conversion respectively compared to 7% for bulk VPO. However, at 500°C the

conversion was up to almost 90% and 70% for the 10wt% and 26wt% α-SiC/VPO samples respectively in comparison to only 34% conversion for bulk VPO. In this study, a 10wt%α-SiC/VPO mixture was found to produce the maximum amount of product.

Higher loadings (Figure 4.8) of α-SiC diluent modified VPO catalysts show no significant increase in conversion as the α-SiC loading was increased beyond 50wt%. Sample 50wt%α-SiC/VPO gave 42% *n*-butane conversion at 420°C in comparison to about 26% conversion for the 80wt%α-SiC loaded VPO sample. The pure α-SiC sample tested did not produce any desired products but rather favored the complete oxidation of *n*-butane. The lower percentage loadings of SiC in VPO samples (6-26wt %) had higher *n*-butane conversion and produced more desired products at the same temperatures when compared to higher loadings (50-90wt%) of SiC in VPO.

It is important to note that in the previous figures and at temperatures higher than 400°C, considerable amounts of CO, CO_2 and water vapor were formed, where water is a product of the partial oxidation reaction to MA. Eventually, when temperatures are high, *n*-butane combustion (complete oxidation) starts as a result of *n*-butane reaction with air to CO_x rather than being partially oxidized over the VPO catalyst.

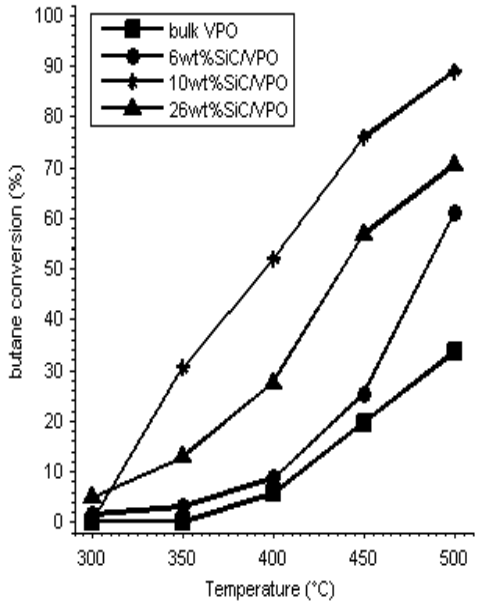

Figure 4.7: *n*-Butane conversion for α-SiC/VPO mixtures (lower loadings). The bulk VPO curve result is shown for comparison. 10wt% loading had the best conversion.

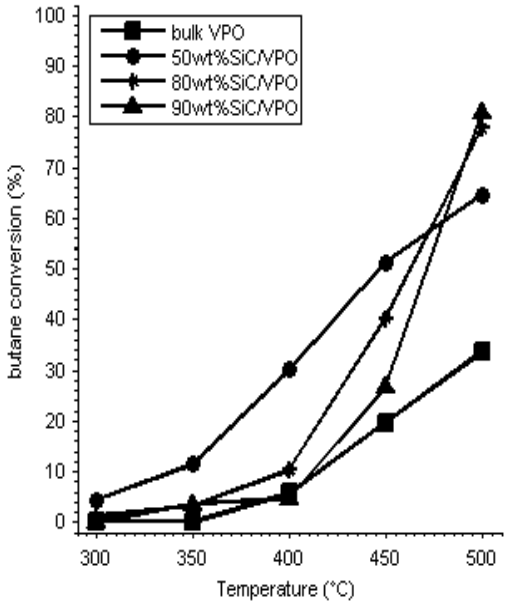

Figure 4.8: *n*-Butane conversion for α-SiC/VPO mixtures (higher loadings). The bulk VPO curve result is shown for comparison. 50wt% loading had the best conversion.

This section concludes that whenever α-SiC (2μm) is present in the sample, the light off *n*-butane conversion temperature is reduced in comparison to bare VPO or α-SiC (2μm) samples. It is also important to note that for the same sample weight, the amount of desired product (MA) produced using α-SiC (2μm) modified VPO catalyst decreased as the weight percentage of α-SiC in VPO increased. This is true since α-SiC has no intrinsic catalytic selectivity to MA.

Figure 4.9 summarizes the results obtained in this section. The VPO sample containing 10wt% α-SiC (2μm) had a 19% and 22% *n*-butane conversion to CO_x, MA and other products at 420°C (reaction temperature) and 450°C respectively. This loading percentage was selected to be used when promoting the VPO catalyst with Pd which will

be discussed in the next section due to its high MA yield. The VPO sample containing 26wt% α-SiC (2μm) had a *n*-butane conversion of 9% and 12% at 400°C and 420°C respectively. For the VPO catalyst system containing 50wt% α-SiC mixed with VPO, the *n*-butane conversion to MA was 17% at 420°C, but increased to 21% at 450°C. From Figure 4.9, it was concluded that the best *n*-butane conversion to MA occurred when the VPO catalyst system had a weight percent range of α-SiC diluent particles between 6 and 25wt% in VPO. This conclusion was also based on the amount of MA obtained (yield) in each of those runs. As expected SiC had no intrinsic selectivity to produce any MA, however, SiC added particles helped increase the conversion of *n*-butane to other products like CO_x as well as water vapor.

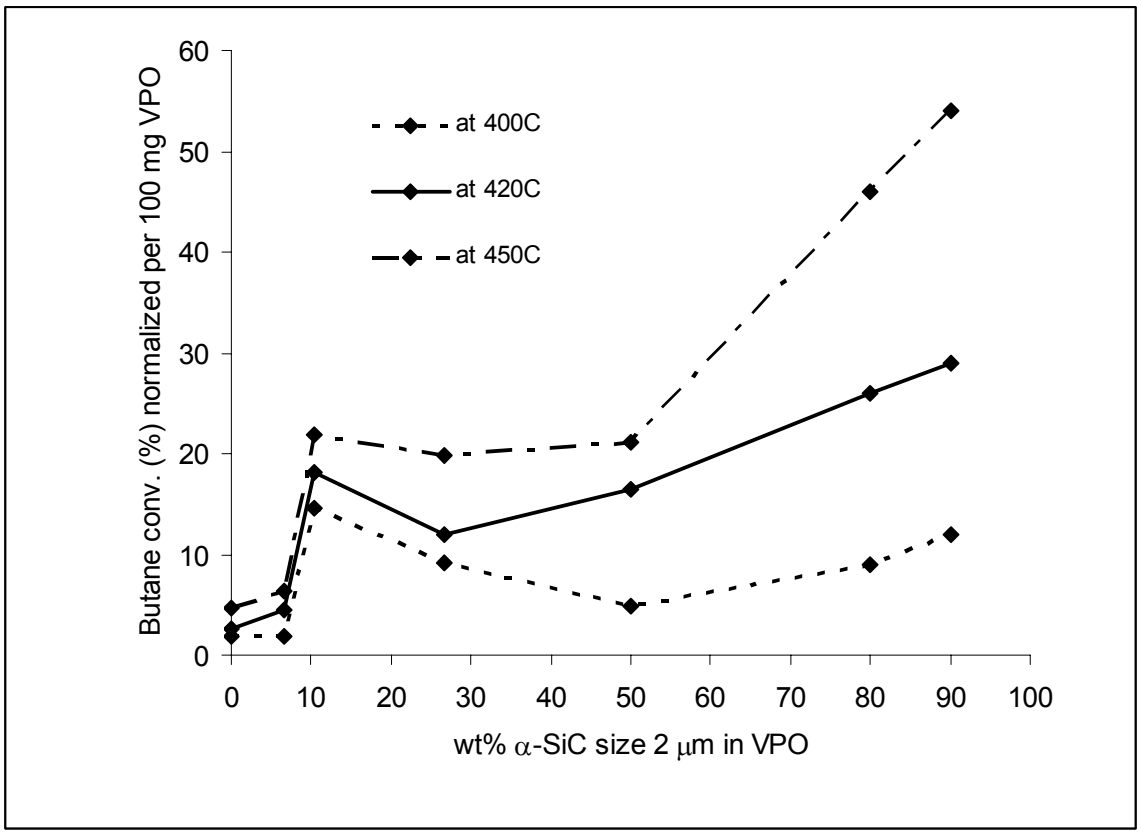

Figure 4.9: Normalized *n*-butane conversion versus α-SiC (2μm) wt%. The 90wt% α-SiC (2μm) had the highest *n*-butane conversion to products at 420 ºC (reaction temperature). However, it produced the least amount of MA product as SiC had no intrinsic selectivity towards MA.

4.6 Reaction Using Pd Promoted VPO Catalysts

Bulk VPO catalysts were promoted with Pd with a loading ranging from 0.5–1.5wt%. The behavior of Pd promoted VPO catalysts with the non-promoted bulk VPO is shown in Figure 4.10. With Pd promotion, oxidation of *n*-butane to products begins at approximately 300°C in comparison to around 400˚C for the bulk VPO. At approximately 550°C, the *n*-butane conversion dropped sharply, indicating a dramatic decrease in catalyst activity most likely due to VPO over oxidation. It is important to

mention that MA was formed in all experiments where the catalyst contains VPO and all catalysts were prepared with the same activation process. However, the amount of *n*-butane converted to MA and other products (*n*-butane conversion) increased when the catalyst is diluted with α-SiC or promoted using Pd.

A summary of the catalytic systems studied in comparison to the optimized novel catalyst system which consisted of 1.5wt%Pd/10wt%α-SiC/VPO is presented in Figure 4.11. This optimized system was obtained by combining the best α-SiC/VPO and Pd/VPO conversion results. It is important to mention here that some of the product (MA) is formed during the initial VPO activation process.

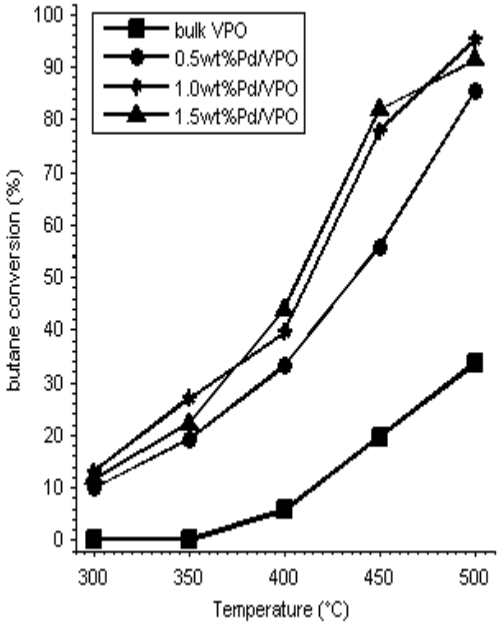

Figure 4.10: *n*-Butane conversion for Pd promoted VPO catalysts. The bulk VPO curve result is shown for comparison. The 1.5wt% Pd/VPO catalyst had the highest *n*-butane conversion and produced the largest MA yield.

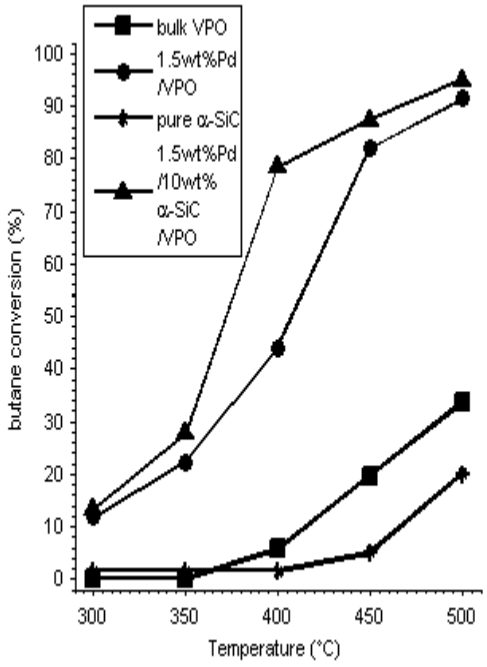

Figure 4.11: Selected results of Pd promoted and α-SiC/VPO catalysts. The 1.5wt%Pd promoted 10wt%α-SiC (2μm) diluted /VPO catalyst system showed the optimum performance (highest yield and conversion).

The product yield refers to the total yield including MA, water, other acids and products of the reaction. Typically, high yields of MA, coupled with high gas flows over the catalyst will maximize the productivity [18]. Productivity or yield will be represented as space time yield (STY), which is defined as the number of grams of product (including MA) produced per kilogram of VPO catalyst charged per hour of operating time. The STY gives a better measure of the yield because it is calculated based on actual catalyst weight used in each run. Table 4.5 shows all tested catalyst sample systems containing VPO, their weight, total product weight (which is mainly MA), actual product yield and STY. After collecting the product in each experiment, the total product was placed in an evaporating dish, and was subjected to moderate heating (50-65°C) so as to vaporize any water, while at the same time not burning the MA. After heating, the product was weighed and listed as the total product weight. Table 4.5 also shows the STY based on 20h of operation since products of the reaction start to form while activating the catalyst with *n*-butane. As expected, the Pd promoted VPO catalysts gave higher actual yields than the unpromoted VPO catalyst, 17.5% versus 7.2% for the 1wt%Pd/VPO and bulk VPO systems respectively. The 10wt%α-SiC/VPO system resulted in a 102 STY value versus 76 STY for the bulk VPO catalyst. The optimized 1.5wt%Pd/10wt%α-SiC (2μm)/VPO catalyst system was found to give a 25% actual yield and a 202 STY.

The STY gives a better measure of the yield because its calculated based on the catalyst weight which is different in some runs. The α-SiC (2μm) mixed VPO catalyst gave higher STY as the α-SiC loading percentage in VPO decreased, with the highest STY obtained with 10wt% α-SiC (2μm)/ VPO system which gave 102 STY value versus 76 STY for the bare VPO catalyst. From Table 4.5, it is noticed that promoting the VPO

catalyst using Pd increased the actual yield and the STY. Modifying the VPO catalyst with α-SiC (2μm) increased the yield at lower weight percentage loadings, but decreased the yield when the weight percentage of α-SiC (2μm) in VPO increased.

The product yield in this section refers to the total product yield including MA, water and other acids. It is important to mention that a lot of the product is formed during the activation by the *n*-butane process, in other words catalyst activity is noticed during the activation process using *n*-butane, and not air. Samples underwent reaction to MA for 7h up to 30h following the *n*-butane activation process. The product amount continuously decreased during that time. This means that at time equal zero, activation by *n*-butane was already done in which some product was formed. The highest total product percentage yield achieved was 27%. Commercial VPO catalysts usually report a yield ranging from 10-35% MA [10,32].

Table 4.5: Total product yield and STY results for all catalyst systems.

Sample	Catalyst weight (g)	Total product weight (g)	Total product actual yield (%)[a]	Space time yield (STY)[b] $\frac{(g)totalproduct}{(kg)catalyst * hours_{operation}}$
VPO only	0.38	0.58	7.20	76
6wt% α-SiC (2μm) /VPO	0.38	0.40	5.01	53
10wt% α-SiC (2μm) /VPO	0.38	0.77	9.67	102
26wt% α-SiC (2μm) /VPO	0.38	0.35	4.38	46
50wt% α-SiC (2μm) /VPO	0.50	0.25	3.13	25
80wt% α-SiC (2μm) /VPO	0.50	0.10	1.25	10
90wt% α-SiC (2μm) /VPO	0.50	0.05	0.62	5
0.5wt%Pd/ VPO	0.50	0.63	7.89	63
1.0wt%Pd/ VPO	0.50	1.40	17.54	140
1.5wt%Pd/ VPO	0.50	1.20	15.04	120
1.5wt%Pd/ 10wt% α-SiC (2μm)/ VPO	0.50	2.02	25.27	202

[a)] Based on total product theoretical yield [b)] 20h of operation
[b)] Yield calculations are shown in Appendix A.

In this study, reaction times of approximately 6-30h at one atmosphere were performed. The optimized 1.5wt%Pd/10wt%α-SiC/VPO system underwent reaction to MA using *n*-butane following the activation process in which the amount of product continuously decreased until the catalyst system lost its entire activity due to oxidation. The total reaction time was 23h which included activation.

Figure 4.12 shows two Pd/ α-SiC (2μm) plot results under the *n*-butane oxidation regime. These experiments were performed to further prove that SiC promoted with Pd

has no intrinsic catalytic activity to produce MA. The loading of Pd is 0.5wt% in α-SiC in both samples. The reduced sample was heated for 2h under N_2 at 80°C, then H_2 was introduced gradually; i.e. 5% then 50% then 100%, the point was to make sure that the nitrate group of the salt was dissolved. The other sample was prepared by mixing the $Pd(NO_3)_2$ salt under agitation with α-SiC (2μm) using dodecanol, initially at moderate temperatures (120°C) and then at about 250°C for 2h. The sample was then placed in a furnace for 2h at a temperature of 500°C to thermally decompose the nitrate group. Figure 4.12 shows clearly that the H_2 reduced sample had a much higher *n*-butane conversion. No desired product (MA) was formed; instead the conversion of *n*-butane was to CO_x gases and water vapor. At 300°C, the etched sample had a *n*-butane conversion of about 80% compared to the unetched sample (3% *n*-butane conversion). The reduced sample of 0.5wt% Pd in α-SiC (2μm) has reduced the combustion temperature of *n*-butane 500°C.

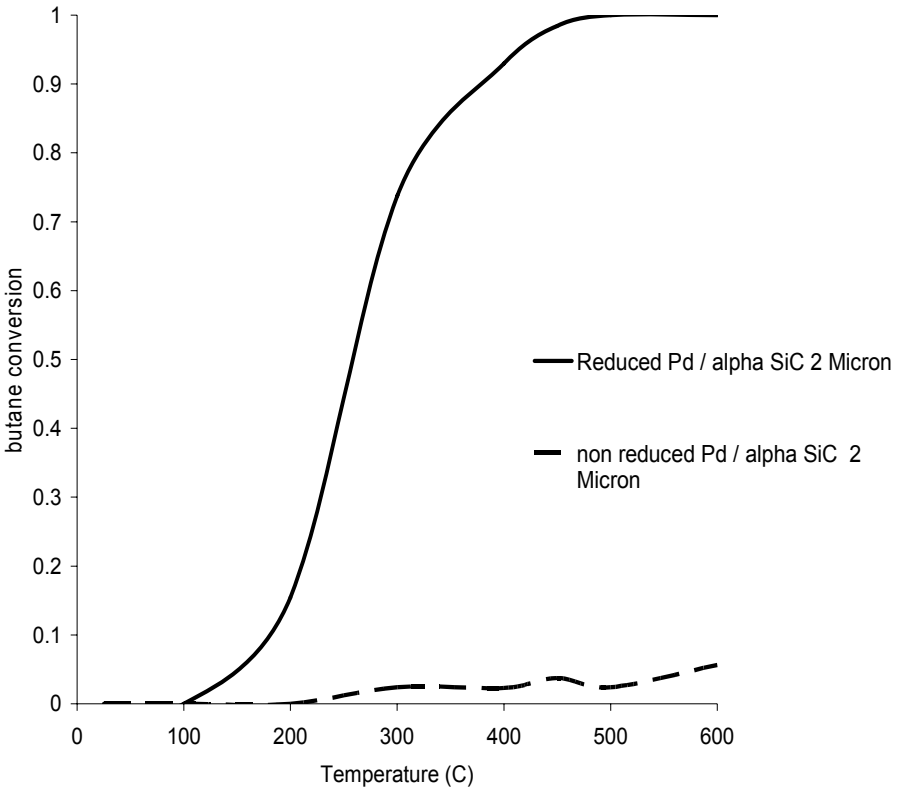

Figure 4.12: Pd/ α-SiC (2μm) partial oxidation reaction results. The reduced sample lowered the combustion temperature of *n*-butane significantly.

4.7 FTIR-ATR and Gas-Cell Analysis of VPO Catalyst and Reaction

A Pike Technologies MIRacle single reflection horizontal attenuated total reflectance (HATR) unit designed for use in FTIR spectrometer was utilized in obtaining spectra of the powder VPO catalyst at different phases. Figure 4.13 shows the FTIR-ATR spectra of fresh bulk VPO, activated bulk VPO, and spent VPO due to over oxidation. Figure 4.14 shows the FTIR-ATR spectra of 10wt% α-SiC/VPO particles fresh before mixing, after activation mixed, and after reaction for the diluted sample. Smoothing (Boxcar 3 points) was used. Both figures show that the peaks corresponding to the fresh

bulk VPO are similar and are in good agreement with the powder IR spectra of VPO catalyst.

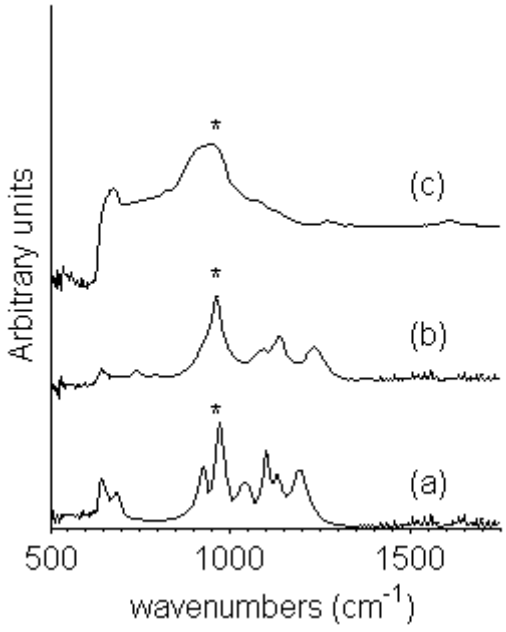

Figure 4.13: FTIR-ATR spectra of bulk VPO particles. (a) Fresh bulk, (b) activated bulk, and (c) after reaction.

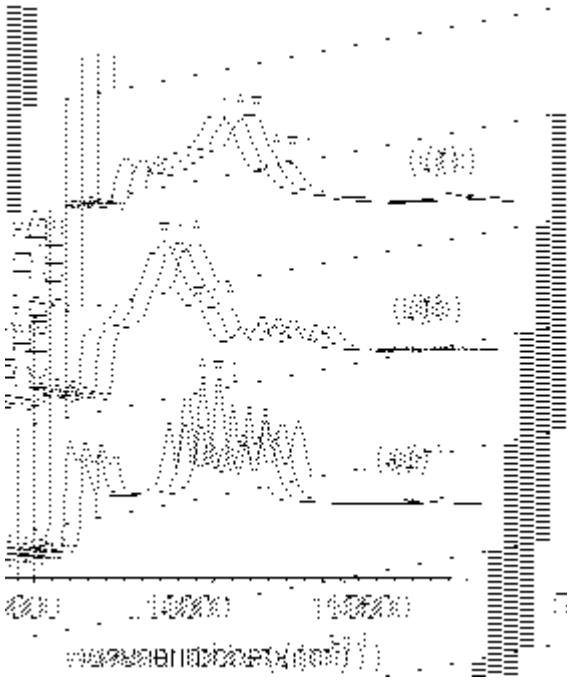

Figure 4.14: FTIR-ATR spectra of 10wt% α-SiC (2μm)/VPO particles. (a) Fresh before mixing, (b) activated mixed, and (c) after reaction.

The presence of a single distinct crystalline phase (revealed by XRD) is believed to be responsible for the single strong sharp band around 950cm^{-1} present in both fresh VPO spectra [33]. The activated bulk VPO spectrum (see Figure 4.13) shows shifted IR band positions in the activated mixed spectrum (Figure 4.14). This is due to diluting VPO particles with the α-SiC particles which is indicated by the IR high intensity bands around 800cm^{-1} characteristic to Si-C IR stretching. The after reaction spectrum (Figure 4.13) shows major band frequency and shape changes in comparison to the activated spectrum, which explains the loss of the catalyst activity in this sample after reaction. On the other hand, the after reaction mixed sample spectrum in Figure 4.14 is almost similar to the one

in Figure 4.13 but shows a band around 1075cm^{-1} which is part of the VPO and a result of the interaction of VPO with the added α-SiC diluent. This may provide an explanation as to why that sample was not totally over oxidized yet and still showed some catalyst activity.

For Figures 4.15-18 and due to the large number of experimental runs, only representative spectra are presented. Unless otherwise indicated, the spectra displayed in each figure have the same intensity scale. Activated VPO indicates orthophosphate phase $(VO)_2P_2O_7$ mixed with α-SiC particles or promoted with Pd or both. The IR wavenumber range is between 500 up to 4000cm^{-1}. The intensity of all the peaks shown in the figures was less than one unit of absorbance. Due to the complexity of the reaction on VPO catalysts, only the formation and consumption of the main constituents of the reaction will be discussed: *n*-butane, maleic anhydride, water, CO and CO_2. Bands at 1845 and 1775 cm^{-1} can be assigned to maleic anhydride, another band near 1720 cm^{-1} is attributed to maleic acid [34]. The bands at 1850 and 1775 cm^{-1} have been used to confirm maleic anhydride formation by oxidation of *n*-butane according to Zhi Yang and Schrader [34]. The strongest band in all the figures between 2800 up to 3000cm^{-1} is due to absorption of gas phase *n*-butane. Strong bands near 1466 and 1392cm^{-1} were also attributed to gas phase *n*-butane (asymmetrical and symmetrical CH_3 deformations, respectively). Water exhibits a band centered at about 1620cm^{-1} as well as the wavenumbers above 3500cm^{-1} which is attributed to the –OH vibrations since water is a product of hydrocarbon oxidation [35]. A strong band between 2300 and 2400cm^{-1} is attributed to CO_2 together with a weaker one around 650cm^{-1}. For CO, a doublet between 2000 and 2250cm^{-1} is responsible for that bond vibration.

Figure 4.15 provides spectra obtained at 300 up to 500°C of the reactor effluent for the 10wt% α-SiC (2μm)/VPO catalyst sample. As the temperature is ramped up, the concentration of gaseous *n*-butane determined by the area under the respective peaks described above is decreased slightly whereas maleic anhydride concentration; also determined by the area under the respective peak(s) is increased with the maximum area under the peak(s) obtained at around 500°C. The associated bands at around 1850 and 1775cm^{-1} indicate the generation of maleic anhydride. The concentration of water and CO_2 also increased slightly; some CO was formed at 500°C.

Figure 4.16 shows FTIR gas-cell reactor effluent spectra for the bulk VPO catalyst sample. Conversion of *n*-butane increases with temperature increase as indicated by the decreased area under the *n*-butane peaks. MA peak intensities gradually increase as temperature is ramped, with higher intensity peak occurring at 450°C. When compared to Figure 4.15, it is noticed that MA peaks are more intense and pronounced at lower temperatures; 300 and 400°C. However, the sample in Figure 4.16 has generated fewer amounts of water and CO_2 than the sample catalyst in Figure 4.15 at the same temperatures. From the spectra in these two figures, it is noticed that the presence of α-SiC as a diluent in the mixture has helped lower the reaction temperature at which MA is formed, indicated by the presence of the MA peaks at lower 300°C.

Figure 4.17 shows the spectra obtained while running a 1.0wt%Pd/VPO catalyst sample. The intensity of the *n*-butane peaks are sharply decreased at 500°C, indicating a high conversion rate of gaseous *n*-butane. The MA peaks apparently have higher intensity using this catalyst sample than any other sample at 500°C. The generation of MA is significantly increased with increasing temperature; however the CO_2 peak intensity is

also sharply increased. Figure 4.18 represents the best combination of Pd and α-SiC modifiers (1.5wt%Pd/10wt% α-SiC/VPO). It is evident that the generation of MA was the largest at 450°C expressed by the high intensity peaks around 1775 and 1825cm^{-1} in comparison to all other spectra shown in the previous three figures. It is also apparent that the *n*-butane peak diminishes quickly when 500°C is reached. Still, however, the peak of CO_2 as well as water vapor is present with high intensity at 500°C.

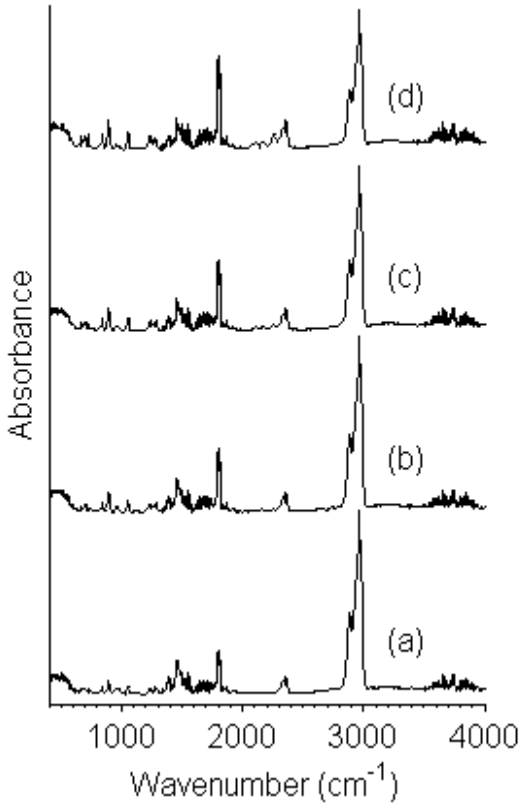

Figure 4.15: FTIR gas-cell effluent for the 10wt% α-SiC/VPO catalyst. The spectra are at different temperatures: (a) 300°C, (b) 400°C, (c) 450°C and (d) 500°C.

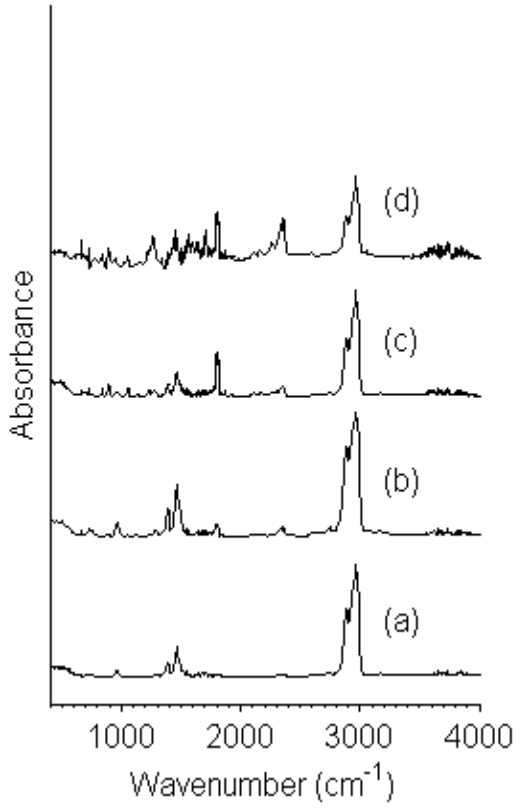

Figure 4.16: FTIR gas-cell effluent for the bulk VPO catalyst. The spectra are at different temperatures: (a) 300°C, (b) 400°C, (c) 450°C and (d) 500°C.

In-situ FTIR spectra of the change in the reactants and products absorbance versus temperature are presented in Appendix B for the 1.5wt%Pd/VPO catalyst sample.

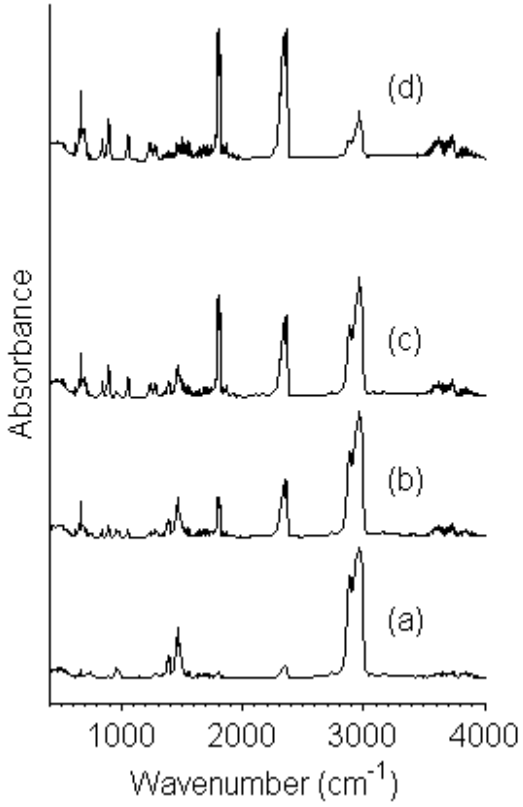

Figure 4.17: FTIR gas-cell effluent for the 1.0wt%Pd/VPO catalyst. The spectra are at different temperatures: (a) 300°C, (b) 400°C, (c) 450°C and (d) 500°C.

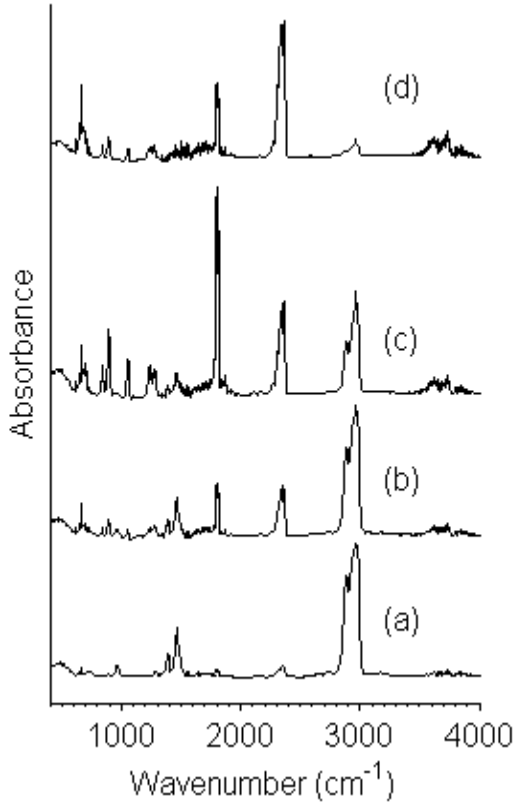

Figure 4.18: FTIR gas-cell effluent for the 1.5wt%Pd/10wt% α-SiC/VPO. The spectra are at different temperatures: (a) 300°C, (b) 400°C, (c) 450°C and (d) 500°C.

4.8 SEM Images of the Powder VPO Catalyst

Various scanning electron microscope (SEM) images via a Hitachi SEM, 20 kV tension are shown in Figures 4.19 and 4.20. The images in Figure 4.19 show bulk VPO in three stages: (a) fresh, (b) activated and (c) after reaction, whereas the ones in Figure 4.20 show the activated and after reaction stages for a sample mixture of 10wt% α-SiC/VPO. For the fresh catalyst (precursor), the platelets are small and agglomerate into the ideal rosette shaped agglomerates (image (a) in Figure 4.19) as reported in literature [36]. For

the activated VPO, the SEM images show what appears to be needle shaped peaks that tend to be a little thicker and less agglomerated when mixed with the α-SiC particles (images (b)-(Figure 4.19) and (a)-(Figure 4.20)). However, after reaction images ((c)-(Figure 4.19) and (b)-(Figure 4.20)) show a significant change of morphology between the bulk over oxidized and the after reaction α-SiC-diluted VPO system. Both show evident signs of disintegration on the surface. The bulk after reaction VPO sample lost all its needle shaped morphology. The α-SiC-mixed VPO sample also became smoother but was less agglomerated than the bulk overoxidized VPO surface [33].

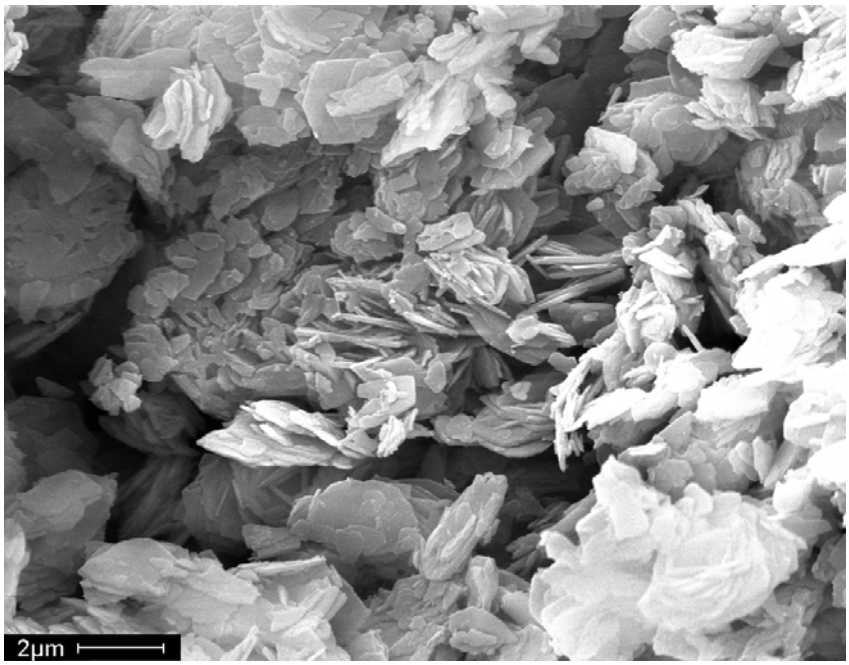

Figure 4.19: SEM images at different stages for bulk VPO sample. The combination of the images is magnified 6000 times. a) VPO fresh (Orthophosphate phase). Ideal rosette shaped phase existence.

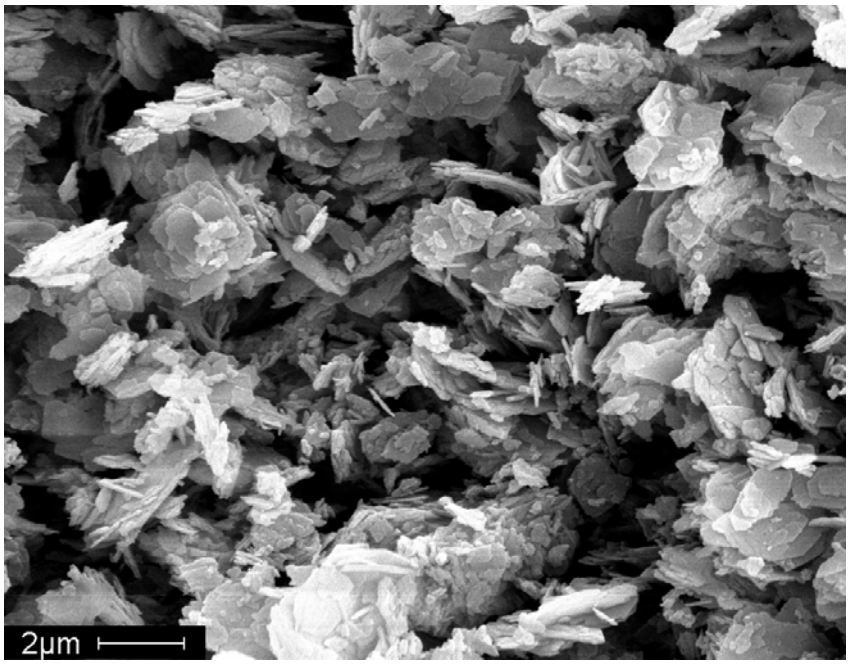

b) VPO activated with *n*-butane (Pyrophosphate phase). Needle shaped peaks morphology.

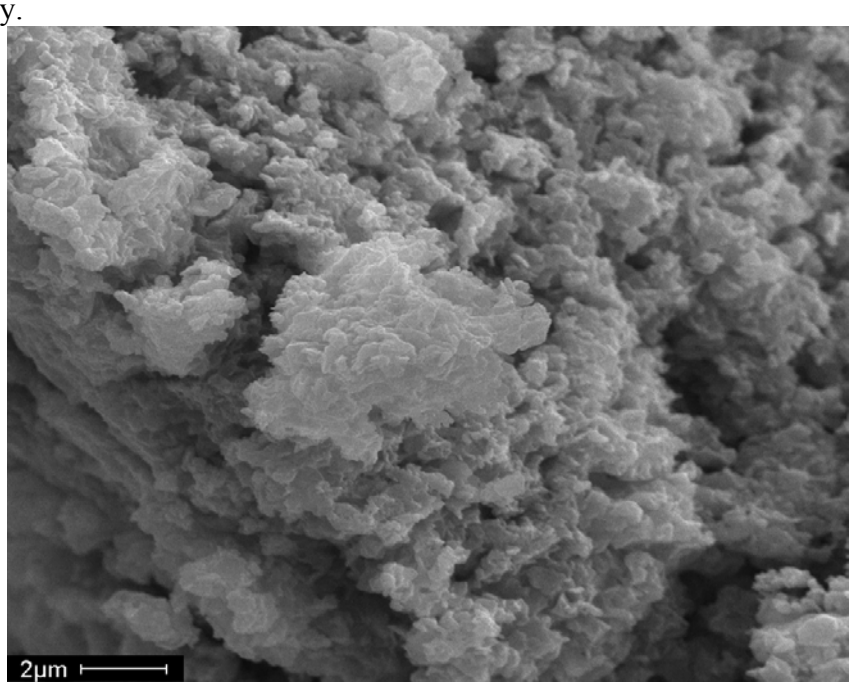

c) VPO oxidized (after 20h of reaction). Particle agglomeration.
Figure 4.19: (Continued).

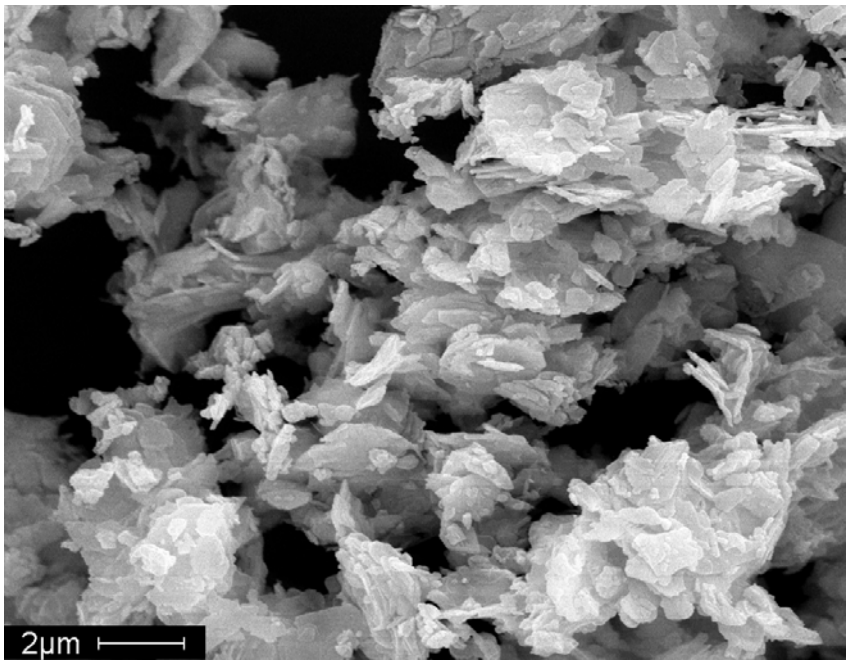

Figure 4.20: SEM images at different stages for the 10wt% α-SiC/VPO sample. The combination of the images is magnified 6000 times. a) 10wt% α-SiC/VPO activated VPO. Needle shaped peaks existence.

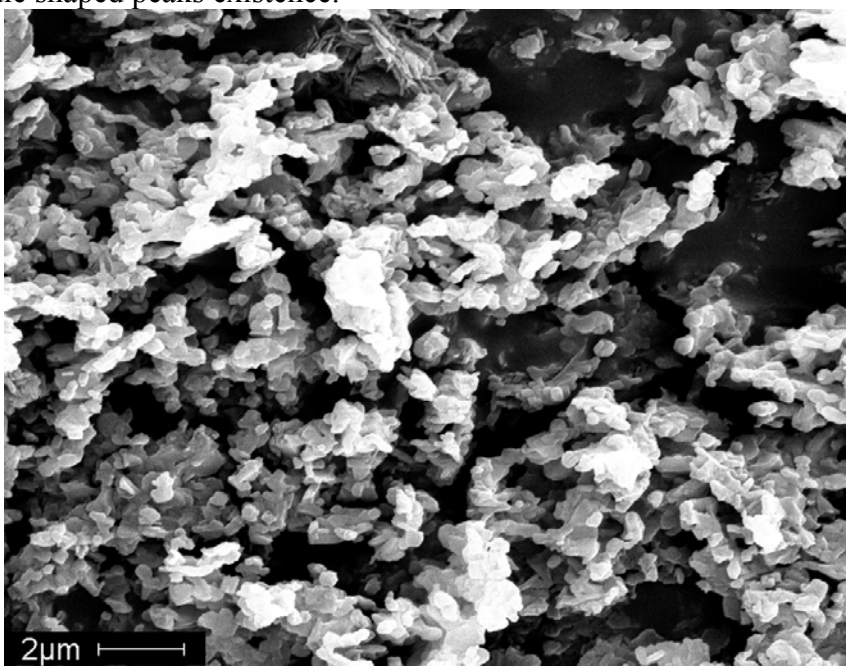

b) 10wt% α-SiC/VPO (after 20h reaction). No agglomeration.

4.9 Summary

This work has demonstrated that a vanadyl pyrophosphate (VPO) catalyst modified with palladium and α-SiC (2μm) diluent crystallites showed at least an 18% increase in yield of maleic anhydride (MA) as compared to bulk VPO. To this end, a low cost, reproducible preparation procedure, coupled with a short activation method, higher mechanical strength and superior heat transfer character over bulk VPO merits investigation.

In this highly exothermic reaction, the maintenance of isothermal operating conditions can lead to increased catalyst productivity. This is mainly accomplished through the elimination of severe hot spotting in the catalyst bed. Operating in this mode required the testing of several catalyst samples. From the results of this study, it was concluded that lower weight percentage loading of α-SiC (2μm) was more favorable than higher weight percentage loadings. For the same catalyst sample weight, the amount of desired product (MA) produced using α-SiC (2μm) mixed VPO catalyst decreased as the weight percentage of α-SiC (2μm) in VPO increased. The best range of loading of α-SiC (2μm) in VPO was found to be between 6-25wt%. Loadings of approximately 10wt% α-SiC (2μm) modified VPO catalysts reduced the temperature of *n*-butane conversion to MA approximately 20% of the reported reaction temperature. This is presumed to be attributed to increased thermal dissipation. Higher loadings showed no increase in yield indicating that α-SiC shows no intrinsic catalytic activity toward MA.

Samples containing Pd as a promoter with or without the addition of α-SiC had a higher selectivity and yield to MA. The optimum system investigated in this study consisted of 1.5wt%Pd/10wt% α-SiC/VPO. This newly developed catalyst formula

lowered the reaction temperature 28% from around 420 to 300°C as compared to bulk VPO resulting in an 84% *n*-butane conversion to products at reaction temperature (420°C) and a 25% total product yield.

Chapter 5: Fischer-Tropsch Synthesis Using Cobalt Silica Supported Catalysts

5.1 Introduction and Literature Review

The Fischer-Tropsch synthesis (FTS) process is a catalyzed chemical reaction in which carbon monoxide and hydrogen (synthesis gas) are converted into gaseous and liquid hydrocarbons. Typical catalysts used are based on iron and cobalt. The reaction is highly exothermic, and the reactor must be designed for adequate heat removal to control the temperature and avoid catalyst deterioration and carbon formation. The sulfur content of the synthesis gas must be extremely low to avoid poisoning the catalyst. In the 1980s, expensive investments in the FTS research and development programs picked up again in major petroleum companies [4]. The global resurgence of interest in FTS has been primarily driven by the problems of utilization of stranded gas, diversification of sources of fossil fuels, and environmental concerns. Synthetic liquid fuels generally have a very low content of sulfur and aromatic compounds compared to gasoline or diesel from crude oil. FTS has been considered as a part of gas to liquids (GTL) technology, which converts natural and associated gases to more valuable middle distillates and lubricants. The abundant reserves of natural gas in many parts of the world have made it attractive to commission new plants based on FTS technology. In 1993, the Shell-Bintulu 12,500 barrels per day (bpd) plant came into operation. In 2006, the Sasol-Oryx 34000 bpd plant was inaugurated. In Nigeria, Shell and Exxon signed the agreement on building 140,000

and 150,000 bpd GTL FTS plants in Qatar [4]. After several decades of research and development, FTS technology has finally come to the stage of full scale industry and worldwide commercialization [37]. In this work, the focus is on cobalt based catalysts. The reasons behind choosing cobalt over iron is its resistance to deactivation compared to iron, cobalt has higher activity and rate of CO conversion, produces pure paraffinic hydrocarbons (HC) and is less affected by water gas shift (WGS) reaction [38,39]. For all these reasons, cobalt based catalysts are considered the state of the art and most promising technology.

Catalyst synthesis, characterization, and evaluation of catalytic performance are the primary and probably most important stages in the design of cobalt FTS catalysts. Different catalyst synthesis routes, promotion with noble metals and metal oxides, catalyst pretreatments, and support effects provide efficient tools to control the structure and chemical, physical, and mechanical properties of cobalt based catalysts. The bulk and surface structure of cobalt supported catalysts can be identified by a wide range of characterization techniques. The most relevant information about the active phases can also be extracted from *in-situ* measurements because the catalyst structure and catalytic performance can evolve during different pretreatments and FT reaction. A fixed-bed reactor with plug flow dynamics which operates in the kinetic regime and in the isothermal mode at (H_2/CO) =2 and 2-3 MPa of total pressure probably provides the most suitable methodology for preliminary evaluation of the performance of cobalt FTS catalysts [40,41] and this was the reason behind choosing a fixed-bed microreactor system in this work.

Information about the nature of the active sites is crucial for the design of cobalt FTS catalysts [42]. There is currently a consensus in the literature that FTS proceeds on cobalt metal particles. The decrease in the number of cobalt active sites (catalyst deactivation) is one of the reasons responsible for the decrease in catalyst performance. In addition to active cobalt metallic phases, a working catalyst contains several other cobalt species: cobalt carbide, cobalt oxides, and cobalt support mixed compounds (silicates). Other than metallic cobalt, the remaining species are not directly involved in FTS. Oxidized cobalt species (Co_3O_4, CoO) do not catalyze FTS since they do not have any active sites [43]. However, upon reduction under H_2, during the activation procedure, the cobalt oxide phases reduce to metallic active cobalt sites on which the FTS reaction takes place. CO adsorbs and dissociates on the active cobalt species in linear, step side or bridge type adsorption, thus initializing the HC chain growth as shown in Figure 5.1. Oxidation of cobalt metallic species during the reaction leads to catalyst deactivation. This is one of the major issues faced in cobalt based FTS catalysts. Although, cobalt based catalysts are considered highly active and maintain its activity over longer periods of time versus iron based FTS catalysts. Still, the studying and investigation of the mechanism and role of these cobalt species will help understand the FTS process and the reaction mechanism [44]. It will also provide the basis for synthesizing better cobalt catalysts.

Catalyst synthesis can be done by the incipient wetness impregnation (IWI) method of any soluble cobalt salt such as cobalt nitrate in an organic or aqueous medium or by precipitation of the salt using an agent. The IWI technique was chosen in a deionized water medium since it disperses the cobalt species solution into the high

surface area dry porous support without the need of any precipitation chemical agents. In the IWI technique, the volume of the added metal containing solution must be equal to the porous volume of the silica support. It also must completely impregnate the support. Capillary action draws the solution into the pores. The incipient wetness occurs when all pores of the support are filled with the liquid and there is no excess moisture over and above the liquid required to fill the pores. Although at the first sight the practical execution of incipient wetness impregnation is simple, the fundamental phenomena underlying impregnation and drying are extremely complex. Reproducible synthesis of cobalt catalyst requires careful control of all impregnation parameters: temperature and time of support drying, rate of addition of impregnating solution, temperature and time of drying. The initial repartition of cobalt on the support depends to a larger extent on the type and concentration of hydroxyl groups on the support surface and pH of the impregnating solution. At the stage immediately after impregnation, the interaction between the metal precursor and the support is relatively weak, thereby allowing redistribution of the active phase over the support body during drying and calcination. Calcining the catalyst is done to drive off the volatile components within the solution, thus depositing the metal on the catalyst surface.

The purpose of this work is to focus on the role of these oxides and other compounds formed during synthesis and reaction and their interaction with the support. The presence of these phases, distribution and the degree of reducibility to active cobalt sites are all major aspects that influence the rate and selectivity to produce desired HC products in the FTS reaction. Characterization using XRD, XPS and FTIR will help

understand the role of the cobalt phases in order to produce optimized catalysts and thus helping improve selectivity and yield.

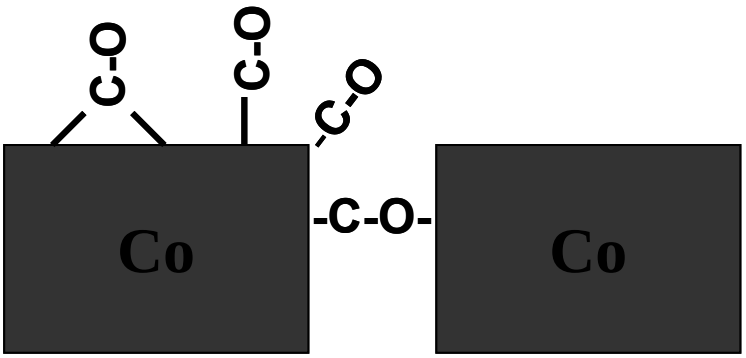

Figure 5.1: Carbon monoxide types of adsorption on an active Co cluster. Linear, step side and bridge type adsorptions. Schematic adapted from reference [45].

Most of the work done on FTS has focused on either development of the reactors and processes or kinetic and mechanistic aspects of this reaction. However, more research needs to specifically address recent developments in the design and characterization of the cobalt mixed oxides and metal support interactions. It is well established that during calcination the cobalt nitrate decomposes to nitrous fumes and CoO [46-48]. This species is oxidized and also migrates to form Co_3O_4 [49,50]. It is also known in literature that Co_3O_4 reduces to CoO under H_2 which then reduces to active metallic cobalt sites [51]. These two oxides are the primary species that determine the rate and activity of the FTS reaction since Co II and Co III oxides are the main source of active cobalt metal sites. However, there is a lot of contradiction in literature on which oxide is formed at a higher rate during calcination. Literature does not provide definite conclusions on the interactions between those two oxides and the silica support in particular. Another species, cobalt silicate is formed due to the reaction between the silica support and the oxides in presence of water [52-54]. Cobalt silicate does not reduce to active metallic

cobalt upon reduction at normal reduction temperatures up to 500°C [55]. Due to that fact, cobalt silicate formation is usually associated with catalyst deactivation [56]. Literature does not provide a conclusion whether cobalt silicate forms during catalyst preparation or after calcination or even after reduction. It has been claimed by some authors that cobalt silicate forms during catalyst preparation [53,54]. Puskas *et al.* claimed recently that cobalt silicate does not form during impregnation or calcinations but is created during the reduction procedure [57]. The goal of this work is to identify cobalt species such as cobalt silicate and determine the conditions and mechanism of its formation. Another goal is to contribute to the literature by clarifying the controversy surrounding the stage at which cobalt silicate is formed. The experimental work was focused on the effects of calcination temperature and support surface area on the formation of this phase and in turn, its effect on the activity of FTS prepared catalysts.

Characterization using XRD, XPS and FTIR will identify these species and their role in order to produce optimized catalysts and thus help improve selectivity and yield. As mentioned, a fixed-bed reactor was used to screen catalyst samples. An FTIR equipped with a gas-cell was also used to analyze the effluent gas from the reactor to evaluate the catalyst performance.

The catalytic performance of FTS catalysts strongly depends on the methods of catalyst preparation. Preparations of cobalt supported catalysts involve several important steps: choice of appropriate catalyst support, choice of method of deposition of the active phase as discussed earlier, catalyst promotion, and oxidative and reductive treatments [58-60].

5.2 Support Selection

Both the structure and performance of cobalt catalysts depend on the catalytic support. The principal function of the catalyst support is to disperse cobalt species and produce stable supported cobalt metal particles in the catalysts after reduction. In addition, the porous structure of the support could control the sizes of supported cobalt particles. FTS is a highly exothermic reaction. Catalytic supports also dissipate the heat released by the FTS reaction and thus reduce a temperature gradient in fixed-bed reactors. The support could also affect the structure and electronic properties of small cobalt metal particles. Ishihara *et al.* suggested that electron donor supports could enrich the electron density of the cobalt active phase and thus ease cleavage of the C-O bond in adsorbed carbon monoxide [48]. The support could react with cobalt species forming cobalt support mixed compounds as discussed earlier. The texture of the support modifies diffusion of reagents and products inside the catalyst grains. In addition, support texture could affect diffusion and capillary condensation of the reaction products in the catalyst pores. Therefore, narrow pores are more likely to be filled by liquid reaction products than wider ones. Capillary condensation in narrow mesopores would lead to diffusion limitations due to more difficult access for the reacting molecules to the catalyst through the gas liquid interface [61,62]. Several authors claim an increase in FTS rate when cobalt is supported on silica versus other supports like alumina and titania. This is due to the fact that silica supports decrease the selectivity to produce water thus lowering catalyst deactivation rate [63]. Another advantage is that cobalt silica interaction is minimal when the catalyst is prepared thus decreasing the rate of undesired phase formation like cobalt silicate [64]. However, the most important reason behind choosing

silica is the ability to disperse cobalt more uniformly on the surface of the support in comparison to other supports. For these reasons, silica was the first choice of support in this work.

5.3 Investigating Metal Support Interaction in Cobalt Silica Catalysts

The cobalt oxide phases (CoO and Co_3O_4) are considered desirable and easily reduced to active metallic cobalt particles [65]. These oxides deposit on the silica surface when the precursor cobalt nitrate solution is decomposed. Synthesis of highly dispersed cobalt catalyst requires strong interaction between the support and the cobalt precursor but such strong interactions generally lower reducibility of such precursors and promote the formation of undesired phases such as cobalt silicate [66]. Cobalt silicate is considered inactive for FTS since it has no cobalt metal sites. Tsubaki *et al.* [66] found that the texture, crystallite phase and acidity of silica are influenced by the hydrothermal treatment with solutions. The reducibility of supported cobalt was closely associated with the silica surface properties. The concentration, distribution, and nature of hydroxyl groups (silanols) on the silica surface also play an important role in the formation of cobalt species and later the dispersion of supported metal on the silica surface [67]. Ming and Baker [68] reported that the catalytic performance of cobalt silica gel FTS catalyst was strongly affected by preparation conditions such as the pH value of the impregnation solution which changed the interaction of cobalt and silica support, resulting in different metal support interaction (MSI), dispersion and reducibility of the supported cobalt species.

5.4 Cobalt Silicate Chemistry

Prior work done on Co/silica supported catalysts has mainly focused on cobalt dispersion, reduction, preparation and pore size distribution. In this study, the cobalt species support interaction leading to the formation of undesired cobalt silicate phase and, its influence on the activity and performance of the catalyst are presented. The reported results suggest disagreement on the chemistry and stage at which cobalt silicate form. Kogelbauer *et al.* [53] found that the presence of cobalt metal is necessary for cobalt silicate formation and is enhanced by the presence of H_2 depending on exposure time and gas phase concentration. Other literature findings [54] have postulated that an intermediate cobalt silicate surface phase is formed during the initial decomposition of the cobalt nitrate precursor during preparation or by a reaction between the aqueous cobalt complexes and surface silanol groups which is enhanced by using metal salts decomposed during thermal treatment. Ernst *et al.* [61] attributed the formation of cobalt silicate during reduction to the reaction of unreduced CoO with silica to form high surface area cobalt orthosilicate:

$$2CoO + SiO_2 \rightarrow Co_2SiO_4 \tag{5.1}$$

Puskas *et al.* [57] proposed a more detailed reaction pathway:

$$CoO + H_2O \rightarrow Co(OH)_2 \tag{5.2}$$

$$Co(OH)_2 + SiO(OH)_2 \rightarrow CoSiO_3 + 2H_2O \tag{5.3}$$

The reaction of finely dispersed cobalt oxide and water during reduction result in molecular cobalt hydroxide formation. Migrating silicic acid then reacts with cobalt hydroxide to produce cobalt silicate. This mechanism can also occur following

impregnation in water during the preparation and drying/calcination stage. The active surface silanol groups form silicic acid which reacts with cobalt hydroxide to form highly amorphous FTS inactive cobalt silicate [53]. The surface area of the silica support can remarkably influence the resultant FTS catalyst performance. The metal support interaction during preparation, drying and calcination is an important aspect in the synthesis of highly active FTS catalysts.

5.5 Catalyst Preparation

Commercially available silica gel (Davisil grade 646, 635 and 710) was used as a support. An aqueous solution of cobalt nitrate was impregnated into the various silica supports by incipient wetness impregnation method using appropriate volume of deionized water. Aqueous ammonium hydroxide was added to keep the pH between 4-5. The loading of cobalt was 20wt% for all catalyst samples. The particle size was kept between 0.25-0.5mm. The series of supported Co catalysts, silica supports structural properties, drying and calcination times and temperatures are shown in Table 5.1.

The calcined samples were reduced in H_2 at 623K for 12h at high space velocity ($2000h^{-1}$) and 1 atm at a ramping rate of 1K/min. Co/silica catalyst sample 300Co-1 was used as a comparing reference. Catalysts 1-3 have different silica support characteristics but were prepared under the same controlled conditions. Catalysts 1, 4 and 5 have the same silica support characteristics (Davisil-646) differing in drying and calcination conditions only.

Table 5.1: Silica support structural properties used in catalyst samples. Drying and calcination conditions are also presented.

Catalyst ID	Silica support properties			Drying Temperature/ Time (K)/ (h)	Calcination Temperature/ Time (K)/ (h)
	Pore vol. (cm^3/g)	Pore Dia. (nm)	BET SA (m^2/g)		
300Co-1	1.15	15	300	298/ 24	573/ 3
480Co-2	0.75	6	480	298/ 24	573/ 3
560Co-3	0.7	5	560	298/ 24	573/ 3
300Co-4	1.15	15	300	393/ 16	673/ 3
300Co-5	1.15	15	300	393/ 16	773/ 3

The FTS reaction was carried out in a fixed-bed catalytic reactor consisting of a tube with an inner diameter of 6mm placed in a programmable furnace. The reduced catalyst of 1.0 g was loaded vertically in the reactor. Void fraction was calculated to be around ~30% by subtracting the volume of the catalyst particles from the volume of the reactor bed. Gas flows were regulated via programmable flow controllers with a static, inline mixer prior to the furnace inlet. The reaction conditions were P (total) = 0.8 MPa, T=503K, CO/H_2=1/2. Gas space velocity was kept at $1500h^{-1}$. The reaction product samples were taken at 1h intervals and analyzed by online FTIR and GC. The analysis of hydrocarbons dissolved in a solvent after condensing in a cold trap was carried out with gas chromatograph-flame ionization detector (GC-FID) using a customized DB-2887 column. Conditioning was reached after 6h time on stream. The reaction time was 48h, and the activity of the catalyst was relatively stable during this time period.

5.6 Catalyst Characterization

Characterization was performed on all powder catalyst samples at three different stages: after preparation before calcination, after calcination before reduction and after

FTS reaction. XRD, XPS, BET and FTIR-ATR were the tools used to characterize these samples as will be discussed in the following sections.

5.6.1 XRD Characterization

The XRD spectra of the catalysts were measured using a Philips Pananlytical X'Pert X-ray diffractometer using Cu Kα radiation in a 0.02° step-scan mode in the 20-75°2θ angular regions. A tube power of 40kV and 30mA was maintained for all runs.

X-ray diffraction was used to verify the co-existence of cobalt oxide species following impregnation /calcination and after 48h reaction time. The XRD patterns of selected catalysts at different stages are illustrated in Figure 5.2.

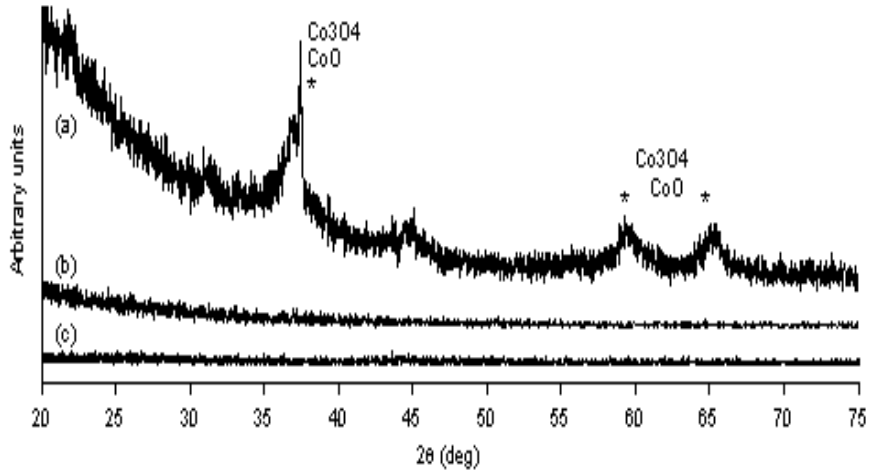

Figure 5.2: The XRD patterns of different cobalt silica supported catalysts. (a) Calcined 560Co-3, (b) after 48h FTS 560Co-3 and (c) after 48h 300Co-5.

Sample 560Co-3 after calcination but before reaction showed diffraction peaks at 36.8°, 45.1°, 59.5° and 65.5° indicating the presence of CoO and Co_3O_4. XRD measurements of the remaining catalysts after calcination showed similar patterns but with different peak intensities. The two oxides can co-exist on the catalyst surface after

calcination. Large clusters of Co_3O_4 can form via oxidative aggregation of small amounts of CoO [65].

Following reduction and 48h FTS, the XRD diffraction peaks of sample 560Co-3 have disappeared, indicating structural irregularity and no cobalt oxide. However, highly amorphous cobalt silicate could exist on the surface after FTS reaction. The used catalyst 300Co-5 XRD patterns also showed no cobalt oxide species on the catalyst surface. Therefore, XRD is not preferred for amorphous cobalt silicate identification. Further characterization using IR spectroscopy was required to verify the effects of surface area and calcination temperature.

5.6.2 FTIR-ATR Analysis

A BIO-RAD Excalibur FTS3000 FTIR equipped with a permanently aligned gas-cell was used to analyze the effluent. The 60mm diameter gas-cell provided an infrared beam path length of 2.4m and consisted of a borosilicate glass body with a KBr window and a total volume of 0.1 liter. An MCT detector was used, with an effective range of analysis between 400 and 4000 cm^{-1} wavenumbers. To obtain spectra of the fresh, calcined and reacted (48h) powder catalysts, a Pike Technologies diamond MIRacle single reflection horizontal attenuated total reflectance (HATR) unit designed for use in the FTIR spectrometer was utilized. 500 scans were recorded for each sample at a resolution of 4 cm^{-1} to ensure consistency in all catalyst sample runs. ATR correction was performed using Digilab Win IR Pro version 3.4 software. Boxcar (3 points) was used as a smoothing function for all collected spectra.

Selected IR spectra are shown in Figure 5.3. All catalyst samples were analyzed using IR spectroscopy to investigate the effect of varying the surface area on the MSI which could lead to the formation of cobalt silicate. Figure 5.3a shows the transmittance of silica (1100, 975, 800 cm^{-1}) for the dried catalyst 300Co-1. The spectrum also confirms the absorbance of the nitrate group (1610, 1365, 842 cm^{-1}) [69] indicating the existence of some cobalt nitrate residue due to low drying temperature. The spinel Co-O bond absorbance peak corresponding to Co_3O_4 is clearly visible around 667 cm^{-1}. Another weak Co-O absorbance peak exists around 580 cm^{-1} probably due to small amounts of CoO formation. The small amounts of CoO are explained by the possible oxidative aggregation of CoO to large clusters of Co_3O_3. Figure 5.3b represents the dried catalyst sample 480Co-2 which has similar IR features as sample 300Co-1 as well as the other dried catalyst samples prepared but with different peak intensities. It is also observed that the ratio of the intensity of the Co-O peak assigned to Co_3O_4 to the Si-O silica stretching peak intensity in spectrum (b) is less than the ratio of the Co_3O_4 peak to the silica peak in spectrum (a) sample 300Co-1. Furthermore, the dried sample 480Co-2 spectrum does not show any indication of CoO formation. This leads to the conclusion that lower surface area sample 300Co-1 contained more desired surface cobalt oxide species than sample 480Co-2. To explain why some catalyst samples contain more desired cobalt oxide species, we go back to the initial mixing of the cobalt precursor and the various surface area silica supports. After mixing, the cobalt positive ions are attracted to the silica support pores by adjusting the pH using aqueous ammonia so as to maintain a negative charge through the silica surface. If the pH value is 2-5 (preferably around 4.5) then the surface is negatively charged and the cobalt ions are dragged to the

pores by capillary action. If the pH value is less than 2 then the silica surface is positively charged, thus repulsing the bulk of cobalt cations from the porous silica surface. Cobalt cations at pH less than 2 and higher than 5 can react with hydrated silica surface (SiOH groups) forming cobalt silicate. In addition, these cations can react with the nitrate ions and the surface SiOH groups forming complexes that could hinder the deposition of cobalt ions in the pores thus affecting the dispersion of cobalt ions and ultimately upon drying and calcination the amount of desired cobalt oxide species formed. Lower support surface area leads to less surface SiOH group formation during preparation and thus less MSI. Puskas *et al.* [69] found using infrared spectroscopy much less than expected Co_3O_4 formation upon calcination when silica was used as a support. This is also explained by the reaction between CoO and SiO_2 during calcination which prevented large amounts of CoO from further oxidation to form Co_3O_4. Interestingly, sample 480Co-2 does not show any nitrate ion peak absorbencies. This is due to a possible interaction between the hydrated silica in the higher surface area sample 480Co-2 and the nitrate ion during preparation. The peak around 1640 cm^{-1} is assigned to hydroxyl groups. The dried sample 480Co-2 contains more hydroxyl groups (SiOH) than the dried sample 300Co-1. Thus, the existence of silanol groups (SiOH) on the silica surface plays an important role in the formation of cobalt species.

The calcined spectrum of sample 300Co-1 (Figure 5.3c) is shown. Si-O stretching bands are clearly visible. As expected, the absorption peaks of Co_3O_4 are confirmed around 667 cm^{-1} and 580^{-1}. The calcined spectra of other samples were essentially the same but with different peak intensities. The spectrum (d) of calcined sample 560Co-3 in Figure 5.2 confirmed the effect of surface area on the resultant cobalt species formed on

the support surface. While Co_3O_4 is confirmed on the surface by the Co-O vibration band at 667 cm^{-1}, it is also noticed that the broad absorbance peak of Si-O (1100 cm^{-1}) has disappeared and a new broad peak around (1020-1036 cm^{-1}) assigned to Si-O-Co bond has formed. This is the characteristic peak assigned to cobalt silicate [57]. The high support surface area of sample 560Co-3 has enhanced the interaction of silica and the cobalt cations during the initial decomposition of the cobalt nitrate precursor upon mixing in the presence of water. This resulted in the formation of aqueous cobalt complexes as well as the attraction of less cobalt ions to the pores. Upon drying and calcination, less cobalt oxide species was formed as evident when comparing the ratio of silica to cobalt oxide absorbance peaks in both spectra (c) and (d). Cobalt silicate formation is enhanced by using metal salts decomposing during thermal treatment [70] and is a result of a reaction between the aqueous cobalt complexes and silanol groups existing on the silica surface. The calcined sample 300Co-5 (not shown) had a similar spectrum as spectrum (d) but with less cobalt silicate peak intensity which indicates that high drying and calcination temperatures also facilitate cobalt silicate formation due to sintering and silica migration as well [57,69,70]. Surface area supports higher than 560 m^2/g resulted in strong interaction between the silica surface and the cobalt cations during preparation leading to the formation of more cobalt complexes and undesired cobalt silicate. Indeed, Puskas *et al.* [69] found that the rate of cobalt silicate formation correlates to the surface area of the silica support.

The last spectrum (e) of sample 480Co-2 after 48 h. FTS confirms the formation of cobalt silicate during the reduction and reaction stage via the unreduced CoO reaction with silica mechanism in the presence of water [61]. Water is formed during H_2 reduction

and as a byproduct during FTS. Furthermore, Puskas *et al.* [69] inferred that the high cobalt loading (13-30wt %) generated more water during reduction resulting in formation of large amounts of cobalt silicate. Our FTIR results agree with their findings, since the loading percentage of cobalt in our samples was kept at 20wt% and that considerable amounts of cobalt silicate were formed upon reduction as a result of the large amount of water generated.

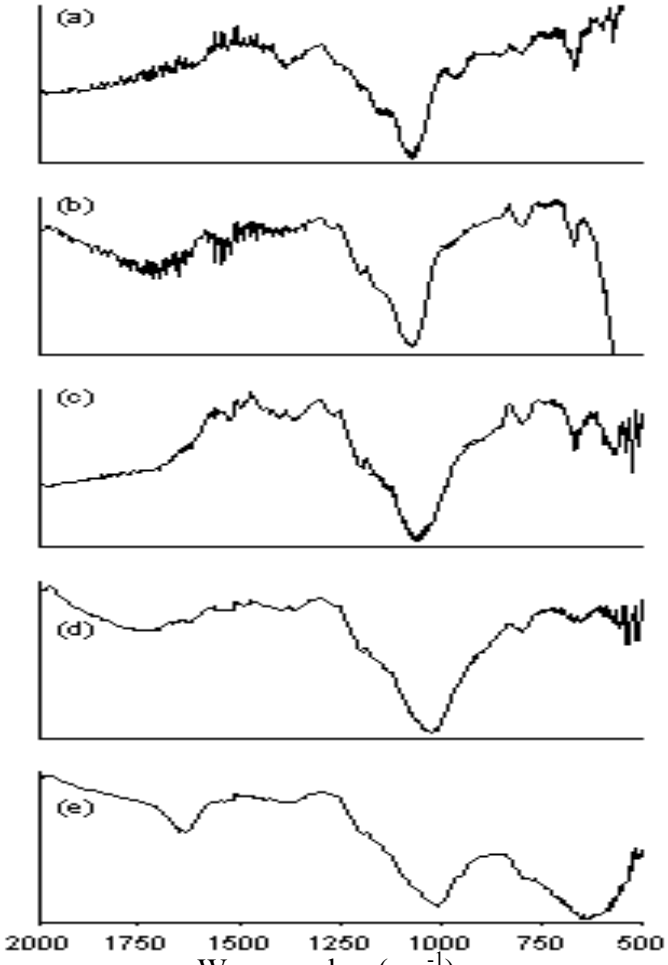

Figure 5.3: Selected IR spectra of different cobalt silica supported catalysts. (a) Dried 300Co-1, (b) dried 480Co-2, (c) calcined 300Co-1, (d) calcined 560Co-3 and (e) after 48h FTS 480Co-2.

Any cobalt species not reducible during the H_2 reduction stage up to 1073K has been identified as cobalt silicate [71]. However, the amount of cobalt silicate formed during reduction differs. An important feature in spectrum (e) is that the intensity of cobalt silicate assigned peak and cobalt oxide assigned peak is almost the same for sample 480Co-2. This result was also true for sample 300Co-1 after 48h reaction time. The amount of cobalt oxide in those two samples after reaction is still considerable meaning those two samples can still carry on FTS for longer periods of time. The ratio of the assigned cobalt oxide peak to the assigned cobalt silicate peak in those two samples is much higher than the same ratio for sample 560Co-3 as shown in spectra (e) and (d) respectively.

5.6.3 XPS Analysis

A Perkin-Elmer Phi 560 ESCA/SAM system was used to verify the loading of the cobalt on the silica support and to investigate the cobalt phase present in the powder catalyst samples after synthesis and after reaction. Al Kα radiation at 1486.6 eV was used as the excitation source. The C 1s line at 284.6 eV was used as a reference. Measurements of the positions and the intensities of the Co $2p_{3/2}$ binding energies provided an opportunity to qualify the existing cobalt phases on the catalyst surface. Figure 5.4 verifies the amount cobalt species on the surface of the catalyst. The survey analysis indicates approximately 20 at% Co on the surface for sample 300Co-1. The concentration of adventitious carbon should be noted. Adventitious carbon is adsorbed on the surface of all samples and is a common contaminant detected by X-ray photoelectron spectroscopy (XPS) on solid surfaces exposed to air [56]. All catalyst samples analyzed

showed similar results and all contained around the same concentration of adventitious carbon.

Figure 5.5 represents the Co 2p orbital high resolution spectra of sample 560Co-3 together with the spectra of pure CoO and Co_3O_4 samples as a reference. The fresh catalyst sample two main Co 2p peaks (blue) are shifted to a higher binding energy than the two oxide references (black), which means higher Co oxidation state. This is due to cobalt silicate formation during the preparation/calcination stage of this high support surface area catalyst which interacts and limits the formation of desired cobalt oxide.

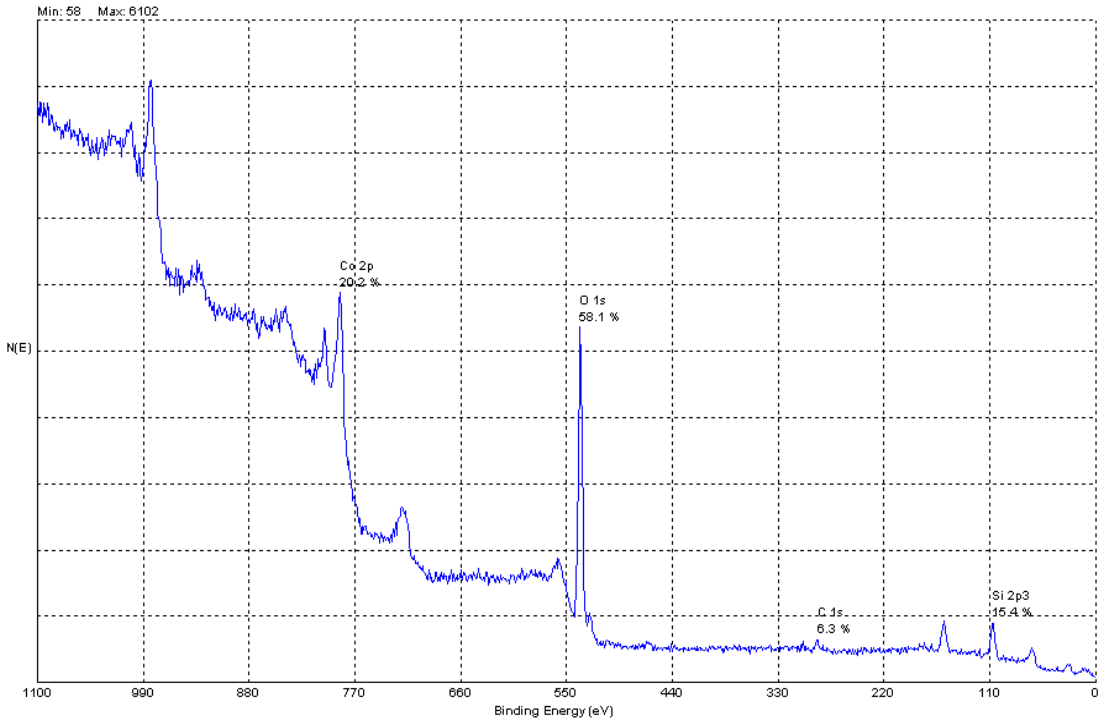

Figure 5.4: XPS survey for sample 300Co-1 showing atomic % of elements. 20 at% Co is present in the system.

The after reaction spectrum show similar binding energy as the fresh before reaction catalyst which means cobalt silicate still existed among other oxides in the

system. However, the intensity was much lower indicating less species concentration which is typical for after calcination sample analysis [61].

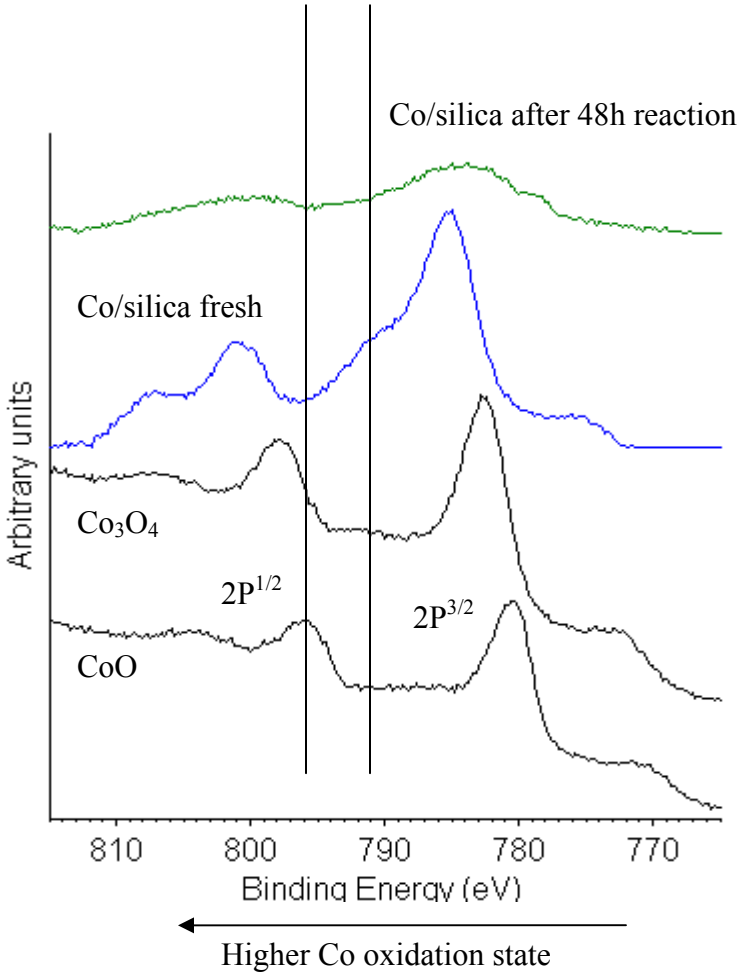

Figure 5.5: XPS high resolution spectra of Co 2p orbital for sample 560Co-3. The spectra are for fresh before reaction and after reaction samples. CoO and Co_3O_4 spectra are shown as a reference.

5.7 Effects of Drying and Calcination Temperature

The BET surface area and pore volume of the catalysts were determined by N_2 physisorption using a Quantachrome AUTOSORB-1 automated system. Each sample was degassed in the system at 573K for 4h prior to N_2 physisorption.

BET was used to study the loss of surface area (SA) for all catalyst samples after calcination and reaction as shown in Table 5.2. All catalysts were degassed for at least 4h at 573K before N_2 physisorption to ensure all products formed in the pores were eluted. It was found that the loss of surface area after calcination depends on the calcination temperature, the higher the calcination temperature the more significant the surface area loss as is evident in sample 300Co-5. This is due to silica migration which occurs at temperatures higher than 573K for silica [69]. It is known that high surface area (>200m^2/g) reactive silica favors silica migration [57]. Furthermore, the loss of SA can also be attributed to the filling of pores with impregnated cobalt species.

Table 5.2: BET surface area and BJH pore volume for all catalyst samples.

Catalyst ID	BJH pore volume (cm^3/g)			BET surface area[a] (m^2/g)		
	Support	Calcined	After 48h	Support	Calcined	After 48h
300Co-1	1.15	0.85	0.73	300	254	231
480Co-2	0.75	0.67	0.57	480	356	319
560Co-3	0.70	0.59	0.50	560	408	375
300Co-4	1.15	0.82	0.66	300	243	206
300Co-5	1.15	0.68	0.48	300	209	168
[a] Error of measurement = ±10%						

The loss in surface area after reaction is attributed to cobalt particle agglomeration which occurs during H_2 reduction where cobalt metal atoms agglomerate forming larger crystalline metal particles. Another reason for this loss is that the long chain HC products which form during the reaction but fail to desorb from the surface result in clogging of the surface pores which leads to further loss in surface area. This explains the drop in the BJH adsorption pore volume for catalyst samples after reaction. It is also noticed that the difference in surface area loss is more evident after calcination than after reaction, this is attributed to the formation of high SA amorphous cobalt silicate as a result of metal support interaction during reduction which counters the loss in surface area due to cobalt

particle agglomeration or silica migration. From the IR and BET results on all sample catalysts after calcination and after 48h reaction, it was found that the activity to FTS was in the following order: sample 300Co-1>480Co-2>300Co-4>560Co-3>300Co-5.

Theoretical calculations of the amount of sintering and activity for all samples are presented in Appendix E.

5.8 Catalyst Performance and Activity

FTS reaction was conducted for 48h in a fixed-bed microreactor for all catalyst samples. Performance parameters after reaching steady state (6h) are reported in Table 5.3. It can be seen from the table that sample 300Co-1 exhibited the highest CO conversion (78.1%) and the lowest CH_4 and CO_2 selectivity. The space time yield (STY) and activity are also the highest for this sample and drop as the surface area of the catalyst increases. As discussed earlier, large surface area of the support increases metal support interaction resulting in formation of cobalt silicate which in turn, limits the number of active metallic sites. The pore size of the silica support affects the rate of CH_4 production as is evident by samples 480Co-2 and 560Co-3 (6 and 5nm respectively). Small pore diameter is expected to promote the formation of CH_4 where a large pore diameter >10 nm increases the probability of longer HC chain formations as is evident in sample 300Co-1. The low reaction pressure (8 bar) decreases the solubility of CO and H_2 thus increasing the reaction rate to form larger amounts of CO_2. Furthermore, the relatively low reaction temperatures (~503K) and partial pressure of CO and water enhance the water gas shift to CO_2 and H_2 production, thus resulting in higher selectivity to CO_2.The drying and calcination temperatures had a higher impact on the catalytic

activity of samples 300Co-4 and 300Co-5 where the CO conversion dropped to below 60% for these two samples in comparison to sample 300Co-1 (78.1%) which has the same surface area (300 m^2/g). The higher temperatures of calcination most likely resulted in the sintering and agglomeration of the cobalt particles thus lowering the cobalt active surface area leading to lower catalytic activity after reduction. The structural properties of the silica supports (surface area and pore diameter) had a lower impact on the activity and yield than the drying and calcination temperatures. Samples 300Co-1, 480Co-2 and 560Co-3 had higher CO conversion, activity and yield than samples 300Co-4 and 300Co-5 where the higher drying and calcination temperatures adversely impacted the catalytic activity.

Table 5.3: Catalytic performance of cobalt silica supported catalysts.

Catalyst ID	STY[a] (g HC L^{-1} h^{-1})	Activity[b] (h^{-1})	CO conv. (%)	Selectivity (%)			
				CH_4	CO_2	C_{2-4}	C_{5+}
300Co-1	137	0.29	78.1	4.7	8.6	7.2	79.5
480Co-2	125	0.26	70.7	10.4	9.3	8.9	71.4
560Co-3	98	0.20	62.4	9.5	14.8	13.6	62.1
300Co-4	86	0.18	59.3	8.4	14.7	9.9	67.0
300Co-5	74	0.15	55.6	8.3	21.0	11.0	59.7

Reaction conditions: 0.8MPa, 503K, CO/H_2 = ½, gas space velocity 1500h^{-1}
Weight of catalyst = 1.0 g, Co loading = 20wt%
[a] Space time yield (STY): grams hydrocarbon product per catalyst bed volume including voids in liters per h operation.
[b] Activity: grams hydrocarbon product/ gram catalyst used per 1h operation.

The activity of Co/silica catalysts was studied with reaction time. Figure 5.6 shows CO conversion as a function of time for samples 300Co-1, 560Co-3 and 300Co-5. All other samples showed similar behavior but with different CO conversion values. The CO conversion increases initially as the catalyst conditions due to higher amounts of CH_4 formation. The conversion drops after 22h, but remains relatively stable for the rest of the run. The drop in CO conversion could be a result of cobalt silicate formation which has

no catalytic FTS activity. Another reason could be the filing of the support pores with HC products which can block the active cobalt sites preventing further CO hydrogenation. Sample 560Co-3 (*) showed significant drop in initial CO conversion in comparison to sample 300Co-1 due to stronger MSI which resulted in cobalt silicate formation. Sample 300Co-5 also exhibited significant CO conversion drop. This can be attributed to sintering effects occurring during the high calcination temperature process.

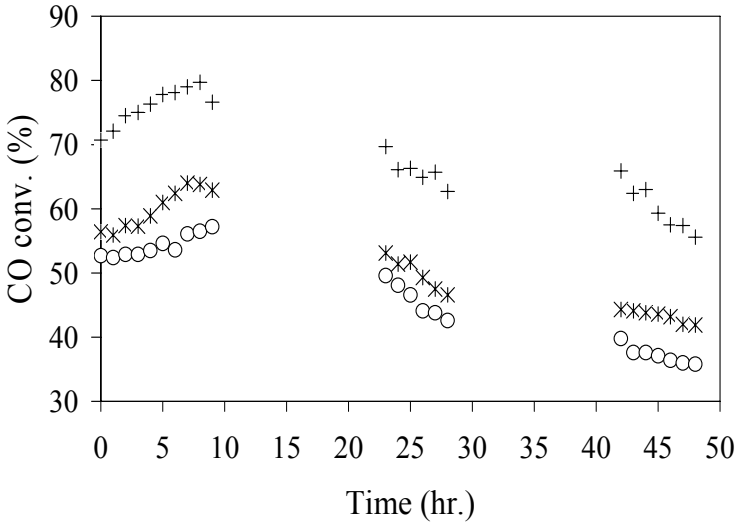

Figure 5.6: CO conversion with time for cobalt silica supported catalysts. 300Co-1 (+), 560Co-3 (*) and 300Co-5 (o). FTS reaction time: 48h.

5.9 GC Product Analysis

An Agilent GC equipped with both TCD and FID detectors was used to analyze the gaseous and liquid HC products respectively. The TCD detector helped, in conjunction with the FTIR gas-cell in the analysis of the gaseous HC in the range of C_{1-4}. Methane and water vapor along with any aromatic product was checked using the FTIR. The FID detector was connected with a customized DB-2887 column. This special column was used to analyze liquid HC in the range of $+C_5$. Jet fuel paraffinic HC range is

known to be between C_9 and C_{15}. The liquid HC product from each catalyst sample run was collected using a cold trap. 1 ml was drawn from each liquid HC product sample to be diluted in 50 times hexane volume. 2 µl injection volumes were administered in the GC inlet to analyze the HC distribution. A sample liquid HC distribution spectrum for sample 300Co-1 is shown in Figure 5.7. The broad initial peaks after 3 min retention time are of the hexane diluent. The HC ranges from C_7 up to C_{23} for this sample. Other catalyst samples HC products showed similar distributions.

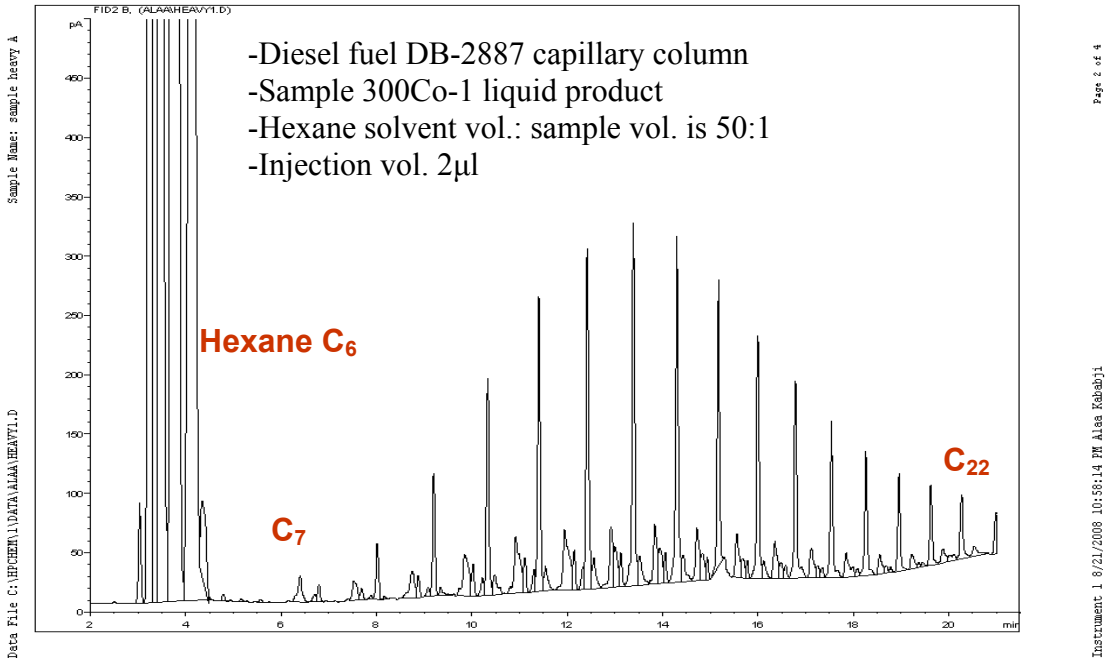

Figure 5.7: GC liquid HC product analysis from sample 300Co-1 after 48h. JP-5 jet fuel contains alkanes with HCs in the range of C_9 –C_{15}. Hexane was used as a product diluent.

Figure 5.8 shows the analysis of the heavy "waxy" product from sample 300Co-1 after injection into the GC. No light HCs were detected. This oily product required mixing with hexane before injection. It only contained the paraffinic HCs C_{14}, C_{17}, and C_{19} besides hexane, the diluent. Other catalyst samples produced similar GC results but with different peak intensities, thus different HC concentration amounts.

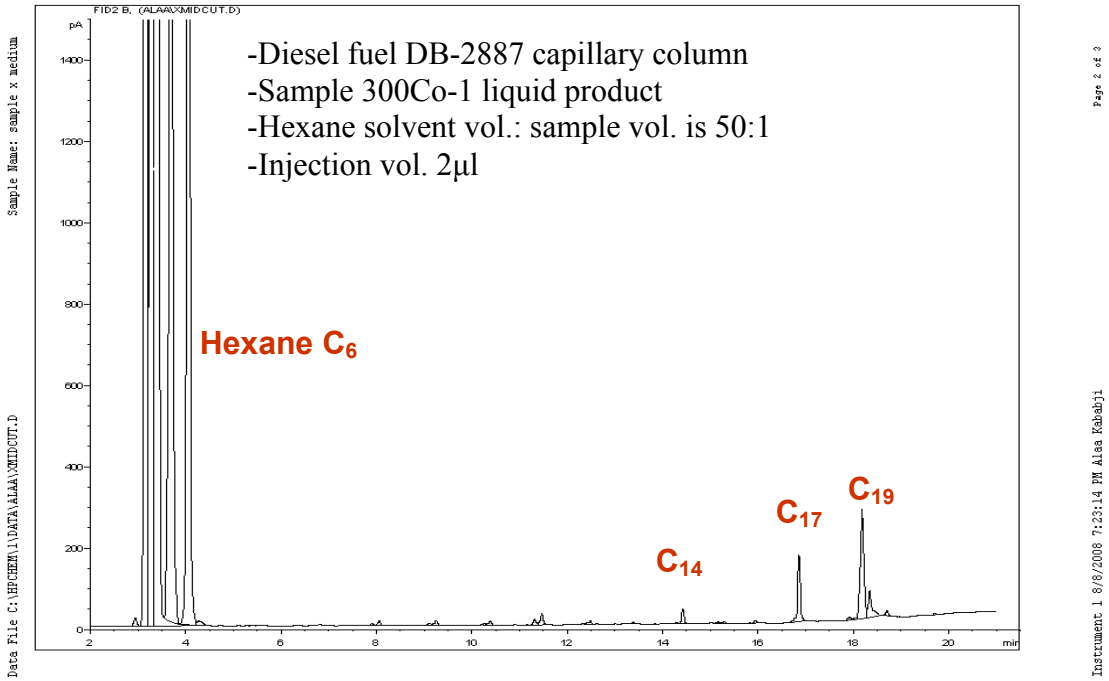

Figure 5.8: GC heavy HC product analysis from sample 300Co-1 after 48h. JP-5 jet fuel contains HCs in the range of C_9 –C_{15}. Hexane was used as a product diluent. No light HC product was detected.

5.10 FTIR-ATR Liquid Product Analysis

To obtain spectra of the liquid HC product, a Pike Technologies diamond MIRacle single reflection horizontal attenuated total reflectance (HATR) unit designed for use in the FTIR spectrometer was utilized. 250 scans were recorded for each sample at a resolution of 1 cm^{-1}.

Figure 5.9 represents the spectrum of the light cut product after running the 300Co-1 catalyst sample. The IR spectrum shows paraffinic alkane C-H vibrations, some olefin product formation (C=C) and also –OH bond stretching vibration indicating some alcohol formation. The clear liquid sample may contain some of the light paraffinic HCs.

GC results also indicated that C_5-C_8 hydrocarbons in addition to alcohols are the main compounds present in this cut.

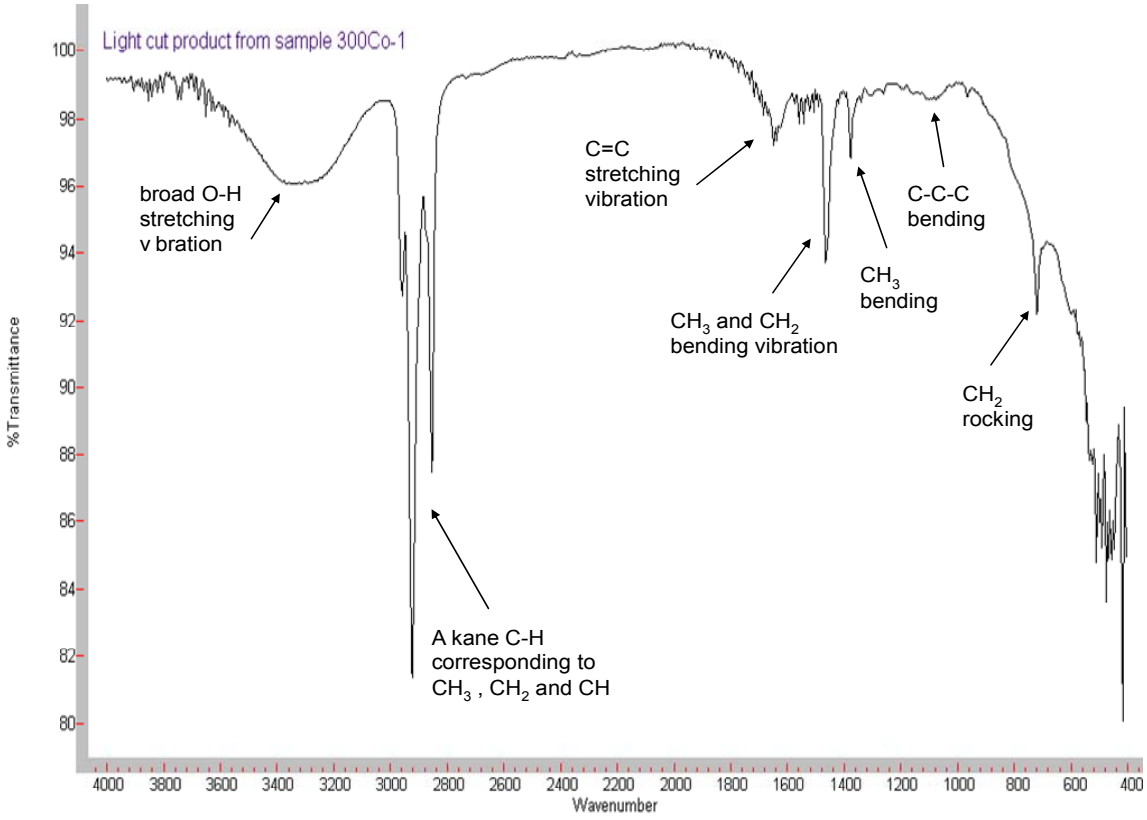

Figure 5.9: ATR spectrum of the light cut product from sample 300Co-1. Small amounts of H-bonded groups are also present. No significant amounts of aromatics are produced.

Figure 5.10 represents the heavy cut oily product from the same catalyst sample 300Co-1. The IR spectrum shows strong alkane C-H bond IR absorptions, very weak alkenes IR absorptions and no indication of any –OH bonded alcohol formation. This oily sample was also run using the GC and produced the analysis shown in Figure 5.7. The paraffinic HC range in this sample was C_6-C_{23}. In addition to the light and oily cuts formed when conducting FTS on all catalyst samples, a wax was also formed in between the gaps of the catalyst bed and also as a product at the bottom of the reactor tube. The

amount of the light cut and oily cut as well as the wax produced differed in each catalyst sample prepared as was explained in Table 5.3.

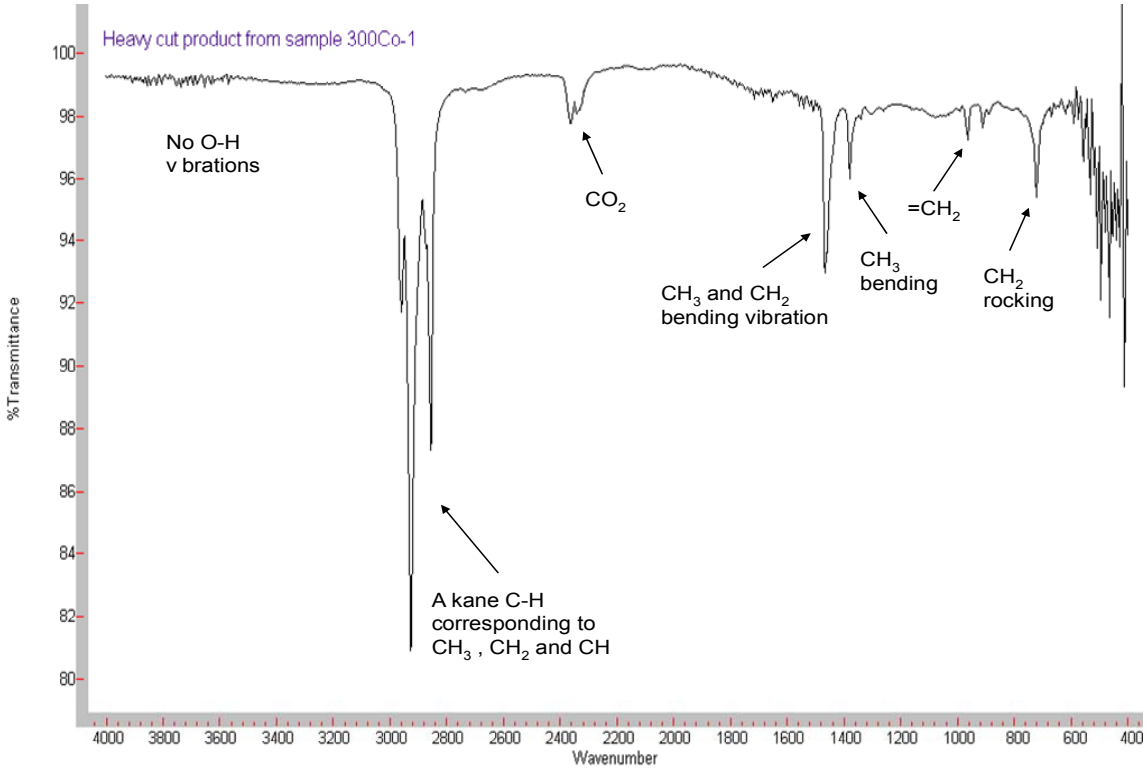

Figure 5.10: ATR spectrum of the heavy oily product from sample 300Co-1. No H-bonded compounds are present. No significant amounts of aromatics are produced.

Figure 5.11 represents the IR spectrum of the waxy product formed in the catalyst bed for sample 300Co-1. The wax accumulates on the reactor walls thus increasing the pressure buildup in the reactor. The Co/silica catalyst particles characteristic IR bond vibrations are also present in the spectrum. The Co-O bond vibration corresponding to cobalt (II) oxide is visible around 680 cm^{-1}. For silica, the Si=O bond IR absorption is clearly visible in the range of 980-1100 cm^{-1}. Small amount of CO_2 and atmospheric water vapor exist in the spectrum. This is due to the fact that some CO_2 and water vapor was trapped between the waxy product and the diamond crystal of the ATR.

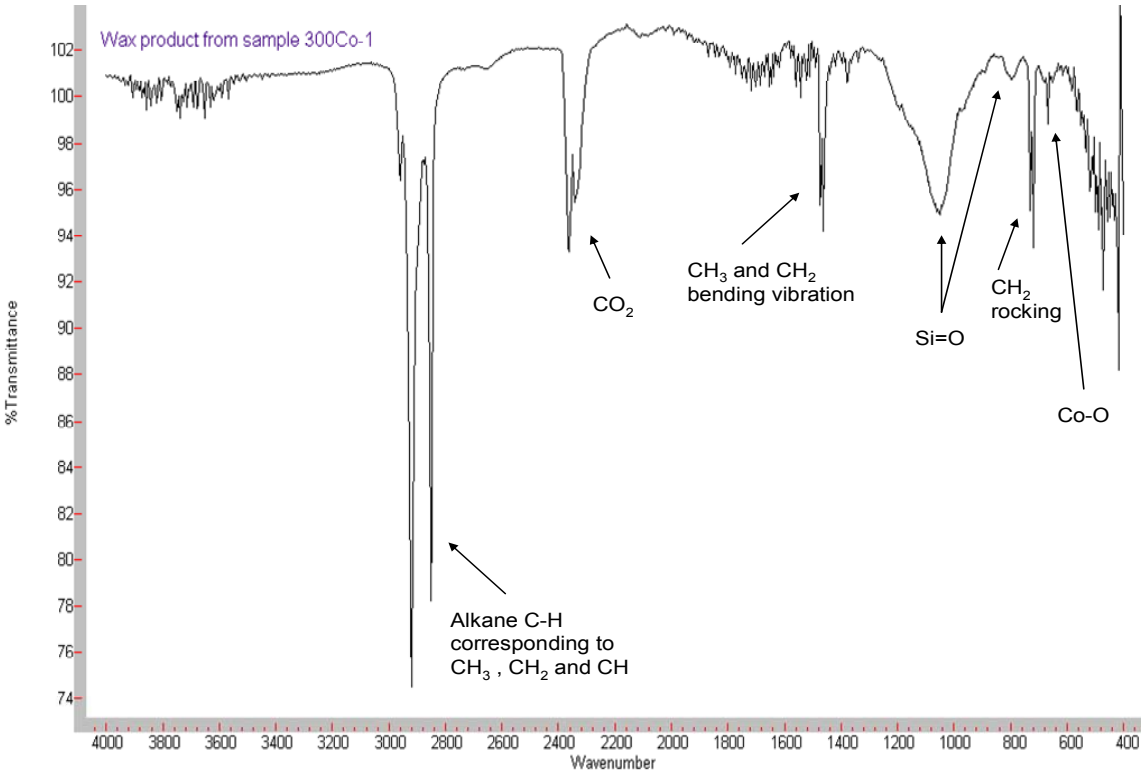

Figure 5.11: ATR spectrum of the wax product from sample 300Co-1. The product forms in between the gaps of the powder catalyst and also accumulates on the reactor tube wall. Alkanes are the main product, no H-bonded compounds are present. No significant amounts of aromatics are produced. The Co/silica catalyst particles representative IR bond absorptions are also visible as cobalt oxide (Co-O) and silica (Si=O).

5.11 Summary

FTS is a very attractive technology since high oil prices continue to persist worldwide. FTS involves the production of ultra high purity synthetic liquid mainly paraffinic fuel from various sources such as biomass, fossil fuels, natural or synthesis gas. In Chapter 5, the effects of calcination temperature and support surface area on the formation of cobalt silicate in Co/silica supported catalysts are explored. FTS catalysts were prepared by incipient wetness impregnation of cobalt nitrate precursor into various

silica supports. Deionized water was used as preparation medium. The properties of catalysts were characterized at different stages using FTIR, XRD and BET techniques. FTIR-ATR analysis of the synthesized catalyst samples before and after 48h reaction identified cobalt species formed during the impregnation/calcination stage and after the reduction/reaction stage. It was found that in the reduction/reaction stage, metal support interaction added to the formation of irreducible cobalt silicate phase. Co/silica catalysts with lower surface area ($300m^2/g$) exhibited higher C_{5+} selectivity which can be attributed to less metal support interaction and higher reducibility and dispersion. The prepared catalysts with different drying and calcination temperatures were also compared. Catalysts dried and calcined at lower temperatures exhibited higher activity and lower cobalt silicate formation. The catalyst sample calcined at 573K showed the highest CO conversion and the lowest CH_4 selectivity.

The results of this study indicate that the support surface area affects the metal support interaction leading to the formation of cobalt silicate. Our results also agreed with the literature conclusion that the bulk of cobalt silicate forms during reduction as a water induced mechanism. It was also concluded that cobalt silicate may form during the catalyst synthesis process depending on many factors such as the pH, cobalt loading percentage and surface area of the silica support and its interaction with the cobalt precursor. The activity and STY of the catalyst samples studied decreased as the surface area of the catalyst increased (300>480>560 m^2/g). This was also true for the CO conversion which dropped as support surface area increased. When catalysts with the same silica support surface area were used, the CO conversion decreased as drying and calcination temperatures increased from 573 to 773K. The same trend was noticed for

activity and STY. This was explained by cobalt particle agglomeration due to sintering and silica migration. The results also indicate that the properties of silica supports affect the product distribution. Catalyst with small pore diameter (<6nm) increased the rate of CH_4 formation.

Chapter 6: Conclusions and Future Work

6.1 Conclusions

This dissertation is focused on two heterogeneous catalytic systems: SiC mixed VPO catalysts for the partial oxidation reaction of *n*-butane to maleic anhydride and cobalt silica supported catalysts for Fischer-Tropsch synthesis. Industrial VPO catalysts undergo severe hotspot formation during the partial oxidation reaction which occurs during the high reaction temperatures of approximately 400°C. The inability to dissipate the heat generated by this highly exothermic reaction affect the catalyst activity, life time and MA yield. The concept of modifying the in-house synthesized bulk VPO catalyst with a thermally conductive material was proposed in this dissertation. α-SiC commercial particles were mixed at different weight ratios with the prepared VPO precursor to investigate the effects of this diluent on the performance of the catalyst. Despite the fact that α-SiC had no intrinsic catalytic activity to produce MA, it did however improve the performance of the VPO catalyst. The experimental work showed that the α-SiC modified VPO catalysts had a 1.5 times longer lifetime than the bulk prepared VPO catalyst. The high thermal conductivity of SiC helped dissipate the heat generated thus lowering the reaction temperature for the sample 10wt% α-SiC (2μm)/VPO approximately 20% than the reported high reaction temperature. Optimum loading of α-SiC was found to be between 6-25wt%. Promoting the VPO catalyst with Pd increased the MA yield

significantly and an optimum catalytic system consisting of 1.5wt%Pd/10wt% α-SiC/VPO lowered the reaction temperature 28% from approximately 420 to 300°C as compared to bulk VPO resulting in an 84% *n*-butane conversion to products at reaction temperature (420°C) and a 25% total product yield. The yield reported in this work is higher than some of the reported MA yield using bulk VPO systems by up to 10%. The work on the SiC modified and Pd promoted VPO catalysts in this dissertation is a pioneering work and literature does not provide sufficient information on addressing this issue regarding VPO catalysts.

The second project in this dissertation was focused on investigating the performance of various cobalt silica supported catalysts used in Fischer-Tropsch synthesis. The goal was to understand the metal support interactions that occur between the cobalt species and the silica support during and after preparation of the Co/SiO_2 supported catalysts. The effects of support surface area and calcinations temperature on the performance of these catalysts were the two main parameters studied. The experiments involved characterizing the various catalysts synthesized at different conditions: after preparation, after calcination and after reaction using various tools such as XPS, XRD, BET and FTIR. The experimental goal was to identify cobalt silicate and try to investigate the chemistry and stage at which it was formed. Cobalt silicate is considered an undesired cobalt phase in FTS. It has no catalytic activity to produce any synthetic paraffinic fuel. FTIR results identified cobalt silicate species in addition to the desired cobalt oxide species. The performance of the catalysts varied and it was found that in the reduction/reaction stage, metal support interaction added to the formation of irreducible cobalt silicate phase. Co/silica catalysts with lower surface area ($300 m^2/g$)

exhibited higher C_{5+} selectivity which can be attributed to less metal support interaction and higher reducibility and dispersion. The prepared catalysts with different drying and calcination temperatures were also compared. Catalysts dried and calcined at lower temperatures exhibited higher activity and lower cobalt silicate formation. The catalyst sample calcined at 573K showed the highest CO conversion and the lowest CH_4 selectivity. The results also agreed with the literature conclusion that the bulk of cobalt silicate forms during reduction as a water induced mechanism. It was also concluded that cobalt silicate may form during the catalyst synthesis process depending on many factors such as the pH, cobalt loading percentage and surface area of the silica support and its interaction with the cobalt precursor. The activity and STY of the catalyst samples studied decreased as the surface area of the catalyst increased (300>480>560 m^2/g). This was also true for the CO conversion which dropped as support surface area increased. When catalysts with the same silica support surface area were used, the CO conversion decreased as drying and calcination temperatures increased from 573 to 773K. The same trend was noticed for activity and STY. This was explained by cobalt particle agglomeration due to sintering and silica migration. The results also indicate that the properties of silica supports affect the product distribution. Catalyst with small pore diameter (<6nm) increased the rate of CH_4 formation.

6.2 Future Work

In this section, future work for the two heterogeneous systems studied is proposed. For the partial oxidation reaction of *n*-butane to produce MA using VPO catalysts, a GC-MS system connected to the bench scale reactor is essential to determine

accurate MA yield and selectivity. The bulk of the results were obtained using an FTIR equipped with a gas-cell. This helped in obtaining *n*-butane conversion as well as qualify the main reaction products.

Investigation into the mechanism of both catalytic reaction systems should be considered. An FTIR equipped with an *in-situ* accessory will investigate the reagents surface adsorption and provide important information on the sequence of the reaction. This will also explain the performance results obtained from both catalytic systems prepared.

A new BTRS-*jr*. reactor was purchased from Autoclave Engineers, Inc. to be used in studying the effect of operating under high pressures on the Co/silica supported catalysts. The results for this project were obtained under relatively low pressure (8 bar) in comparison to reported operating pressures due to safety concerns and equipment limitations.

The preparation of the VPO catalysts is a very complex process. Characterization using specific tools such as ESR and XAFS should provide important information on the evolution of this catalyst. Titration experiments should also provide additional information on the valence number of V and the important P/V ratio which, in turn, determines the activity.

Finally, characterization during reaction using an *in-situ* tool such as XRD is an extraordinary way of investigating the cobalt phases formed during reduction as well as the cobalt metal sites formed. The results of this work has provided an insight on the cobalt oxide species formed in addition to cobalt silicates but the ability to investigate the

evolution and formation of the cobalt metal clusters and their size will help in predicting the performance of these catalyst systems and the reaction mechanism.

List of References

[1] M. Ruitenbeek, *Characterization of Vanadium-Based Oxidation Catalysts,* Thesis, Universiteit Utrecht, (1999).

[2] R. Masel, *Chemical Kinetics and Catalysis*,Wiley Interscience, (2001).

[3] www.nist.gov (1999) 11-23-08, <http://www.atp.nist.gov/focus/cabt.htm>

[4] www.mcgraw-hill.com (2003) 11-26-08, <http:///www.chemguide.co.uk/physical/catalysis/introduction.html#top>

[5] S. Jaras, M. Zwinkels, P. Menon, and T. Griffin, *Catal. Rev. Sci. Eng. ,* 35, 319, (1993).

[6] Y. Chao, R. Friedman and M. Vannice, *Appl. Catal., A,* 20, 91, (1986).

[7] Bruce Gates, University of California-Davis (2001) 1-30-09, <http://www.scribd.com/doc/11080604/Catalysis>

[8] C. Bartholomew and R. Farrauto, *Fundamentals of Industrial Catalytic Processes*, Second ed., John Wiley & Sons, Inc., (2006).

[9] Amanda Lee, Louisiana State University (2002) 04-22-04, <http://www.che.lsu.edu/COURSES/4205/2000/Lee/paper.htm>

[10] B. Elvers, S. Hawkins, and G. Schulz, *Maleic Anhydride*, Ullman's Encyclopedia of Chemical Industry, A16, 54, (1990).

[11] K. Othmer, *Maleic Anhydride, Maleic Acid, and Fumaric Acid*, Encyclopedia of Chemical Technology, 14, 770, (1981).

[12] C. Satterfield, *Heterogeneous Catalysis in Industrial Practice*, Second ed., Kreiger Publishing Co, Malabar, FL, (1991).

[13] www.piketech.com (2005) 2-4-09, <www.piketech.com/products/product-documentation pdfs/MIRacle_PDS.pdf>

[14] NIST Chemistry Webbook (2005) 10-14-04, <http://webbook.nist.gov/cgi/cbook.cgi?Name=butane&Units=SI>

[15] M. Ledoux, DuPont Co., *Vanadium Phosphorous Oxide Catalysts Having a Thermally Conductive Support*, US Patent 6,660,681 (2003).

[16] B Kubias, U Rodemerck, H. Zanthoff, and M. Meisel, *Catal. Tod.,* 32**,** 243, (1996).

[17] X. Wen and G. Yang, *AICHE Jour.,* 49, 465, (2003).

[18] J. Bither, DuPont Co., *Catalysis for Vapor Phase Oxidation of n-Butane to Maleic Anhydride,* US Patent 4,442,226 (1984).

[19] I. Ayub, D. Su, A. Kharlamov, L. Ushkalov, and R. Schlogl, *Electron Microscope Study of Mechanical Activation of VPO Catalyst,* Kiev, Ukraine, (1996).

[20] M. Abon and J. Volta, *Appl. Catal. A.,* 157, 173, (1997).

[21] M. Ledoux, C. Crouzet, C. Pham-Huu, V. Turines, K. Kourtakis, P. Mills, and J. Lerou, *Jour. Catal.,* 203, 495, (2001).

[22] Y. Taufiq-Yap, M. Looi, K. Waugh, and M. Zobir-Hussein, *The Effect of Cobalt Doping on Vanadyl Pyrophosphate Catalyst,* Department of Chemistry, Universiti Putra Malaysia, Selangor, Malaysia, (1999).

[23] Spectrum Laboratory Inc., Chemical Fact Sheet (2003) 02-18-09, <http://www.speclab.com/elements/palladium.htm>

[24] L. Cornaglia, S. Irusta, E. Lomabardo, M. Durupty, and J. Volta, *Catal. Tod.,* 78, 291, (2003).

[25] S. Roy, M. Dudukovic, and P. Mills, *Catal. Tod.,* 61, 73, (2000).

[26] M. Dente, S. Pierucci, E. Tronconi, M. Cecchini, and F. Ghelfi, *Chem. Eng. Sci.,* 58, 643, (2003).

[27] S. Shen, J. Zhou, F. Zhang, L. Zhou, and R. Li, *Catal. Tod.,* 74, 37, (2002).

[28] M. Witko, R. Tokarz, J. Haber, and K. Hermann, *Jour. of Mol. Catal. A,* 166**,** 59, (2001).

[29] B. Hodnett, *Catal. Rev. Sci. Eng. ,* 27, 373, (1985).

[30] E. Bordes, P. Courtine, and J. Johnson, *Jour. Solid State Chem.,* 55, 270, (1984).

[31] Z. Sobalik, G. Carrazan, S. Ruiz, and B. Delmon, *Jour. Catal.,* 185, 272, (1999).

[32] Timothy Felthouse, Huntsman Petrochemical Corporation, (2001) 05-23-04, <http://www.huntsman.com/performance_products/Media/KOMaleic.pdf>

[33] N. Govender, H. Friedrich, and M. van Vuuren, *Catal. Tod.,* 97, 315, (2004).

[34] Z. Xue, and G. Schrader, *Jour. Catal. ,* 184, 87, (1999).

[35] S. Puttock, and C. Rochester, *Jour. Chem. Soc. Faraday Trans.,* 82, 2773, (1986).

[36] A. Duarte de Farias, W. Gonzalez, P. Pries de Oliveira, J. Eon, J. Herrmann, M. Aouine, S. Loridant, and J. Volta, *Jour. Catal.,* 208, 238, (2002).

[37] Synfuels International Corportation, (2006) 06-23-08, <http://www.synfuels.com/technology.html>

[38] A. Steynberg, and M. Dry, *Stud. Surf. Sci. Catal. ,* 152, 223, (2004).

[39] J. Keyser, M. van Dyk; and M. Coertzen, *Int. Jour. Coal Geol.,* 65, 243, (2006).

[40] B. van Berge, P. Jager; and A. Steynberg, *Stud. Surf. Sci. Catal.,* 136, 63, (2001).

[41] A. Steynberg, R. Jager, and B. Vosloo, *Appl. Catal. A,* 186, 41, (1999).

[42] S. Iglesia, E. Soled, R. Fiato; J. Baumgartner, H. Vroman, and S. Miseo, *Top. Catal.,* 26, 101, (2003).

[43] G. Bitter, J. Bezemer, H. Kuipers, H. Oosterbeek, J. Holewijn, X. Xu, F. Kapteijn, A. van Dillen, and K. de Jong, *Jour. Am. Chem. Soc.,* 128, 3956, (2006).

[44] S. Aris, and R. Lee, *Catal. Rev. Sci. Eng.,* 27, 207, (1985).

[45] T. Cleys, M. Riedel, G. Schulz, G. Schaub, S. Nam, K. Jun, M. Choi, G. Kishan, and K. Lee, *Appl. Catal. A,* 186, 201, (1999).

[46] Z. Qing, K. Fang Zhu, J. Chen, and Y. Sun, *Fuel Chem. Tech.,* 33, 506, (2005).

[47] Y. Hanayama, K. Zhang; and N. Tsubaki, *Catal. Comm.,* 7, 251, (2006).

[48] T. Egichi, K. Ishihara, and H. Arai, *Jour. Mol. Catal.,* 72, 253, (1992).

[49] A. Claeys, M. Saib, and E. Steen, *Catal. Tod.,* 71, 395, (2002).

[50] D. Li, and J. Song, *Jour. Mol. Catal.,* 247, 206, (2006).

[51] S. Occeli, and M. Biz, *Catal. Rev. Sci. Eng.,* 40, 329, (1998).

[52] V. Evans, A. Zholobenko, D. Plant, and S. Holmes, *Micro. Meso. Mater.,* 793, 345, (2001).

[53] J. Weber, A. Kogelbauer,and J. Goodwin, *Catal. Lett ,* 34, 259, (1995).

[54] A. Sault, and K. Coulter, *Jour. Catal.,* 154, 56, (1995).

[55] G. Sewell, E. Steen, R. Makhote, C. Micklethwaite, H. Manstein, C. O'Connor, and M. de Lange, *Jour. Catal.,* 162, 220, (1996).

[56] S. Libs, B. Ernst, P. Chaumette, and A. Kiennemann, *Appl. Catal. A,* 86, 145, (1999).

[57] T. Fleisch, I. Puskas, J. Hall, B. Meyers, and R. Roginski, *Jour. Catal.,* 134, 615, (1992).

[58] F. de Groot, F. Morales, O. Gijzeman, A. Mens, O. Stephan, and B. Weckhuysen, *Jour. Catal.,* 230, 301, (2005).

[59] T. Cleys, M. Riedel, G. Schulz, G. Schaub, S. Nam, K. Jun, M. Choi, G. Kishan, and K. Lee, *Appl. Catal. A,* 186, 201, (1999).

[60] F. Gijzeman, O. Morales, O. Cano, F. de Groot, and M. Weckhuysen, *Stud. Surf. Sci. Catal. ,* 147, 271, (2004).

[61] B. Ernst, and A. Kiennemann, *Catal. Tod ,* 50, 413, (1999).

[62] T. Ding, Y. Wang, J. Xiong, L. Yan, H. Zhu, Y. Lu, and L. Lin, *Catal. Lett.,* 107, 47, (2006).

[63] G. Butala-Huber, S. Lee, and C. Bartholomew, *Catal. Lett.,* 74, 45, (2001).

[64] Y. Nagamori, S. Zhang, S. Hinchiranan, T. Vitidsant, and N. Tsubaki, *Energy Fuels,* 20, 417, (2006).

[65] J. Chen, J. Zhang, J. Ren and Y. Sun, *Appl. Catal. A,* 243, 121, (2003).

[66] Y. Liu, Y. Zhang, G. Yang, S. Sun, and N. Tsubaki, *Appl. Catal. A,* 321, 79, (2007).

[67] R. Iler, *The Chemistry of Silica*, Wiley, New York, (1979).

[68] H. Ming and B. Baker, *Appl. Catal. A,* 123, 23, (1995).

[69] T. Fleisch, I. Puskas, J. Kaduk, C. Marshall, and B. Meyers, *Appl. Catal. A,* 316, 197, (2007).

[70] G. Sewell, E. van Steen, R. Makhote, C. Micklethwaite, H. Manstein, M. de Lange, and C. O'Connor, *Jour. Catal.,* 162, 220, (1996).

[71] M. Wolcyrz, J. Jablonski, and L. Krajczyk, *Jour. Catal.,* 173, 530, (1998).

[72] Vadim Siklitsky, www.ioffe.ru (2003) 04-05-04,. <http://www.ioffe.ru/SVA/NSM/Semicond/SiC/thermal.html#Thermal conductivity>

[73] M. Dry, *Catal. Tod.*, 71, 227, (2002).

[74] E. Iglesia, *FTS CO Dissociation Mechanism*, Proceedings of the 20th Meeting of the North American Catalysis Society, (2007).

[75] H. Fogler, *Elements of Chemical Reaction Engineering*, Fourth ed., Prentice Hall, (2005).

[76] Y. Jun, L. Ying, Z Yuanming, and T. Yu, *Chem. Jour.,* 6, 4, (2004).

Appendices

Appendix A: Theoretical and Actual MA Yield Calculations

The balanced partial oxidation reaction of *n*-butane to MA is:

$$C_4H_{10} + 3.5O_2 \rightarrow C_4H_2O_3 + 4H_2O \quad \text{(A.1)}$$

Since lean mixtures of *n*-butane in air are used, then *n*-butane is the limiting reactant. The values used to calculate the theoretical yield shown in Table 4.5 are as follows: *n*-butane flow rate = 1.46 sccm, total operating time = 20h (since activation by *n*-butane of the VPO catalyst also produced MA), density of gaseous *n*-butane = 2.7 kg/m^3, molecular weight of *n*-butane = 58.12 g/mol and molecular weight of maleic anhydride = 98.0 g/mol.

From the balanced equation, the number of moles of *n*-butane is equal to the number of moles of MA, so calculating the number of moles of *n*-butane gives 0.0814 mols *n*-butane, which is equal to 0.0814 mols MA. This gives 7.98g MA as theoretical yield. Other tabulated results were calculated in the same way.

Appendix B: *In-situ* FTIR Spectral Change Versus Temperature

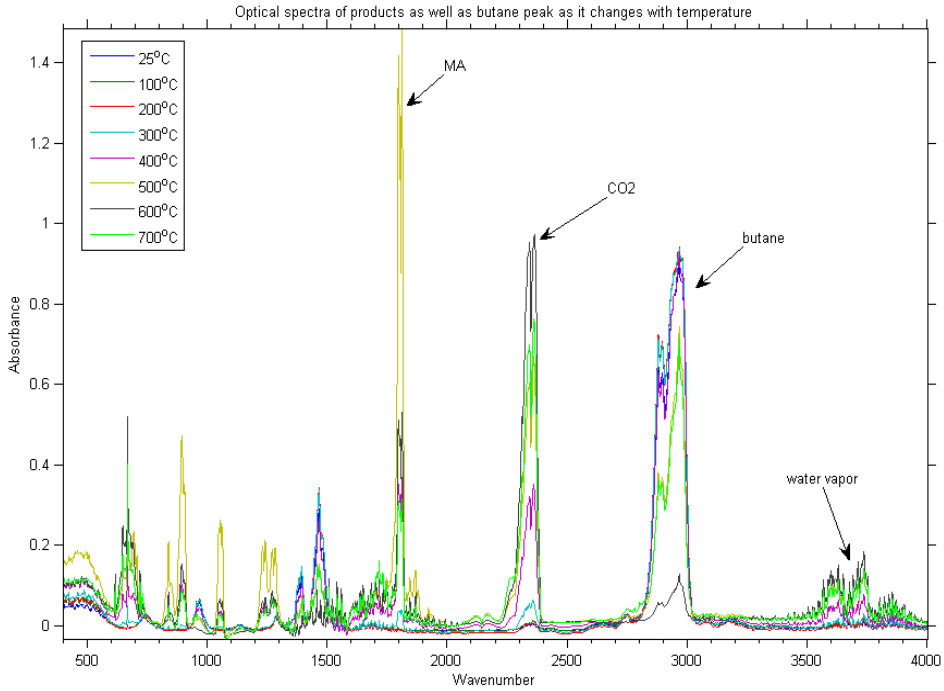

Figure B.1: *In-situ* FTIR spectra of products and *n*-butane IR peaks. The spectra are shown at different temperatures for the 1.5wt%Pd/VPO catalyst sample.

Appendix B: (Continued)

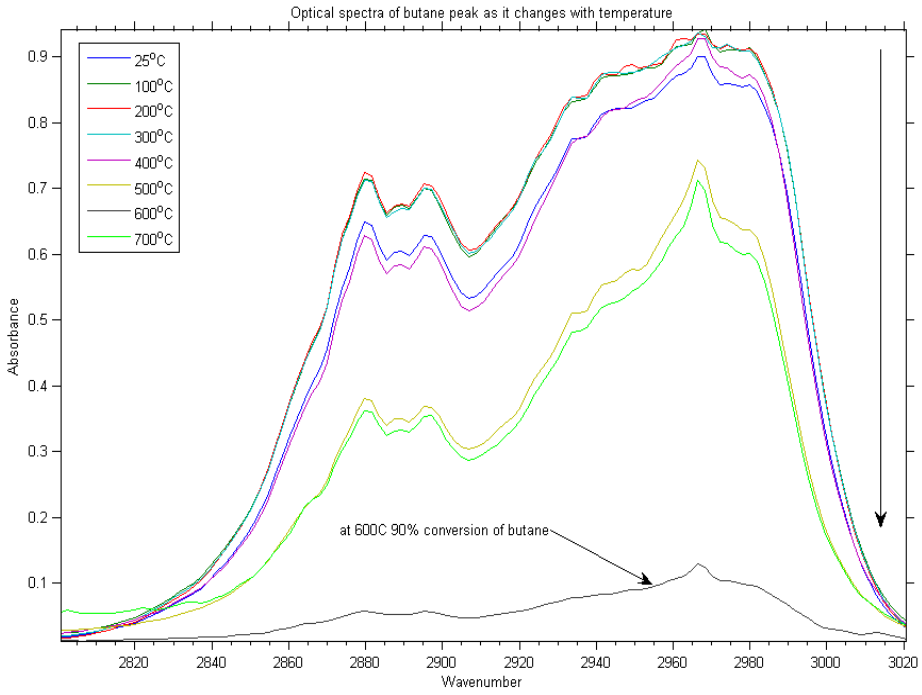

Figure B.2: *In-situ* FTIR spectra of *n*-butane characteristic IR peak. The spectra are shown at different temperatures for the 1.5wt%Pd/VPO catalyst sample.

Appendix B: (Continued)

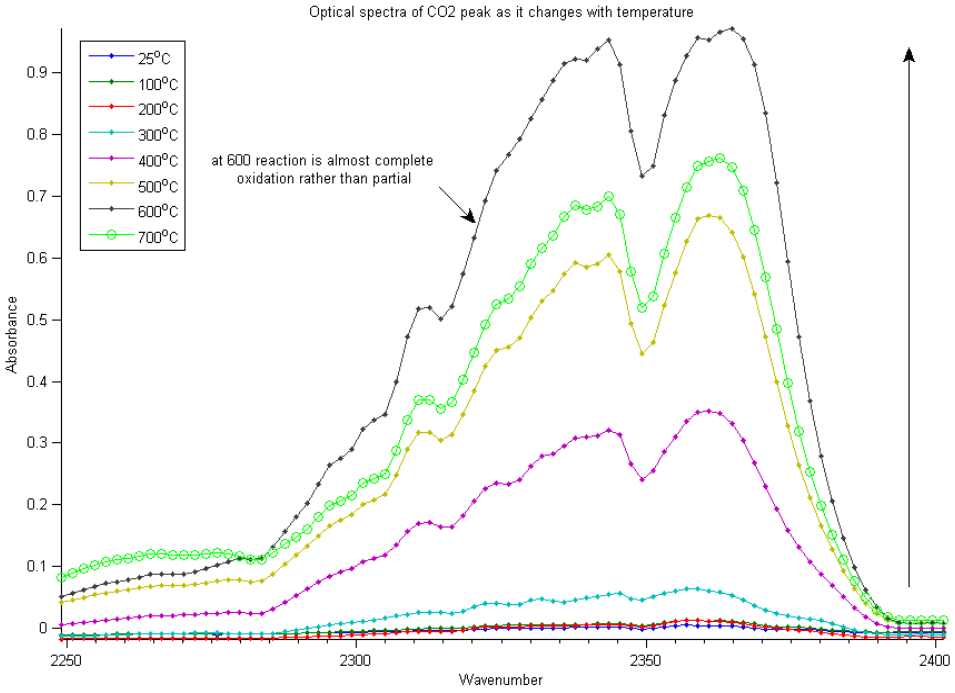

Figure B.3: *In-situ* FTIR spectra of CO_2 characteristic IR peak. The spectra are shown at different temperatures for the 1.5wt%Pd/VPO catalyst sample.

Appendix B: (Continued)

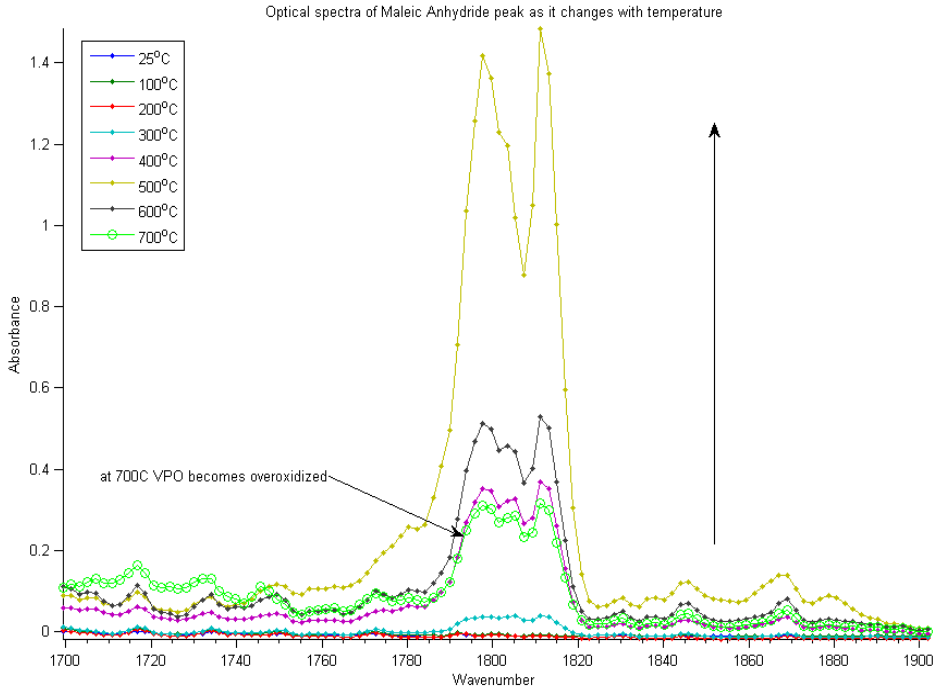

Figure B.4: *In-situ* FTIR spectra of maleic anhydride characteristic IR peak. The spectra are shown at different temperatures for the 1.5wt%Pd/VPO catalyst sample.

Appendix C: Calculating Temperature Gradient in SiC/VPO Catalyst

For film ΔT resistance, one can equate the rate of heat removal through the film with the rate of heat generated or absorbed by the reaction within the diluent or support. Thus for the general heterogeneous catalytic reaction, A→B:

$$Q_{generated} = \left(V_{particle}\right)\left(-r_{A,obs}\right)\left(-\Delta H_r\right) \tag{C.1}$$

$$Q_{removed} = U\left(S_{particle}\right)\left(T_g - T_s\right) \tag{C.2}$$

And on combining we find:

$$\Delta T_{film} = \left(T_g - T_s\right) = \frac{L\left(-r_{A,obs}\right)\left(-\Delta H_r\right)}{U} \tag{C.3}$$

Where L is the characteristic pellet size (1.5 mm for all catalyst samples), Q is the heat duty, T_g and T_s are bulk and surface temperatures respectively, ($-r_{A,obs}$) is the observed reaction rate calculated using rate constant of 0.01 m^3/mol.s [1] and assuming second order reaction with respect to *n*-butane only, since atomic lattice oxygen is consumed in the reaction rather than reactant O_2 [1,10,11]. Other parameters used are: inlet *n*-butane concentration of 1.4 vol%, *n*-butane density of 2.52 kg/m^3 at 1 atm and *n*-butane molecular weight of 58 g/mol. This gives: inlet molar concentration (C_0) =1.4cm^3/100cm^3 *2.52kg/m^3/58g/mol*10^3 g/kg= 0.61mol/m^3, but $C_{n\text{-butane}}=C_0$ (1-x), where x is the *n*-butane conversion. In this case, the conversion at reaction temperature of 400°C for bulk VPO was selected, the value was 6% (Figure 4.7). This gives ($-r_{A,obs}$) =3.28*10^{-3} mol/m^3.s. ΔH_r for the partial reaction is equal to -1236kJ/mol *n*-butane (Table 2.3) and

U is the heat transfer coefficient (conductance) which equals to the material thermal conductivity divided by the distance between the ends or tube thickness ($h=k/\Delta x$). U was found to be 0.195 $W/m^2.°C$, since the effective thermal conductivity of the bed was $0.78*10^{-3}$ W/m.°C at 400°C [1]. The distance between both ends is the reactor tube diameter which is constant for all experiments and equals to 0.004m.

Solving for ΔT gives 31.2°C. This means that for a bulk gas temperature T_g of 400°C, the surface particle temperature T_s is 431.2°C.

For α-SiC mixed VPO catalysts, effective thermal conductivity is calculated using the following empirical formula [72]:

$$k = \frac{611}{(T - 115)} \tag{C.4}$$

This gives a value of 214 W/m.°C, and a conductance value of 53,500.00 $W/m^2.°C$. For a 10wt% α-SiC/VPO catalyst, the thermal conductivity is assumed to be averaged based on the weight ratios. This gives an average effective thermal conductivity of: $0.195*0.9+53,500.00*0.1=5350.00$ $W/m^2.°C$ which is basically the SiC effective thermal conductivity. The conversion for this sample at 400°C is 53%. This gives a reaction rate of $8.2*10^{-3}$ $mol/m^3.s$.

Solving for ΔT gives 0.003°C, meaning that the surface particle temperature is essentially the same as the gas phase temperature. Since these experiments were done using a 4 mm diameter tube, then isothermal conditions can be assumed. Still, SiC high

thermal conductivity should easily help dissipate the heat generated in this highly exothermic reaction. Utilizing SiC as a catalytic diluent material greatly increases both h and k. This translates to reduced temperature effects and increased catalyst life time, selectivity, and reduced thermal run away and reaction temperatures.

Appendix D: Fischer-Tropsch Stepwise Growth Process Mechanism

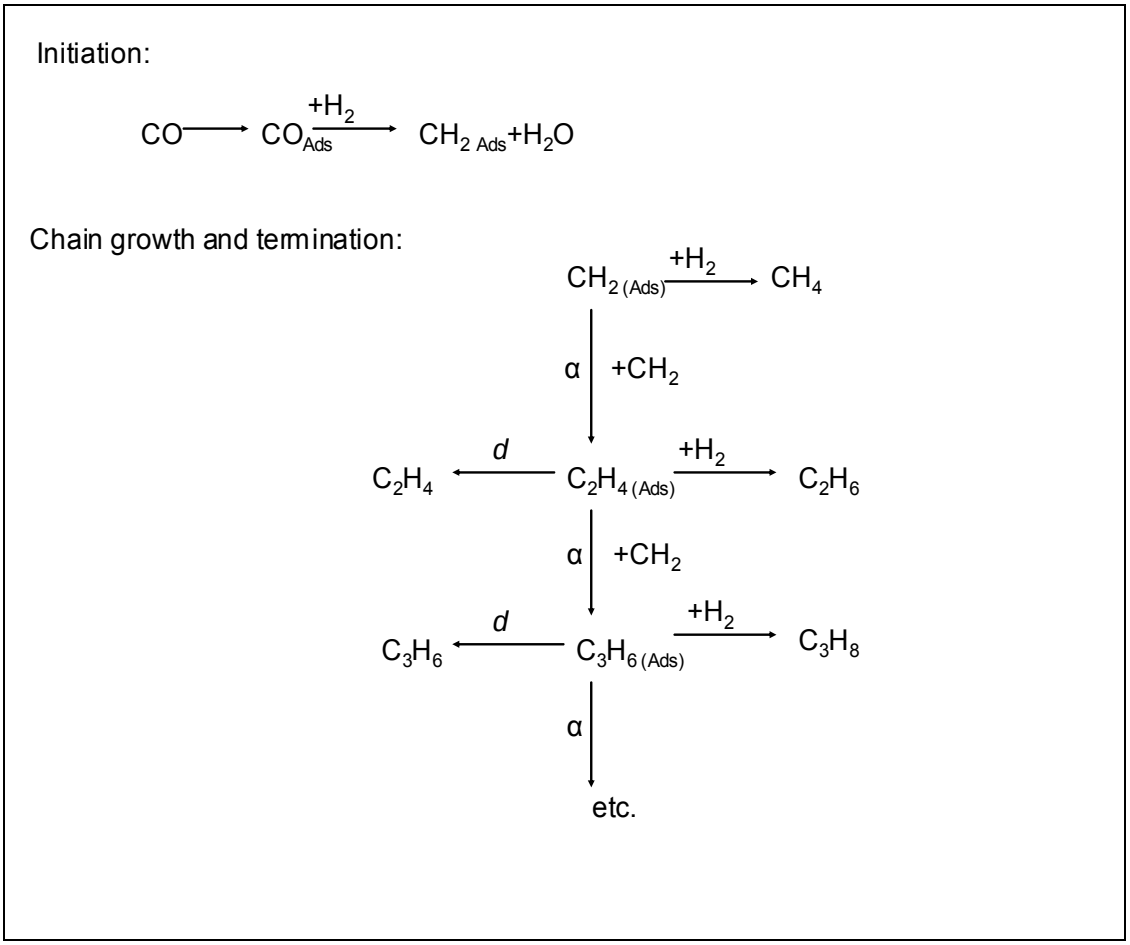

Figure D.1: Fischer-Tropsch growth process. Notice that no specific chemical mechanism is implied in the sequence. Schematic adapted from reference [73].

Two mechanisms have been proposed by Iglesia [74] for the CO dissociation versus H-assisted CO dissociation: Carbide mechanism with direct CO dissociation

$$CO_{(g)} + \boldsymbol{S} \leftrightarrow CO.\boldsymbol{S} \tag{D.1}$$

$$H_{2(g)} + 2\boldsymbol{S} \leftrightarrow 2H.\boldsymbol{S} \tag{D.2}$$

$$CO.\boldsymbol{S} + \boldsymbol{S} \leftrightarrow C.\boldsymbol{S} + O.\boldsymbol{S} \tag{D.3}$$

$$C.\boldsymbol{S} + H.\boldsymbol{S} \rightarrow CH.\boldsymbol{S} + \boldsymbol{S} \tag{D.4}$$

$$CH.\boldsymbol{S} + H.\boldsymbol{S} \leftrightarrow CH_2.\boldsymbol{S} + \boldsymbol{S} \tag{D.5}$$

$$CO.\boldsymbol{S} + O.\boldsymbol{S} \leftrightarrow CO_{2(g)} + 2\boldsymbol{S} \tag{D.6}$$

The rate equation for this mechanism is:

$$r = \frac{k(P_{CO})^{0.5}\left(P_{H_2}\right)^{0.75}}{(1 + KP_{CO})^2} \tag{D.7}$$

Where k is the reaction rate constant and K is the equilibrium constant which equals to the adsorption rate constant divided by the desorption rate constant. Carbonyl insertion with H-assisted CO dissociation:

$$CO_{(g)} + \boldsymbol{S} \leftrightarrow CO.\boldsymbol{S} \tag{D.8}$$

$$H_{2(g)} + 2\boldsymbol{S} \leftrightarrow 2H.\boldsymbol{S} \tag{D.9}$$

$$CO.\boldsymbol{S} + H.\boldsymbol{S} \leftrightarrow HCO.\boldsymbol{S} + \boldsymbol{S} \tag{D.10}$$

$$HCO.\boldsymbol{S} + H.\boldsymbol{S} \rightarrow CH.\boldsymbol{S} + OH.\boldsymbol{S} \tag{D.11}$$

$$CH.\boldsymbol{S} + H.\boldsymbol{S} \leftrightarrow CH_2.\boldsymbol{S} + \boldsymbol{S} \tag{D.12}$$

$$OH.\boldsymbol{S} + H.\boldsymbol{S} \rightarrow H_2O_{(g)} + 2\boldsymbol{S} \tag{D.13}$$

The rate equation for this mechanism is:

$$r = \frac{kP_{CO}P_{H_2}}{(1 + KP_{CO})^2} \tag{D.14}$$

The carbonyl insertion mechanism is favored for cobalt catalysts.

Appendix E: Theoretical Deactivation by Sintering Calculations

Sintering, also referred to as aging, is the loss of catalytic activity due to a loss of active surface area resulting from the prolonged exposure to high gas phase temperatures. The active surface area may be lost either by crystal agglomeration and growth of the metals deposited on the support or by narrowing or closing of the pores inside the catalyst pellet. Although other forms of the sintering decay rate laws exist, one of the most commonly used decay laws is second order with respect to the present activity [75].

$$r_d = k_d.a^2 = -\frac{da}{dt} \tag{E.1}$$

Integrating with a = 1 at time t = 0 yields:

$$a(t) = \frac{1}{1 + k_d t} \tag{E.2}$$

The amount of sintering is usually measured in terms of the active surface area of the catalyst S_a

$$S_a = \frac{S_{a_0}}{1 + k_d t} \tag{E.3}$$

The sintering decay constant, K_d follows the Arrhenius equation [75]:

$$k_d = k_d(T_0)\exp\left[\frac{E_d}{R}\left\{\frac{1}{T_0} - \frac{1}{T}\right\}\right] \tag{E.4}$$

Where E_d is the decay activation energy. For FTS, the chain growth activation energy is 60.55 $kJ.mol^{-1}$ [76] and was assumed to be equal to the decay activation energy.

Appendix E: (Continued)

The parameters used in solving for k_d are: R=80314 J/mol.K, T_0=298K, T=503K and k_d (T_0)= $1.8*10^{-16}$ s^{-1}. This gives k_d= $1.8*10^{-6}$ s^{-1} or 0.0065h^{-1}. So for catalyst sample 300Co-1, assuming high cobalt dispersion and 100% reduction of the cobalt oxide species to metallic $Co^{(0)}$ sites under H_2. The initial active surface area S_{a0} is equal to the calcined surface area of 254m^2/g (Table 5.2).

Solving gives S_a (48h)= 194m^2/g active surface area after 48h FTS reaction. The experimental value was 231 m^2/g (Table 5.2). The reason why the experimental value was much higher than the theoretical value is the fact that the theoretical calculations were based on cobalt decay constant only but not Co/silica systems, the decay activation energy was for chain growth. On the other hand, the cobalt melting point is approximately 1495°C lower than that of silica which is approximately 1700°C. Based on this, one can conclude that sintering in FTS Co/silica systems can be mainly due to metal Co particle agglomeration rather than silica structure damage or migration. Good dispersion of cobalt in the silica porous frame and high reduction percentages can enhance the activity and life time of this catalytic system. Cobalt particles that are not completely dispersed can easily agglomerate during reduction to form large cobalt clusters, thus reducing the amount of active Co metal sites exposed. Another reason for the high experimental values of surface area is due to cobalt silicate formation during reduction which counters the sintering (loss of active surface area) effects since it has a high surface area amorphous structure. Also, the theoretical calculations do not take into

effect the interaction between the high surface area silica with the cobalt species during reduction and reaction. The theoretical values of the amount of sintering and activity are presented in Table E.1 for all samples. Experimental values of activity and after reaction surface area are also included.

Table E.1: Calculated theoretical and experimental activity and sintering. Results are shown for all catalyst samples used in the FTS experiments.

Catalyst ID	Theoretical			Experimental		
	Activity[a] (h^{-1})	Calcined[b] S_a (m^2/g)	After 48h S_a (m^2/g)	Activity (h^{-1})	Calcined S_a (m^2/g)	After 48h S_a (m^2/g)
300Co-1	0.76	254	194	0.29	254	231
480Co-2	0.76	356	271	0.26	356	319
560Co-3	0.76	408	311	0.20	408	375
300Co-4	0.76	243	185	0.18	243	206
300Co-5	0.76	209	159	0.15	209	168

[a] Theoretical activity estimated at t = 48h.
[b] Experimental calcined S_a was used. No data was available to calculate calcined S_a.

The theoretical activity for all samples at t= 48h was $0.76h^{-1}$. The reason why the theoretical value was much higher compared to the actual values is because the theoretical activity was calculated based on 100% reduction of the cobalt species, complete dispersion of the catalyst and no cobalt silicate formation during preparation or reduction which obviously is not the case. Another reason is that when waxy HC product is formed during FTS, sometimes it does not desorb from the silica pores thus accumulating within the catalyst bed. This in turn decreases the value of the experimental activity which is based on the collected HC product.

About the Author

Ala'a Hamed Kababji received a Bachelor's degree in Chemical Engineering from the Jordan University of Science and Technology (JUST) in 2001. Since that time, he has been pursuing his Master's and Doctor of Philosophy degrees in Chemical Engineering at the University of South Florida. His research focus is on catalysis and reaction engineering: VPO catalysts for the production of maleic anhydride, Fischer-Tropsch synthesis and methane nonoxidative aromatization to hydrogen and benzene. His work was performed at the Department of Chemical and Biomedical Engineering Applied Surface Science Laboratory and was supported by DOE, ONR and NASA grants. His dissertation work has been presented at the 2005 and 2008 AICHE annual conferences, the 2009 AIAA 47th meeting, the 2005 MRS spring meeting, and lastly at the 2005 AVS meeting. Ala'a has a patent pending filed with the US patent office. He also has one publication, a book chapter and two conference proceedings.